Dissertation

submitted to the Combined Faculties for the
Natural Sciences and Mathematics
of the Ruperto – Carola University of Heidelberg
for the degree of
Doctor of Natural Sciences

presented by
Diplom-Physiker Hans Christian Krahl
born in Konstanz, Germany

Oral Examination: July 25, 2007

Antiferromagnetism and d-wave Superconductivity in the Hubbard Model

Referees: Prof. Dr. Christof Wetterich
PD. Dr. Jan Martin Pawlowski

Antiferromagnetismus und d-Wellen-Supraleitung im Hubbard-Modell

Zusammenfassung

Das zweidimensionale Hubbard Modell gilt als vielversprechendes, effektives Modell zur Beschreibung der Freiheitsgrade der Elektronen in den Kupferoxidschichten von Hochtemperatursupraleitern. Wir stellen einen Zugang zu diesem Modell mithilfe der funktionalen Renormierungsgruppe mit Fokus auf Antiferromagnetismus und d-Wellensupraleitung vor. Um die relevanten Freiheitsgrade auf allen Längenskalen explizit zugänglich zu machen, führen wir zusammengesetzte bosonische Felder ein, welche die Wechselwirkung zwischen den Fermionen vermitteln. Das spontane Brechen einer Symmetrie spiegelt sich in einem nichtverschwindenden Erwartungswert eines bosonischen Feldes wieder. Wir zeigen wie durch Spinwellenfluktuationen eine d-Wellenkopplung erzeugt wird. Des Weiteren berechnen wir die höchste Temperatur, bei der die Wechselwirkungsstärke der Elektronen im Renormierungsgruppenfluss divergiert sowohl für Antiferromagnetismus als auch für d-Wellensupraleitung über einen weiten Dotierungsbereich. Diese "pseudokritische" Temperatur signalisiert das Einsetzen von lokaler Ordnung. Ausserdem wird die Temperaturabhängigkeit der d-Wellensupraleitung in einem vereinfachten Modell, welches sich durch eine Kopplung lediglich im d-Wellenkanal auszeichnet, studiert. Wir finden einen Phasenübergang vom Kosterlitz-Thouless-Typ.

Antiferromagnetism and d-wave Superconductivity in the Hubbard Model

Abstract

The two-dimensional Hubbard model is a promising effective model for the electronic degrees of freedom in the copper-oxide planes of high temperature superconductors. We present a functional renormalization group approach to this model with focus on antiferromagnetism and d-wave superconductivity. In order to make the relevant degrees of freedom more explicitly accessible on all length scales, we introduce composite bosonic fields mediating the interaction between the fermions. Spontaneous symmetry breaking is reflected in a non-vanishing expectation value of a bosonic field. The emergence of a coupling in the d-wave pairing channel triggered by spin wave fluctuations is demonstrated. Furthermore, the highest temperature at which the interaction strength for the electrons diverges in the renormalization flow is calculated for both antiferromagnetism and d-wave superconductivity over a wide range of doping. This "pseudo-critical" temperature signals the onset of local ordering. Moreover, the temperature dependence of d-wave superconducting order is studied within a simplified model characterized by a single coupling in the d-wave pairing channel. The phase transition within this model is found to be of the Kosterlitz-Thouless type.

Contents

Chapter 1

Introduction

Interacting many-body systems in condensed matter physics are usually discussed in terms of effective models which incorporate only a comparatively small number of degrees of freedom. Of course, the complexity of taking into account all microscopic degrees of freedom such as the core atoms as well as their electron shells and energy bands would be prohibitive. In order to understand macroscopic properties, such as the phase diagram, it is furthermore questionable whether all these microscopic degrees of freedom are needed. Hence, one of the challenges is to identify the relevant microscopic degrees of freedom and to formulate a microscopic theory which potentially comprises all the information needed to explain the macroscopic behavior.

A famous example of such a microscopic model for interacting fermions is the Hubbard model [1, 2, 3]. Besides many other applications the two-dimensional version of the Hubbard model is regarded as a promising candidate for a description of the electron degrees of freedom in the copper-oxide planes of cuprate high temperature superconductors [4] since it resembles important features of these materials. Particularly, the ground state of this model is antiferromagnetically ordered for a half-filled lattice and is expected to become a superconductor with d-wave pairing symmetry slightly away from half-filling [5, 6]. Recently, the Hubbard model was also proposed for ultra-cold fermionic atoms in two-dimensional optical lattices [7, 8]. These systems may provide an ideal testing ground for this model since they are comparatively clean and as a bonus the ratio of the parameters is tunable. Experiments in optical lattices may also shed light on the question which degrees of freedom are responsible for high temperature superconductivity.

A common feature of such an interacting many-body system is that its behavior depends qualitatively on the energy or momentum scale. For instance, in high temperature superconductors ordering phenomena such as d-wave superconductivity are separated by several orders of magnitude in energy from the bare Coulomb interaction. The intermediate scales are dominated by short-range magnetic correlations. A calculation of macroscopic properties involves an integration over fluctuations on all scales. However, it is hard to treat the

fluctuations on all scales at the same time since the appropriate degrees of freedom change qualitatively with scale. In particular, perturbative approaches are plagued by infrared divergences and therefore are often not applicable, especially in low dimensions.

Among the most promising approaches to the Hubbard model are renormalization group studies [9, 10, 11, 12]. Fluctuations from different scales are treated successively starting from the highest present momentum scale. This allows to very efficiently describe the transition from the microscopic scale where the effective model is defined, to macroscopic scales where collective phenomena may occur. In recent years an increasing number of renormalization group studies of the two-dimensional Hubbard model have been published [13, 14, 15, 16, 17, 18, 19, 20]. The results are encouraging and indeed suggest an antiferromagnetic instability at half-filling and the dominance of d-wave superconductivity slightly away from half-filling. However, all of these studies analyze the scale dependence of the fermionic coupling directly in a purely fermionic language. The information about the various phases and properties is contained in the complicated momentum structure of the four fermion coupling developed in the renormalization flow to lower momentum scales. Spontaneous breaking of a symmetry is reflected in the divergence of the fermionic coupling in the corresponding channel on a finite momentum scale. However, the symmetry broken phase is not entered by these studies and also higher fermionic operators which play an important role in the vicinity of a phase transition are neglected. In [21, 22] the symmetric phase is studied with the functional renormalization group in a fermionic formulation while the symmetry broken regime is treated for both antiferromagnetism and d-wave superconductivity by a mean field calculation.

Our functional renormalization group approach is based on the awareness that in the renormalization flow to lower momentum scales the relevant degrees of freedom change. On high momentum scales the electrons are the appropriate degrees of freedom which is reflected in the fermionic Hubbard model. However, on lower momentum scales and especially in the vicinity of a phase transition the fluctuations are more efficiently integrated out in terms of composite bosons such as e.g. Cooper-pairs. We accommodate for this fact by a bosonization of the initially fermionic model via a Hubbard-Stratonovich transformation [23, 24]. As a consequence, the interaction between the fermions is mediated by bosonic fields which become dynamic in the renormalization flow. Within this formulation the former divergence of the fermionic coupling indicating the onset of local ordering in a fermionic language is translated into a vanishing mass term of the corresponding bosonic field if the transition is continuous. Importantly, the broken phase can be penetrated in the renormalization flow and is identified by a finite expectation value of a bosonic field

and by a massless Goldstone-mode in case of a broken continuous symmetry. Our approach focuses on antiferromagnetism and d-wave superconductivity and their mutual influence depending on the chemical potential. In particular we generalize [25] to finite doping (chemical potential) and demonstrate the emergence of a coupling in the d-wave channel generated by antiferromagnetic spin fluctuations [5]. The spirit of this work is that competing instabilities are described in a bosonized language. This formulation is well-adapted to cope with the diversity of relevant degrees of freedom and their mutual influence on different scales in the renormalization flow. Both the occurrence of an instability and the thereby caused broken phase at lower momentum scales are explicitly accessible within this framework.

Dissertation Outline

This thesis is organized in the following way: In chapter 2 a short introduction to high temperature superconductivity and the Hubbard model is provided. Furthermore the partition function which is the starting point of all further investigations is formulated as a coherent state path integral over fermionic and composite bosonic degrees of freedom.

Functional renormalization group equations which build the methodical basis of this thesis are discussed in chapter 3. Moreover, the concept of scale-dependent field transformations is introduced, which is applied in order to bosonize the antiferromagnetic and d-wave pairing channel properly on all scales.

In chapter 4 we present a formulation which is well-suited to study antiferromagnetism and d-wave superconductivity over a wide range of the chemical potential. The symmetric phase is studied numerically and it is pointed out how the discussion can be enhanced into the symmetry broken regimes in a straightforward manner.

The temperature dependence of the phase transition to d-wave superconductivity is studied in chapter 5 within a simplified effective model which is characterized by a single coupling in the d-wave pairing channel [26]. The emergence of such a model is motivated by the results of chapter 4.

A summary and conclusion is provided in chapter 6.

Chapter 2

Interacting Electrons

This chapter is intended to motivate the Hubbard model as an effective model for correlated electrons. Moreover, the bridge to the calculational techniques developed in the third chapter is built.

The first section provides a brief introduction to cuprate superconductors and the qualitative features of their phase diagram. In the next section we present the idea of effective field theories and subsequently introduce the Hubbard model as an effective model for electron degrees of freedom. Since we are interested in thermodynamic properties in equilibrium, the partition function is the suitable starting point for further investigations. In order to make contact to the powerful functional techniques of quantum field theory we formulate the partition function as coherent state path integral.

The spirit of our approach is the bosonization of the initially purely fermionic Hubbard model. Thereby we want to achieve an optimal description of the relevant degrees of freedom on all length scales. Particularly close to the critical temperature of a phase transition the long range fluctuations are dominated by bosonic composite operators. Spontaneous symmetry breaking is very efficiently studied in terms of bosonic fields. A finite expectation value of a bosonic field reflects the amount of symmetry breaking in the respective channel. Technically, we introduce suitable bosonic fields by means of a Hubbard-Stratonovich transformation.

An appropriate formulation of the partition function for a functional renormalization group approach to antiferromagnetism and d-wave superconductivity in the Hubbard model is derived in the last section of this chapter.

2.1 High Temperature Superconductivity

In the early 1980[ies] J. G. Bednorz and K. A. Müller searched for superconductivity in oxides of different metals. This was an unconventional approach, since these ceramic oxides are mostly insulators at room temperature. However, in the year 1986 they measured a transition temperature T_c to superconductivity

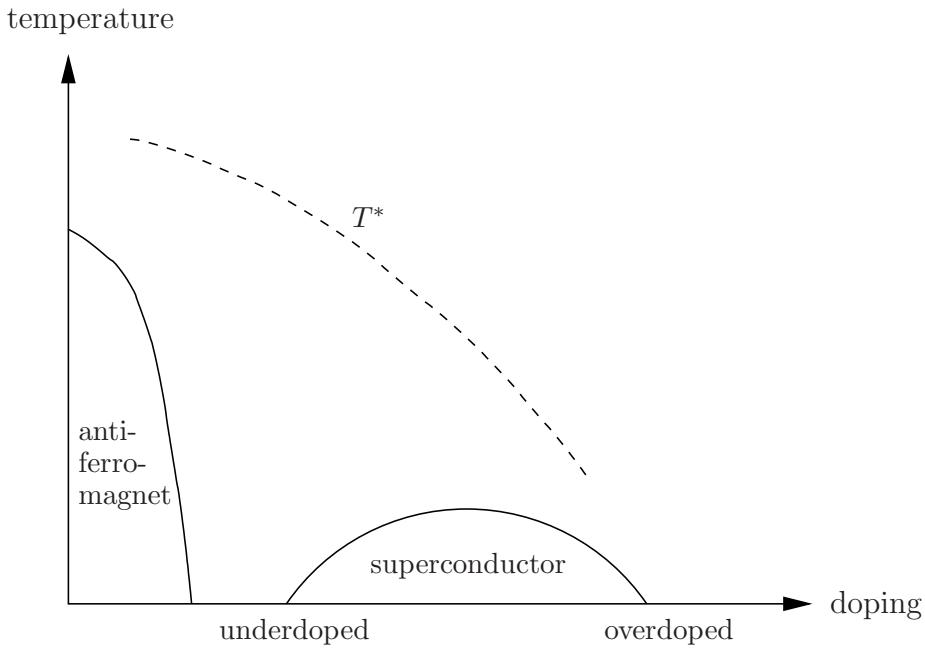

Figure 2.1: Schematic phase diagram of a cuprate superconductor.

of approximately 35 K in compounds of $(\mathrm{La}, \mathrm{Ba})_2\mathrm{CuO}_4$ [27]. This sensational discovery was the starting point of considerable experimental effort. In the following years the record was raised to 134 K in materials with similar structure, such as yttrium barium copper oxides (YBCO). Most of these materials belong to the so called *cuprates*. Their common feature is an anisotropic structure consisting of CuO_2 layers separated by layers containing other atoms, e.g LaO_2 or YO_2 blocks. The electric properties of the cuprates can be changed by modifying the composition of the blocks separating the CuO_2 layers. A replacement of atoms may add electrons (n-doping) or holes (p-doping) to the CuO_2 layers.

In figure 2.1 the schematic phase diagram of such cuprate superconductors is shown. For equal concentration of electrons and holes in the copper-oxide layers the material shows a strong antiferromagnetic interaction between the Cu atoms in the CuO_2 layers below a few hundred Kelvin and the material is an insulator. The long range antiferromagnetic order disappears for an increased level of doping, and the system becomes a superconductor in a certain range of doping [28]. Another interesting phenomenon is indicated by the dashed line in figure 2.1. In the region below T^* (below the dashed line) unusual thermal and transport properties are observed. The origin of these effects is associated with a "pseudo gap", and the transition into this region is rather a cross-over than a real phase transition. Although various possible explanations were proposed

the issue is still unclear, see [29] for a review.

Conventional superconductivity is explained by the BCS theory [30, 31], where the emergence of the attractive interaction between the electrons responsible for the formation of Cooper pairs is mediated by phonons. BCS theory does not apply to the materials considered here since the transition temperature is too high and the thermal energy is therefore too large. In addition, it is shown experimentally [32, 33, 5] that in high temperature superconductors the electron pairs are in states with d-wave symmetry rather than s-wave symmetry. This d-wave symmetry is also reflected in a momentum dependent gap function for the electrons. The energy gap has zeros on the Fermi surface. The origin of the pairing mechanism is still under discussion. However, antiferromagnetic spin fluctuations are regarded to play an important role and may generate the attractive interaction in the d-wave channel [5]. Furthermore, it is speculated that an understanding of the pseudo gap region may be essential for an understanding of the pairing mechanism yielding d-wave superconductivity.

In many rather phenomenological descriptions, superconductivity is discussed with temperature being the relevant parameter. If the temperature falls below a certain critical temperature the materials undergo a transition into the superconducting state. But superconductivity also depends, e.g. on the strength of external magnetic fields. For sufficiently weak fields the famous Meissner effect appears and the external field does not penetrate into the material. The external field is compensated by supercurrents on the surface of the material. However, this works only up to a critical field strength B_{c1}. For stronger fields the energy costs of preventing the external field from penetrating into the material exceeds the condensation energy into the superconducting state. There are two possible scenarios for field strengths above B_{c1}. In so called type I superconductors the field is no longer expelled from the material and the superconductivity disappears completely. Whereas in type II superconductors below a field strength of B_{c2} with $B_{c2} > B_{c1}$ the formation of thin vortices, where the normal state of matter is reestablished, is energetically favorable. For fields above B_{c2} superconductivity breaks down, too. High temperature superconductors are of type II.

2.2 Hubbard Model

The Hubbard model was introduced independently by Hubbard, Kanamori and Gutzwiller [1, 2, 3] in the 1960$^{\text{ies}}$. The physical systems for which the Hubbard model is intended are systems where the fermion (electron) degrees of freedom dominate, or at least play the essential role for the understanding of certain

properties of interest. In an important class of solids the electrons are assumed to be tightly bound to the atoms defining a lattice. This is reflected by the fact that the model is formulated on a lattice where the electrons take only discrete locations in position space. Furthermore, it is assumed that for the low energy properties only one non-degenerate orbit of the atoms is relevant. For this reason one single lattice site can only be occupied by two electrons with opposite spin, which repel each other due to their Coulomb repulsion. This motivates the (one-band) Hubbard model which is defined by the Hamiltonian

$$\hat{H} = \sum_{ij,\sigma} t_{ij} c^\dagger_{i,\sigma} c_{j,\sigma} + U \sum_i n_{i,\uparrow} n_{i,\downarrow} \,. \tag{2.1}$$

Here, $c^\dagger_{i,\sigma}$ and $c_{i,\sigma}$ are creation and annihilation operators for fermions on lattice site i with spin projections $\sigma \in \{\uparrow, \downarrow\}$. The hopping matrix t_{ij} contains transition amplitudes from lattice site j to i. For $U > 0$, the second term describes the local, repulsive interaction of electrons on the same lattice site. $n_{i,\sigma} = c^\dagger_{i,\sigma} c_{i,\sigma}$ defines the number operator for fermions on lattice site i and spin projection σ. All physical information of the model is contained in the dimensionless ratio of the coupling U to the hopping parameters t_{ij}, and the topology of the lattice. We restrict ourselves to nearest $(-t)$ and next to nearest $(-t')$ neighbor coupling on a square lattice.

Despite its formal simplicity the Hubbard model was proposed as an effective model to describe many different phenomena of interacting fermions. Historically, it was first proposed in the context of solids with narrow energy bands (e.g. transition metals), but it is also used for magnetic phenomena such as ferro-, antiferro- and ferrimagnetism. In addition, it is applied to electrical phenomena, namely metal-insulator transition (Mott-transition) and superconductivity. Since its ground state is antiferromagnetically ordered at half filling and is expected to become a d-wave superconductor slightly away from half-filling [5, 6], the model is regarded to be a promising candidate for a description of the electron degrees of freedom in the copper-oxide planes of high temperature superconductors, see e.g. [4]. However, in these materials it is not a priori clear what the degrees of freedom are which render it superconducting. Experiments with ultra-cold fermionic atoms in two-dimensional optical lattices may help to clarify this point in the near future [7, 8]. One may gain a better understanding whether the two-dimensional fermions alone are responsible for d-wave superfluidity, or whether there are other degrees of freedom, e.g. lattice vibrations, needed in addition. Anyway, these experiments may offer the great possibility to test the Hubbard model for various ratios of coupling U and hopping t.

Theoretically, the model is hard to solve even approximately. In two dimensions there are known only very few exact results, mostly in special regions

of the parameter space or for finite systems, see e.g. [34]. Solely in one dimension an exact solution [35] has been found. Although a lot of calculational techniques have been developed and applied to the model, none of these has turned out to be capable to address all aspects. Here, we consider the Hubbard model only at comparable small coupling $U/t \simeq 3$. However, in the context of high temperature superconductivity a coupling larger than the bandwidth, $U/t > 8$, would be more realistic.

2.3 Functional Integral Representation of the Partition Function

The aim of our functional renormalization group study is to explore statistical equilibrium properties of the Hubbard model (2.1). The thermodynamics of a system in contact with a heat bath and a particle reservoir is completely described by its grand canonical partition function

$$Z = \mathrm{Tr}\, e^{-\beta(\hat{H}-\mu\hat{N})}\,, \tag{2.2}$$

where $\beta = 1/T$ is the inverse of the temperature, $\hat{H}$ is the Hamiltonian, $\hat{N}$ the particle number operator, and μ the chemical potential[1]. The trace runs over all physical states of the system.

In our approach we use the well explored functional techniques in quantum field theory. Therefor we write the thermodynamic partition function as a coherent state path integral. Following e.g. [36, 37] we work with Graßmann valued fermionic fields

$$\hat{\psi}_i(\tau) = (\hat{\psi}_{i,\uparrow}(\tau), \hat{\psi}_{i,\downarrow}(\tau))^T\,, \quad \hat{\psi}_i^\dagger(\tau) = (\hat{\psi}^*_{i,\uparrow}(\tau), \hat{\psi}^*_{i,\downarrow}(\tau))\,, \tag{2.3}$$

and similar for the Graßmann valued sources $\eta\,, \eta^\dagger$, and obtain

$$Z[\eta,\eta^\dagger] = \int_{\substack{\hat{\psi}_i(\beta) = -\hat{\psi}_i(0),\\ \hat{\psi}_i^\dagger(\beta) = -\hat{\psi}_i^\dagger(0)}} \mathcal{D}(\hat{\psi},\hat{\psi}^\dagger) \exp\big(-S_F[\hat{\psi},\hat{\psi}^\dagger] + \eta^\dagger\hat{\psi} + \eta^T\hat{\psi}^*\big)\,, \tag{2.4}$$

with the short hand notation $\eta^\dagger\hat{\psi} = \int_0^\beta d\tau \sum_i \eta_i^\dagger(\tau)\hat{\psi}_i(\tau)$. The Euclidean time τ parameterizes a torus with circumference β and the functional integral is constrained by antiperiodic boundary conditions for fermionic fields. The action of the Hubbard model is defined as

$$S_F[\hat{\psi},\hat{\psi}^\dagger] = \int_0^\beta d\tau \Big[\sum_{i,j} \hat{\psi}_i^\dagger\left([\partial_\tau - \mu]\delta_{ij} + t_{ij}\right)\hat{\psi}_j + \frac{U}{2}\sum_i \left(\hat{\psi}_i^\dagger\hat{\psi}_i\right)^2\Big]\,, \tag{2.5}$$

[1] We use natural units, e.g. $k_B = \hbar = 1$.

where we have suppressed the argument τ of the fermionic fields. The kinetic term contains besides the chemical potential μ the hopping matrix t_{ij}. For simplicity, we assume

$$t_{ij} = \begin{cases} -t\,, & \text{if i and j are nearest neighbors } (NN), \\ -t'\,, & \text{if i and j are next to nearest neighbors } (NNN), \\ 0\,, & \text{else.} \end{cases} \tag{2.6}$$

The connection between the interaction term in the action (2.5) and the normal ordered Hamiltonian is given by the replacement rule,

$$\begin{aligned} H_{\rm int}[c, c^\dagger] &= U \sum_i n_{i,\uparrow} n_{i,\downarrow} = -U \sum_i c^\dagger_{i,\uparrow} c^\dagger_{i,\downarrow} c_{i,\uparrow} c_{i,\downarrow} \\ \longleftrightarrow H_{\rm int}[\hat\psi, \hat\psi^\dagger] &= -U \sum_i \hat\psi^*_{i,\uparrow} \hat\psi^*_{i,\downarrow} \hat\psi_{i,\uparrow} \hat\psi_{i,\downarrow} = \frac{U}{2} \sum_{i,\sigma} \hat\psi^*_{i,\sigma} \hat\psi_{i,\sigma} \hat\psi^*_{i,-\sigma} \hat\psi_{i,-\sigma} \\ &= \frac{U}{2} \sum_i \left(\hat\psi^\dagger_i \hat\psi_i\right)^2 . \end{aligned} \tag{2.7}$$

Conveniently, most of the calculations are performed in momentum space rather than in position space. We write $\hat\psi(X) = \hat\psi(\tau, \mathbf{x}) = \hat\psi_i(\tau)$ with $\mathbf{x} \in \mathbb{Z}\times\mathbb{Z}$ and define the Fourier transforms

$$\hat\psi(X) = \sum_Q \hat\psi(Q) e^{iQX}, \quad \hat\psi^\dagger(X) = \sum_Q \hat\psi^\dagger(Q) e^{-iQX}\,, \tag{2.8}$$

with short hand notations

$$X = (\tau, \mathbf{x}), \quad Q = (\omega_Q, \mathbf{q}), \quad QX = \omega_Q \tau + \mathbf{x}\cdot\mathbf{q}\,. \tag{2.9}$$

The fact that the Euclidian time is compactified on a torus translates into a sum over discrete Matsubara frequencies [36] in Fourier space. The Matsubara frequencies for the fermions are $\omega_Q = (2n+1)\pi T$, $n \in \mathbb{Z}$. For bosons this has to be replaced by $\Omega_Q = 2n\pi T$, $n \in \mathbb{Z}$. Accordingly, we define sums and delta distributions in position and momentum space

$$\begin{aligned} \sum_X = \int_0^\beta d\tau \sum_{\mathbf{x}}, \quad \sum_Q = T \sum_{n=-\infty}^{\infty} \int_{-\pi}^{\pi} \frac{d^2q}{(2\pi)^2}\,, \\ \delta(X - X') = \delta(\tau - \tau')\delta_{\mathbf{x},\mathbf{x}'}\,, \\ \delta(Q - Q') = \beta\delta_{n,n'}(2\pi)^2 \delta(\mathbf{q} - \mathbf{q}')\,. \end{aligned} \tag{2.10}$$

We measure all components of X and Q in units of the lattice distance a, i.e. $\mathbf{x} \to a\mathbf{x}$, $\mathbf{q} \to \mathbf{q}/a$, therefore they aquire the same canonical dimension. Here,

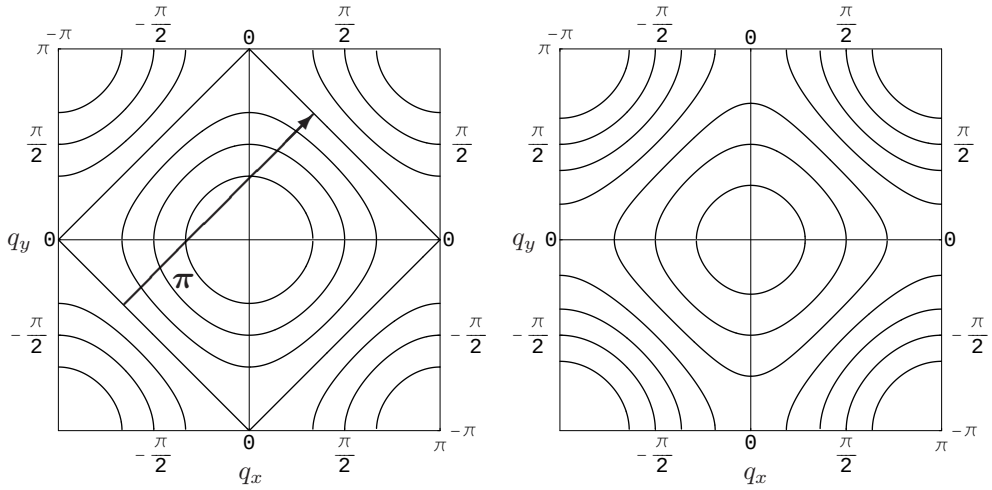

Figure 2.2: Fermi surfaces ($\epsilon_{\mathbf{q}} = \mu$) for $\mu = (-3, -2, -1, 0, 1, 2, 3)t$ from the interior to the exterior, respectively. Figure (a) corresponds to $t' = 0$, (b) to $t' = -0.1$. The vector $\boldsymbol{\pi}$ in (a) is defined by $\boldsymbol{\pi} = (\pi, \pi)$.

we set $a = 1$. Note that all functions are 2π-periodic in spatial momentum. For the fermionic action (2.5) we obtain in momentum space,

$$\begin{aligned} S_F[\hat{\psi}, \hat{\psi}^\dagger] &= \sum_Q \hat{\psi}^\dagger(Q)[i\omega_Q - \xi_Q]\hat{\psi}(Q) \\ &+ \frac{U}{2} \sum_{Q_1,Q_2,Q_3} \hat{\psi}^\dagger(Q_1)\hat{\psi}(Q_2)\hat{\psi}^\dagger(Q_3)\hat{\psi}(Q_1 - Q_2 + Q_3)\,, \end{aligned} \tag{2.11}$$

with

$$\xi_Q \equiv \xi_{\mathbf{q}} = -\mu - 2t(\cos q_x + \cos q_y) - 4t' \cos q_x \cos q_y\,, \tag{2.12}$$

The inverse fermionic propagator $P_F(Q) = i\omega_Q - \xi_{\mathbf{q}}$ has zeros at $T = 0$ on the Fermi surface defined by $\xi_{\mathbf{q}} = 0$. For the zeros of $\xi_{\mathbf{q}}$ see figure 2.2 for different values of the chemical potential μ/t and the hopping parameter t'/t. In figure 2.2 (a) it is $t' = 0$ and the quadratic Fermi surface corresponds to $\mu = 0$. This is the case where the number of states below equals the number of states above the Fermi surface, the lattice is half-filled. Electron (hole) doping corresponds to positive (negative) chemical potential in our convention. Even at finite temperature, modes with momenta in the vicinity of the Fermi surface dominate in the scattering processes. Hence, the physical properties of the system depend strongly on the topology of the Fermi surface. For instance, for a half-filled lattice, scattering processes with space-like momentum exchange of $\boldsymbol{\pi} = (0, 0)$ play an essential role. The electrons are scattered from one

side of the Fermi surface to the other side, see figure 2.2 (a). This translates into an alternating sign of the spin density between neighboring lattice sites in position space which is the same as a tendency towards antiferromagnetic order. For $t' = 0$, $\epsilon_{\mathbf{q}} = \xi_{\mathbf{q}} + \mu$ has the nesting property $\epsilon_{\mathbf{q}+\boldsymbol{\pi}} = -\epsilon_{\mathbf{q}}$, and an antiferromagnetic instability for arbitrarily small coupling $U > 0$ at half-filling is a consequence.

Symmetries

The action of the Hubbard model (2.5) is invariant under global $U(1)$ and $SU(2)$ transformations:

$$\begin{aligned} U(1) \quad &: \quad \hat{\psi}(X) \to e^{i\theta}\hat{\psi}(X), \quad \hat{\psi}^\dagger(X) \to e^{-i\theta}\hat{\psi}^\dagger(X) \\ SU(2) \quad &: \quad \hat{\psi}(X) \to e^{i\boldsymbol{\theta}\cdot\boldsymbol{\sigma}}\hat{\psi}(X), \quad \hat{\psi}^\dagger(X) \to \hat{\psi}^\dagger(X)e^{-i\boldsymbol{\theta}\cdot\boldsymbol{\sigma}}, \end{aligned} \tag{2.13}$$

with the Pauli matrices $\boldsymbol{\sigma} = (\sigma^1, \sigma^2, \sigma^3)^T$. The $U(1)$ symmetry is reflected in charge (particle number) conservation, while the $SU(2)$ symmetry corresponds to the invariance under spin rotations.

Of course, the symmetries of the lattice are also respected. On a translation invariant square lattice the action is invariant under translations, discrete rotations, and reflections.

The partition function is invariant under the following transformation together with a corresponding transformation of the sources,

$$\begin{aligned} \hat{\psi}_i(\tau) \to -\hat{\psi}_i(\beta - \tau), \quad \hat{\psi}_i^\dagger(\tau) \to -\hat{\psi}_i^\dagger(\beta - \tau), \\ t_{ij} \to -t_{ij}, \quad \mu \to -\mu\,. \end{aligned} \tag{2.14}$$

This transformation is similar to time reversal.

Certain restrictions to the lattice and the hopping matrix t_{ij} may provide additional symmetries. For instance, in a system with a restriction to nearest neighbor coupling ($t' = 0$) on a square lattice we may divide the lattice into two sub-lattices L_1, L_2. L_1 is defined by the lattice sites $i \in (2\mathbb{Z}, 2\mathbb{Z})$, L_2 by the remaining sites. t_{ij} has non vanishing entries only for i and j on different sub-lattices. Such a lattice is called bipartite lattice and the partition function here is invariant under the transformations,

$$\begin{aligned} \hat{\psi}_{i\in L_1} \to \hat{\psi}_{i\in L_1}, \quad \hat{\psi}_{i\in L_2} \to -\hat{\psi}_{i\in L_2}, \\ \hat{\psi}^\dagger_{i\in L_1} \to \hat{\psi}^\dagger_{i\in L_1}, \quad \hat{\psi}^\dagger_{i\in L_2} \to -\hat{\psi}^\dagger_{i\in L_2}, \\ t_{ij} \to -t_{ij}\,. \end{aligned} \tag{2.15}$$

The partition function on a bipartite lattice depends only on the absolute value of μ as can be seen from eq. (2.15) and the time reversal symmetry (2.14).

For vanishing μ there is an additional $SU(2)$ symmetry on a bipartite lattice which breaks down to the usual $U(1)$ symmetry (2.13) away from half filling. With regard to high temperature superconductors there is even an approximative $SO(5)$ symmetry for antiferromagnetism and superconductivity under discussion, see [38] for a review.

Supplementary, we mention the invariance under the rescaling with respect to $\alpha \in \mathbb{R}$:

$$\tau \to \tau/\alpha, \quad T \to \alpha T, \quad \mu \to \alpha\mu, \quad t \to \alpha t, \quad U \to \alpha U\,. \tag{2.16}$$

Therefore only dimensionless ratios are physical, e.g. T/t, μ/t and U/t.

2.4 Partial Bosonization

Initially, the Hubbard model is defined as a purely fermionic model (2.5) which seems to be the natural microscopic description for electrons on a lattice. However, a calculation of the partition function (2.4) involves an integration over the degrees of freedom on all length or momentum scales. The struggle comes from the fact that the four fermion coupling U of the Hubbard model develops a complicated momentum dependence and the information about the various phases and properties is encrypted in this momentum structure. Among the most promising approaches are renormalization group studies. For an introduction to this method see next chapter and references therein. The largest amount of renormalization group calculations has been performed in a purely fermionic formulation [13, 14, 15, 16, 17, 18, 19, 20]. In these approaches spontaneous symmetry breaking is reflected by the divergence of the four fermion coupling in the corresponding channel in the renormalization flow. This may limit the use of a purely fermionic formulation to the symmetric phase. However, there are also ideas concerning a continuation of the fermionic renormalization group flow into phases with broken symmetry [39]. Furthermore, there are approaches which combine functional renormalization flow with a mean field theory for the spontaneous symmetry broken phases [21, 22].

At this point the question arises, how the optimal description of the relevant degrees of freedom on all scales can be achieved within a functional renormalization group study. It is well known that also bosonic degrees of freedom, e.g. Cooper pairs, play an important role on larger length scales. On the one hand we want to accommodate the purely fermionic model on high momentum scales, on the other hand we want to study phase transitions and critical behavior. In the vicinity of the critical temperature the long range fluctuations are dominated by bosonic composite operators. The aim is to make this fact more explicit in our formulation. Particularly with regard to spontaneous

symmetry breaking a bosonized formulation, or at least a combination of a fermionic and a bosonized formulation seems to be advantageous. The divergence indicating the onset of spontaneous symmetry breaking, and limiting the use of purely fermionic formulations, is mirrored in a vanishing of a bosonic mass parameter. Also an inclusion of higher fermionic operators, which are likely to play an important role close to a phase transition, would be desirable. For this reasons, it seems to be advantageous to introduce bosonic fields mediating the interaction between the fermions via a Hubbard-Stratonovich transformation [23, 24]. This is visualized in figure 2.3 and will be formalized in the next subsection.

2.4.1 Hubbard-Stratonovich Transformation

The idea behind a Hubbard-Stratonovich transformation is to transform the purely fermionic theory into a Yukawa-type theory where the four fermion interaction is replaced by bosonic fields (e.g. $\hat{\phi}$) coupled to the fermions. For instance, a bosonization of the fermionic interaction into a Cooper channel can be written schematically as

$$\lambda_\psi^\phi(\hat{\psi}^\dagger\hat{\psi})^2 \to m_\phi^2\hat{\phi}^*\hat{\phi} - h_\phi(\hat{\phi}^*\hat{\psi}\hat{\psi} + \text{h.c.})\,. \tag{2.17}$$

Following [25, 40, 41, 42, 43], we decompose the Hubbard interaction into fermion bilinears corresponding to charge density, magnetization and Cooper pairs in different channels,

$$\begin{aligned}
\tilde{\rho}(X) &\equiv \tilde{\rho}_i = \hat{\psi}_i^\dagger\hat{\psi}_i,\\
\tilde{\mathbf{m}}(X) &\equiv \tilde{\mathbf{m}}_i = \hat{\psi}_i^\dagger\boldsymbol{\sigma}\hat{\psi}_i,\\
\tilde{s}(X) &\equiv \tilde{s}_i = \hat{\psi}_i^T\epsilon\hat{\psi}_i, \quad \tilde{s}^*(X) \equiv \tilde{s}_i^* = -\hat{\psi}_i^\dagger\epsilon\hat{\psi}_i^*\\
\tilde{c}_x(X) &\equiv \tilde{c}_{xi} = \hat{\psi}_i^T\epsilon\hat{\psi}_{i+\mathbf{e}_x}, \quad \tilde{c}_x^*(X) \equiv \tilde{c}_{xi}^* = -\hat{\psi}_{i+\mathbf{e}_x}^\dagger\epsilon\hat{\psi}_i^*\\
\tilde{c}_y(X) &\equiv \tilde{c}_{yi} = \hat{\psi}_i^T\epsilon\hat{\psi}_{i+\mathbf{e}_y}, \quad \tilde{c}_y^*(X) \equiv \tilde{c}_{yi}^* = -\hat{\psi}_{i+\mathbf{e}_y}^\dagger\epsilon\hat{\psi}_i^*\,,
\end{aligned} \tag{2.18}$$

with the Pauli matrices $\boldsymbol{\sigma} = (\sigma^1, \sigma^2, \sigma^3)^T$, the totally antisymmetric tensor $\epsilon = i\sigma^2$ and $\mathbf{e}_{x,y}$ is the unit vector in x,y direction. The interaction term in the action (2.5) can be written in different ways,

$$(\hat{\psi}_i^\dagger\hat{\psi}_i)^2 = \tilde{\rho}_i^2 = -\frac{1}{3}\tilde{\mathbf{m}}_i^2 = \frac{1}{2}\tilde{s}_i^*\tilde{s}_i\,. \tag{2.19}$$

Note the relation

$$\tilde{c}_{xi}^*\tilde{c}_{xi} - \frac{1}{2}\tilde{\rho}_i\tilde{\rho}_{i+\mathbf{e}_x} + \frac{1}{2}\tilde{\mathbf{m}}_i\cdot\tilde{\mathbf{m}}_{i+\mathbf{e}_x} = 0\,, \tag{2.20}$$

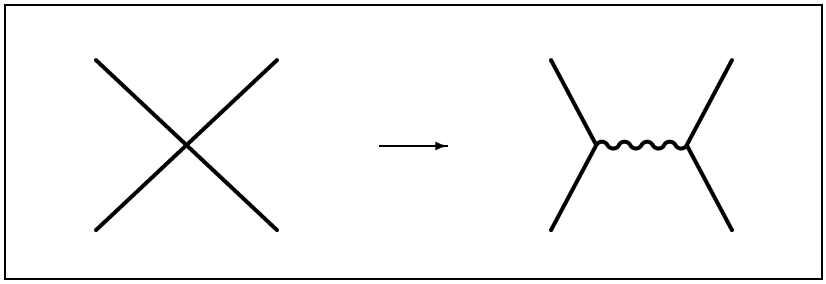

Figure 2.3: Bosonization of the four fermion interaction. Solid lines represent fermions, wiggly lines bosons.

and similar for $x \to y$.

The main idea is now to introduce a suitable 1 into the path integral representation of the partition function (2.4). According to Hubbard and Stratonovich, the 1 is represented by a Gaussian functional integral over auxiliary bosonic fields,

$$1 = \mathcal{N} \int \mathcal{D}\hat{B} e^{-S_{HS}[\hat{B}]} = \mathcal{N} \int \mathcal{D}\hat{B} e^{-S_{HS}[\hat{B}-\tilde{B}]} \,. \tag{2.21}$$

Here, we have collected all sorts of bosonic fields into a vector notation,

$$\hat{B}(X) = (\hat{\rho}, \hat{\mathbf{m}}^T, \hat{s}, \hat{s}^*, \hat{c}_x, \hat{c}_x^*, \hat{c}_y, \hat{c}_y^*)^T(X) \,, \tag{2.22}$$

and the factor $\mathcal{N}$ ensures the proper normalization. The quadratic function in the exponential of equation (2.21), referred to as $S_{HS}[\hat{B}]$, can be chosen to be

$$\begin{aligned} S_{HS}[\hat{B}] \;=\; & \sum_X \Big\{ \frac{1}{2} U_\rho \hat{\rho}_i^2 + \frac{1}{2} U_m \hat{\mathbf{m}}_i^2 + U_s \hat{s}_i^* \hat{s}_i \\ & + U_x [\hat{c}_{xi}^* \hat{c}_{xi} - \frac{1}{2} \hat{\rho}_i \hat{\rho}_{i+\mathbf{e}_x} + \frac{1}{2} \hat{\mathbf{m}}_i \cdot \hat{\mathbf{m}}_{i+\mathbf{e}_x}] + U_y [x \to y] \Big\} \,, \end{aligned} \tag{2.23}$$

with suitable coefficients U_i, $i \in \{\rho, m, s, x, y\}$. In the second equality in (2.21) the bosonic fields are shifted about the corresponding fermion bilinears defined in (2.18). In order to ensure the validity of (2.21) the couplings U_i have to fulfill the constraints

$$\begin{aligned} U_i \;&>\; 0 \,, \quad i \in \{\rho, m, s, x, y\} \,, \\ U_\rho, U_m \;&>\; U_x + U_y \,. \end{aligned} \tag{2.24}$$

The insertion of (2.21) into the fermionic partition function yields[2]

$$Z[j_B, \eta, \eta^\dagger] = \int \mathcal{D}(\hat{B}, \hat{\psi}, \hat{\psi}^\dagger) e^{-S_F[\hat{\psi},\hat{\psi}^\dagger] - S_{HS}[\hat{B}-\tilde{B}] + j_b \hat{B} + \eta^\dagger \hat{\psi} + \eta^T \hat{\psi}^*} , \qquad (2.25)$$

where we have dropped an irrelevant normalization factor. For the bosonic source term we use a short hand notation similar as in (2.4). Note, $S_{HS}[\hat{B}-\tilde{B}]$ commutes with all other terms in the exponential of (2.25).

The goal is to achieve a cancellation of the four fermion interactions in the exponential of (2.25). Therefore, we use (2.19) together with (2.20) and constrain the couplings to

$$U = 3U_m - U_\rho - 4U_s \, . \qquad (2.26)$$

Finally, the action is a sum of a kinetic part which is bilinear in the fermionic and bosonic fields, and a Yukawa part containing the couplings of the bosons to the fermions,

$$\begin{aligned} S[\hat{B}, \hat{\psi}, \hat{\psi}^\dagger] &= S_{\text{kin}}[\hat{B}, \hat{\psi}, \hat{\psi}^\dagger] + S_Y[\hat{B}, \hat{\psi}, \hat{\psi}^\dagger] \\ &\equiv S_F[\hat{\psi}, \hat{\psi}^\dagger] + S_{HS}[\hat{B} - \tilde{B}] \, . \end{aligned} \qquad (2.27)$$

We give the explicit formulae for S_{kin} and S_Y at the end of the next subsection.

Importantly, the expectation values of the fermion bilinears and the corresponding bosonic fields are equal,

$$\langle \hat{B} \rangle = \frac{\delta}{\delta j_B} \ln Z[j_B, \eta, \eta^\dagger] \Big|_{j_B=0,\eta,\eta^\dagger=0} = \langle \tilde{B} \rangle \, . \qquad (2.28)$$

The left equality follows from the definition of expectation values. The right equality can be easily seen by integrating out the bosons and applying the functional derivative with respect to the sources afterwards.

2.4.2 d-wave Operators

The motivation for introducing bosonic fields was to make the relevant degrees of freedom more accessible in the formalism. However, in the Hubbard model the Cooper pairs which we want to describe by appropriate bosonic fields are expected to be in a d-wave state. Operators which have d-wave symmetry can be constructed by performing a linear transformation of field variables, see e.g. [25, 40, 41],

$$\begin{aligned} \hat{e} &= \hat{c}_x + \hat{c}_y, \quad \hat{c}_x = \frac{1}{2}(\hat{e} + \hat{d}), \\ \hat{d} &= \hat{c}_x - \hat{c}_y, \quad \hat{c}_y = \frac{1}{2}(\hat{e} - \hat{d}) \, , \end{aligned} \qquad (2.29)$$

[2] We assume boundary conditions as in eq. (2.4) for the fermionic fields and periodic boundary conditions for the bosonic fields, $\hat{B}_i(\beta) = \hat{B}_i(0)$.

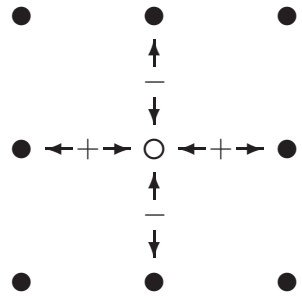

Figure 2.4: d-wave symmetry. The $\mathbf{q} = \mathbf{0}$ mode of $\tilde{d}(Q)$ at the lattice site $\circ$ visualized in its local form, see equation (2.32). Note the invariance under reflections along the axis and the change of sign under a rotation by 90°.

and similar for the complex conjugated operators.

While the Fourier transforms of the bosonic fields $\hat{\rho}$, $\hat{\mathbf{m}}$, and $\hat{s}$ ($\hat{s}^*$) are defined analogously to the fermionic case (2.8), we use for the Fourier transforms of the fields $\hat{c}_j$, $\hat{c}_j^*$ with $j = (x, y)$,

$$\hat{c}_j(X) = \sum_Q e^{iQX + iq_j/2} \hat{c}_j(Q) \quad \text{and} \quad \hat{c}_j^*(X) = \sum_Q e^{-iQX - iq_j/2} \hat{c}_j^*(Q)\,. \quad (2.30)$$

For bosonic frequencies we use $\Omega_Q = 2n\pi T$ instead of $\omega_Q = (2n+1)\pi T$ in the fermionic case ($n \in \mathbb{Z}$ both for fermions and bosons). The d-wave fermion bilinear in momentum space is correspondingly

$$\tilde{d}(Q) = \tilde{c}_x(Q) - \tilde{c}_y(Q)\,. \quad (2.31)$$

It is instructive to consider the spatially homogeneous case, the $\mathbf{q} = \mathbf{0}$ mode of $\tilde{d}(Q)$ reads

$$\begin{aligned} \tilde{d}(Q=0) &= \sum_K (\cos k_x - \cos k_y) \hat{\psi}^T(K) \epsilon \hat{\psi}(-K) \\ &= \frac{1}{2} \sum_X \big(\hat{\psi}^T(X) \epsilon \hat{\psi}(X + \mathbf{e}_x) + \hat{\psi}^T(X) \epsilon \hat{\psi}(X - \mathbf{e}_x) \\ &\qquad - \hat{\psi}^T(X) \epsilon \hat{\psi}(X + \mathbf{e}_y) - \hat{\psi}^T(X) \epsilon \hat{\psi}(X - \mathbf{e}_y) \big)\,. \end{aligned} \quad (2.32)$$

This means that each lattice site is connected by the operator $\tilde{d}(Q=0)$ to the adjacent neighbors on the x-axis with a plus sign and to the adjacent neighbors in the y-axis with a minus sign (see the illustration in figure 2.4). Such an operator indeed presents a $d_{x^2-y^2}$-wave as it changes its sign under rotation by 90° and is invariant under reflection along the axes. For a more extensive discussion, see e.g. [5].

Finally, we want to make the d-wave symmetry explicit in the Hubbard-Stratonovich transformed action (2.27). Therefor, it remains to replace the $\hat{c}_x$- and $\hat{c}_y$- fields by the $\hat{d}$- and $\hat{e}$-fields. This can be easily achieved by insertion of the transformation of variables (2.29). Furthermore, we set $U_x = U_y = U_c$ and modify our vector notation for the bosonic fields in a self-evident way,

$$\hat{B}(X) = (\hat{\rho}, \hat{\mathbf{m}}^T, \hat{s}, \hat{s}^*, \hat{d}, \hat{d}^*, \hat{e}, \hat{e}^*)^T(X)\,. \tag{2.33}$$

The quadratic part of the finally obtained action, also referred to as the kinetic part, reads in momentum space

$$\begin{aligned} S_{\mathrm{kin}}[\hat{B}, \hat{\psi}, \hat{\psi}^\dagger] = \sum_Q \Big\{ & \hat{\psi}^*(Q)[i\omega_Q + \xi_Q]\hat{\psi}(Q) \\ & + \frac{1}{2}\big(U_\rho - U_c(\cos q_x + \cos q_y)\big)\hat{\rho}(Q)\hat{\rho}(-Q) \\ & + \frac{1}{2}\big(U_m + U_c(\cos q_x + \cos q_y)\big)\hat{\mathbf{m}}(Q)\cdot\hat{\mathbf{m}}(-Q) \\ & + \frac{1}{2}U_c\{\hat{e}^*(Q)\hat{e}(Q) + \hat{d}^*(Q)\hat{d}(Q)\} + U_s\hat{s}^*(Q)\hat{s}(Q)\Big\}\,. \end{aligned} \tag{2.34}$$

Besides the kinetic part of the fermionic action (2.11) there are also quadratic parts of the introduced bosonic fields. The part of the action which contains the couplings of the bosons to the corresponding fermion bilinears, referred to as Yukawa-terms, looks like

$$\begin{aligned} S_Y[\hat{B}, \hat{\psi}, \hat{\psi}^\dagger] = \sum_{K,Q,Q'} \Big[& \delta(K - Q + Q') \times \\ & \Big\{\big(U_\rho - U_c(\cos k_x + \cos k_y)\big)\hat{\rho}(K)\hat{\psi}^\dagger(Q)\hat{\psi}(Q') \\ & + \big(U_m + U_c(\cos k_x + \cos k_y)\big)\hat{\mathbf{m}}(K)\cdot\hat{\psi}^\dagger(Q)\boldsymbol{\sigma}\hat{\psi}(Q')\Big\} \\ & + \delta(K - Q - Q') \times \\ & \Big\{U_s[\hat{s}^*(K)\hat{\psi}^T(Q)\epsilon\hat{\psi}(Q') - \hat{s}(K)\hat{\psi}^\dagger(Q)\epsilon\hat{\psi}^*(Q')] \\ & + \frac{U_c}{2}\big(\cos(\frac{q_x - q'_x}{2}) + \cos(\frac{q_y - q'_y}{2})\big) \\ & \times[\hat{e}^*(K)\hat{\psi}^T(Q)\epsilon\hat{\psi}(Q') - \hat{e}(K)\hat{\psi}^\dagger(Q)\epsilon\hat{\psi}^*(Q')] \\ & + \frac{U_c}{2}\big(\cos(\frac{q_x - q'_x}{2}) - \cos(\frac{q_y - q'_y}{2})\big) \\ & \times[\hat{d}^*(K)\hat{\psi}^T(Q)\epsilon\hat{\psi}(Q') - \hat{d}(K)\hat{\psi}^\dagger(Q)\epsilon\hat{\psi}^*(Q')]\Big\}\Big]\,. \end{aligned} \tag{2.35}$$

The restrictions and relation to the coupling in the Hubbard model U of the

couplings U_i , $i \in \{\rho, m, s, c\}$ are in summary,

$$\begin{aligned} U_i &> 0\,, \quad i \in \{\rho, m, s, c\}\,, \\ U_\rho, U_m &> 2U_c\,, \\ U &= 3U_m - U_\rho - 4U_s\,. \end{aligned} \tag{2.36}$$

Obviously, the values of the couplings U_i , $i \in \{\rho, m, s, c\}$ are not determined uniquely by the relations (2.36). The origin of this ambiguity is the possibility of a Fierz reordering of the local four fermion interaction. This ambiguity is unphysical and physical quantities should not depend on the particular choice of the couplings U_i. However, since we are forced to make approximations, results such as critical temperatures may depend on our specific choice. For instance, in [44] it is shown that in a mean field approximation the dependence on unphysical parameters which describe the choice of the mean field is strong. An inclusion of bosonic fluctuation beyond mean field theory (MFT) may drastically reduce this Fierz-ambiguity, see [25, 40].

Chapter 3

Functional Renormalization Group Equations

In this chapter we develop the main part of the formalism used in this thesis. Starting point is a functional integral formulation of Quantum Field Theory (QFT). In the first section, we provide some basics of QFT and clarify our notation. For a more detailed reading of standard QFT see, e.g., [45, 46, 47]. The following section is devoted to an introduction of the effective average action Γ_k and the derivation of an exact flow equation for Γ_k [10]. This flow equation is the central result of this chapter and starting point of all further investigations. It describes the evolution of the effective action under the influence of fluctuations with increasing length or decreasing momentum scales. In terms of correlation functions this means that the microscopic correlation functions are exactly connected with the desired full correlation functions by the flow equation which describes a continuous process of integrating out fluctuations. Hence, solving the flow equation is equivalent to solving the full theory. Importantly, this concept applies both for quantum and statistical field theories [48]. A rigorous introduction to the functional renormalization group is given in [49, 50]. The applicability to Fermi systems is emphasized in [51, 52, 53, 54].

Scale-dependent field transformations and the corresponding modifications of the flow equation are introduced in the last section of this chapter. This topic plays an important role for a proper bosonization of the theory on all scales.

3.1 Functional Integral Formulation of QFT

In Quantum Field Theory the objects which are most directly related to the physical information are the correlation functions. For a moment, we consider only the case of real scalar fields. In Euclidean QFT all field configurations

are weighted with an exponential of the action $S[\varphi]$,

$$\langle\hat{\varphi}(x_1)\cdots\hat{\varphi}(x_n)\rangle = \mathcal{N}\int_\Lambda \mathcal{D}\hat{\varphi}\hat{\varphi}(x_1)\cdots\hat{\varphi}(x_n)e^{-S[\hat{\varphi}]}\,, \tag{3.1}$$

with the normalization factor

$$\mathcal{N}^{-1} = \int_\Lambda \mathcal{D}\hat{\varphi}e^{-S[\hat{\varphi}]}\,, \tag{3.2}$$

ensuring that $\langle 1\rangle = 1$. We assume a proper regularized measure denoted by the ultraviolet cutoff (UV) Λ, which should also preserve all symmetries of the theory. For instance, the inverse lattice distance may provide a natural UV cutoff scale Λ. It is convenient to introduce the generating functional

$$Z[J] = \int_\Lambda \mathcal{D}\hat{\varphi}e^{-S[\hat{\varphi}]+\int J\hat{\varphi}}\,, \tag{3.3}$$

where $\int J\hat{\varphi} = \int d^Dx J(x)\hat{\varphi}(x)$. All n-point correlators are obtained by functional derivatives of $Z[J]$ with respect to the sources J:

$$\langle\hat{\varphi}(x_1)\cdots\hat{\varphi}(x_n)\rangle = \frac{1}{Z[0]}\frac{\delta^n Z[J]}{\delta J(x_1)\cdots\delta J(x_n)}\bigg|_{J=0}\,. \tag{3.4}$$

The generalization to more general (Nambu-)fields is merely a question of notation. We combine different types of fields into a vector notation

$$\begin{aligned}\hat{\chi}(X) &= (\hat{\mathbf{a}}^T,\hat{d},\hat{d}^*,\hat{\psi}^T,\hat{\psi}^{*T})^T(X)\,,\\ J(X) &= (\mathbf{j}^{\mathbf{a}T},j^{d^*},j^d,\eta^{*T},\eta^T)^T(X)\,.\end{aligned} \tag{3.5}$$

Appropriate to our applications we have introduced a vector field with $O(3)$ symmetry and a complex field, denoted by $\hat{\mathbf{a}}$ and $(\hat{d},\hat{d}^*)$, respectively. Hereby, the generating functional $Z[J]$ is

$$Z[J] \equiv e^{W[J]} = \int_\Lambda \mathcal{D}\hat{\chi}e^{-S[\hat{\chi}]+J\cdot\hat{\chi}}\,, \tag{3.6}$$

with short hand notation $J\cdot\hat{\chi} = \int_X J(X)\cdot\hat{\chi}(X)$. We also have introduced the functional $W[J] = \ln Z[J]$, which generates the *connected correlators*. The *classical fields* are now defined as the expectation values of the corresponding quantum fields

$$\chi := \langle\hat{\chi}\rangle = \frac{1}{Z[0]}\frac{\delta Z[J]}{\delta J}\bigg|_{J=0} = \frac{\delta W[J]}{\delta J}\bigg|_{J=0}\,. \tag{3.7}$$

The *effective action* is defined as the Legendre transform of $W[J]$ with respect to the classical fields χ

$$\Gamma[\chi] = \sup_J (J \cdot \chi - W[J]) \,. \tag{3.8}$$

The source J depends on the field χ, such that $J \cdot \chi - W[J]$ approaches its supremum at $J_{sup} = J[\chi]$. This definition guarantees the convexity of Γ. In addition, we get with $J = J_{sup}$

$$0 = \frac{\delta}{\delta J(X)}(J \cdot \chi - W[J]) \quad \Longrightarrow \quad \chi = \frac{\delta W[J]}{\delta J} = \langle \hat{\chi} \rangle_J \,, \tag{3.9}$$

which shows, that χ is the expectation value of $\hat{\chi}$ in presence of the source J. The *quantum equation of motion*, which takes all quantum fluctuations into account, is obtained by derivation with respect to χ at $J = J_{sup}$

$$\begin{aligned} \frac{\delta \Gamma[\chi]}{\delta \chi_i(X)} &= \frac{\delta J_j(Y)}{\delta \chi_i(X)} \chi_j(Y) + M_{ij} J_j(X) - \frac{\delta J_j(Y)}{\delta \chi_i(X)} \frac{\delta W[J]}{\delta J_j(Y)} \\ &= M_{ij} J_j(X) = J_j(X) M_{ji} \,, \end{aligned} \tag{3.10}$$

where summation (integration) over repeated indices is understood. Furthermore, it is

$$M = M^T = \mathrm{diag}(\mathbf{1}_{3\times 3}, 1, 1, -\mathbf{1}_{2\times 2}, -\mathbf{1}_{2\times 2}) \,. \tag{3.11}$$

For later convenience, note the identity

$$\frac{\delta W[J]}{\delta J_i(X)} \frac{\overleftarrow{\delta}}{\delta J_l(Z)} \left(\frac{\delta \Gamma[\chi]}{\delta \chi_l(Z)} \frac{\overleftarrow{\delta}}{\delta \chi_j(Y)} \right) \equiv W^{(2)}_{iX,lZ} \Gamma^{(2)}_{lZ,jY} = M_{ij} \delta(X - Y) \,. \tag{3.12}$$

A useful, more implicit equation for the effective action can be derived from the generating functional,

$$e^{-\Gamma[\chi]} = \int_\Lambda \mathcal{D}\hat{\chi} \exp\big(- S[\chi + \hat{\chi}] + M \frac{\delta \Gamma[\chi]}{\delta \chi} \cdot \hat{\chi} \big) \,. \tag{3.13}$$

Note that we have performed a shift of the integration variable, $\hat{\chi} \to \chi + \hat{\chi}$. Since the effective action is the generating functional of the *one-particle irreducible (1-PI) proper vertices* it is appropriate to expand $\Gamma[\chi]$ into monomials of fields, where the coefficients of this *vertex expansion* are the 1-PI vertices $\Gamma^{(n)}$:

$$\Gamma[\chi] = \sum_{n=0}^{\infty} \frac{1}{n!} \sum_{X_1,\ldots,X_n} \Gamma^{(n)}_{i_1,\ldots,i_n}(X_1,\ldots,X_n) \chi_{i_1}(X_1) \cdots \chi_{i_n}(X_n) \,. \tag{3.14}$$

The insertion of equation (3.14) into equation (3.13) yields an infinite tower of coupled integro-differential equations for the $\Gamma^{(n)}$, the *Dyson-Schwinger equations*. This method can be used to construct approximative solutions to the theory by using a finite truncation of this series. Here, we do not proceed into this direction. We use functional renormalization group techniques as discussed in the next sections.

3.2 Flow Equation for the Effective Average Action

A powerful tool to construct approximative solutions in non-perturbative contexts in QFT are renormalization group methods [9, 12, 10]. The basic idea is to use Wilson's idea [11] of integrating out fluctuations momentum shell by momentum shell, instead of integrating out all fluctuations at once.

Our renormalization group approach [10, 48] is based on functional integral techniques developed in the last section. More concretely, we employ the concept of the *effective average action* Γ_k, where k is a momentum parameter. Γ_k interpolates between the bare action S_Λ, for $k \to \Lambda$ and the full quantum effective action Γ, for $k \to 0$:

$$\lim_{k\to\Lambda} \Gamma_k \simeq S_\Lambda \,, \quad \lim_{k\to 0} \Gamma_k = \Gamma \,. \tag{3.15}$$

The main idea is to pose this interpolation procedure as initial value problem and derive an exact flow equation for Γ_k. How this can be achieved is demonstrated in the following lines. Firstly, we introduce the scale parameter k by a scale dependent infrared (IR) regulator term in the classical action[1],

$$S[\hat{\chi}] \to S_k[\hat{\chi}] = S[\hat{\chi}] + \Delta S_k[\hat{\chi}] \,, \tag{3.16}$$

where the regulator part is quadratic in the fields and can be viewed as scale and momentum dependent mass term. It reads in momentum space,

$$\Delta S_k[\hat{\chi}] = \frac{1}{2} \int_Q \hat{\chi}^T(Q) R_k(Q) \hat{\chi}(Q) \,, \tag{3.17}$$

and has to satisfy several criteria. In order to implement an IR regularization, it should hold

$$\lim_{Q^2/k^2\to 0} R_k(Q) > 0 \,. \tag{3.18}$$

[1] Choosing the regulator term quadratic in the fields yields the one-loop structure of the flow equation (3.24).

For instance, if $R_k \sim k^2$ for $Q^2 \ll k^2$, the IR modes are endued with a mass term $m^2 \sim k^2$. Secondly, the condition

$$\lim_{k^2/Q^2 \to 0} R_k(Q) = 0\,, \tag{3.19}$$

ensures that the regulator vanishes for $k \to 0$, as it is necessary to obtain the standard effective action in this limit, $\lim_{k\to 0} \Gamma_k = \Gamma_k$. The third condition is

$$R_k(Q) \to \infty \quad \text{for} \quad k^2 \to \Lambda \to \infty\,, \tag{3.20}$$

in order to recover $\Gamma_{k\to\Lambda} = S_\Lambda + \text{const.}$. More precisely, this condition leads to the dominance of the stationary point in the functional integral.

However, equation (3.16) introduces a scale dependence on the generating functional,

$$W_k[J] = \ln Z_k[J] = \ln \int \mathcal{D}\hat{\chi} \exp(-S_k[\hat{\chi}] + J \cdot \hat{\chi})\,. \tag{3.21}$$

Keeping the sources J scale independent, the derivative with respect to k yields

$$\begin{aligned}
\partial_k W_k[J] &= -\frac{1}{2Z_k[J]} \int_Q \int \mathcal{D}\hat{\chi} (\partial_k R_{k,ij}(Q)) \hat{\chi}_i(Q) \hat{\chi}_j(Q) \exp(-S_k[\hat{\chi}] + J \cdot \hat{\chi}) \\
&= -\frac{1}{2} \int_Q (\partial_k R_{k,ij}(Q)) \langle \hat{\chi}_i(Q) \hat{\chi}_j(Q) \rangle_J \\
&= -\frac{1}{2} \int_Q (\partial_k R_{k,ij}(Q)) \{ \langle \hat{\chi}_i(Q) \hat{\chi}_j(Q) \rangle_{c,J} + \langle \hat{\chi}_i(Q) \rangle_J \langle \hat{\chi}_j(Q) \rangle_J \} \\
&= -\frac{1}{2} \int_Q (\partial_k R_{k,ij}(Q)) W^{(2)}_{k,ji}(Q) - \partial_k \Delta S_k[\chi]\,,
\end{aligned} \tag{3.22}$$

where $\langle \cdots \rangle_c$ stands for connected correlators, generated by $W[J]$ itself.

In the definition of the effective average action Γ_k we use a slightly modified Legendre transform[2],

$$\Gamma_k[\chi] = \sup_J (J \cdot \chi - W_k[J]) - \Delta S_k[\chi]\,. \tag{3.23}$$

The subtraction of the IR cutoff term is crucial in order to fulfill $\lim_{k\to\Lambda} \Gamma_k \simeq S_\Lambda$. Finally, we have all ingredients and can derive a flow equation for Γ_k for

[2]Convexity of Γ_k is restored in the limit $k \to 0$.

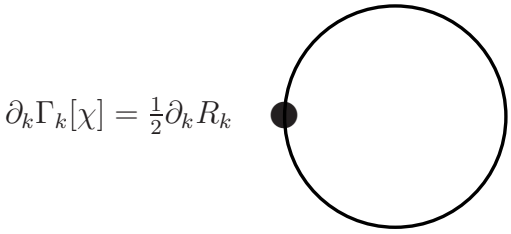

Figure 3.1: Diagrammatic representation of the flow equation (3.24). The rhs has one-loop structure and involves the full scale dependent propagator $[\Gamma_k^{(2)}[\chi] + R_k]^{-1}$ (solid line) and the insertion of $\partial_k R_k$ (filled circle).

fixed χ at $J = J_{sup}$:

$$\begin{aligned}
\partial_k \Gamma_k[\chi] &= \partial_k J \cdot \chi - \partial_k W[J]|_\chi - \partial_k \Delta S_k[\chi] \\
&= -\partial_k W[J]|_J - \partial_k \Delta S_k[\chi] \\
&= \frac{1}{2}\int_Q (\partial_k R_{k,ij}(Q)) W^{(2)}_{k,ji}(Q) \\
&= \frac{1}{2}\int_Q (\partial_k R_{k,ij}(Q)) M_{jl}[\Gamma_k^{(2)}[\chi] + R_k]^{-1}_{li}(Q) \\
&= \frac{1}{2}\mathrm{STr}\{(\partial_k R_k)[\Gamma_k^{(2)}[\chi] + R_k]^{-1}\}\,. \qquad (3.24)
\end{aligned}$$

From the second to the third line, we have used equation (3.22) and in the following step equation (3.12) in momentum space. The "supertrace" STr introduced in the last line runs over field type, momentum and internal indices, and has an additional minus sign for fermionic entries. The flow equation (3.24) is the central result of this chapter and the methodical starting point of all further investigations.

3.3 Scale-Dependent Field Transformations

The flow equation for the effective average action (3.24) derived in the last section applies for scale independent fields χ. As demonstrated in [55], it is sometimes advantageous to consider scale dependent bosonic fields. An important application arises in the situation described in the following lines. The idea of partial bosonization is to transform certain channels of a fermionic two-particle operator $\lambda_\psi^\phi(\psi^\dagger\psi)^2$ into a Yukawa interaction $h_\phi \phi \psi^\dagger \psi$, where an appropriate bosonic field ϕ mediates the interaction between the fermions. This can be achieved by a Hubbard-Stratonovich transformation on a fixed momentum scale, e.g. Λ. On this scale Λ, the purely fermionic interaction in the "ϕ-channel", denoted by the coupling λ_ψ^ϕ, is completely transformed into

the Yukawa interaction. However, at lower momentum scales $\Lambda - \delta k$ a coupling $\Delta\lambda_\psi^\phi$ in this channel reappears due to the box diagrams, see figure 4.5, and other diagrams containing the remaining fermionic couplings of other channels. In truncations we use here, we take only the fermionic channels into account, which are most relevant and expected to develop instabilities in appropriate parameter regions. These fermionic interactions are bosonized on the UV scale Λ. Their reappearance during RG transformations to lower scales would degrade the use of the concept of bosonization. Scale dependent bosonic fields are introduced to *rebosonize* the newly generated purely fermionic couplings on all scales. This is discussed later in more detail.

The task is now to derive a modified flow equation for the effective average action taking scale-dependent field transformations into account. Here, we follow [55, 49, 56]. Firstly, we introduce a modified generating functional

$$Z_k[J] = e^{W_k[J]} = \int \mathcal{D}\hat{\chi} \exp\Big(- S[\hat{\chi}] - \frac{1}{2}\int \hat{\chi}_k^T R_k \hat{\chi}_k + J\cdot\hat{\chi}_k\Big)\,, \qquad (3.25)$$

where we have coupled scale-dependent bosonic fields to the source and the regulator, $\hat{\chi}_k = (\hat{\mathbf{a}}_k^T, \hat{d}_k, \hat{d}_k^*, \hat{\psi}, \hat{\psi}^*)^T$. The expectation values are defined in a standard way,

$$\chi_k = \langle\hat{\chi}_k\rangle = \frac{\delta W_k[J]}{\delta J}\,. \qquad (3.26)$$

The scale derivative of the functional $W_k[J]$ is

$$\begin{aligned}
\partial_k W_k[J] \;&=\; \frac{1}{Z_k[J]}\int \mathcal{D}\hat{\chi}\Big(- \frac{1}{2}\int \hat{\chi}_k^T(\partial_k R_k)\hat{\chi}_k - \int \hat{\chi}_k^T R_k \partial_k\hat{\chi}_k + J\cdot\partial_k\hat{\chi}_k\Big) \\
&\qquad\qquad \times\exp\big(- S[\hat{\chi}] - \Delta S_k[\hat{\chi}_k] + J\cdot\hat{\chi}_k\big) \\
&=\; -\frac{1}{2}\int (\partial_k R_{k,ij}) W^{(2)}_{k,ji} - \frac{1}{2}\int (\partial_k R_{k,ij})\chi_{k,i}\chi_{k,j} \\
&\quad +\big(J - \chi_k^T R_k\big)\cdot\langle\partial_k\hat{\chi}_k\rangle - \int \frac{\delta}{\delta J_i} R_{k,ij}\langle\partial_k\hat{\chi}_{k,j}\rangle\,, \qquad (3.27)
\end{aligned}$$

where we have used the relation $\langle\hat{\chi}_{k,i}\partial_k\hat{\chi}_{k,j}\rangle = \big(\frac{\delta}{\delta J_i} + \chi_{k,i}\big)\langle\partial_k\hat{\chi}_{k,j}\rangle$. Correspondingly, the effective average action reads,

$$\Gamma_k[\chi_k] = \sup_J(J\cdot\chi_k - W_k[J]) - \frac{1}{2}\int \chi_k^T R_k\chi_k\,. \qquad (3.28)$$

We perform the scale derivative as usual at $J = J_{sup} = J[\chi_k]$ and obtain,

$$\begin{aligned}\partial_k\Gamma_k[\chi_k] &= \frac{1}{2}\int(\partial_k R_{k,ij})W^{(2)}_{k,ji} + \int\frac{\delta}{\delta J_i}R_{k,ij}\langle\partial_k\hat{\chi}_{k,j}\rangle \\ &\quad +(J-\chi_k^T R_k)\cdot(\partial_k\chi_k - \langle\partial_k\hat{\chi}_k\rangle) \\ &= \frac{1}{2}\int(\partial_k R_{k,ij})W^{(2)}_{k,ji} + \int W^{(2)}_{k,il}\frac{\delta}{\delta\chi_{k,l}}R_{k,ij}\langle\partial_k\hat{\chi}_{k,j}\rangle \\ &\quad +(J-\chi_k^T R_k)\cdot(\partial_k\chi_k - \langle\partial_k\hat{\chi}_k\rangle)\,. \end{aligned} \tag{3.29}$$

One can work out $\langle\partial_k\hat{\chi}_k\rangle$ for a given scale-dependent field transformation $\partial_k\hat{\chi}_k$, which is a functional of all fields. In general, it is $\langle\partial_k\hat{\chi}_k\rangle \neq \partial_k\chi_k = \partial_k\langle\hat{\chi}_k\rangle$. However, we use the flow equation together with an truncation of Γ_k. We assume that at least on the level of a truncation the condition,

$$\langle\partial_k\hat{\chi}_k\rangle \stackrel{!}{=} \partial_k\chi_k\,, \tag{3.30}$$

can be satisfied. In this case, the last term in equation (3.29) cancels and we obtain

$$\begin{aligned}\partial_k\Gamma_k[\chi_k]\big|_{\chi_k} &= \partial_k\Gamma_k[\chi_k] - \int(\partial_k\chi_{k,i})\frac{\delta\Gamma_k[\chi_k]}{\delta\chi_{k,i}} \\ &= \frac{1}{2}\mathrm{STr}\{[\Gamma^{(2)}_k[\chi_k]+R_k]^{-1}\partial_k R_k\} + \int W^{(2)}_{k,il}\frac{\delta}{\delta\chi_{k,l}}R_{k,ij}\partial_k\chi_{k,j} \\ &\quad -\int(\partial_k\chi_{k,i})\frac{\delta\Gamma_k[\chi_k]}{\delta\chi_{k,i}}\,. \end{aligned} \tag{3.31}$$

The first term on the rhs is the standard term (3.24). The third term is the desired one which we use, for instance, to ensure $\partial_k\lambda^{\phi}_{\psi} \stackrel{!}{=} 0$ during the flow. The second contribution comes from the renormalization flow of the operator insertion $\partial_k\hat{\chi}_k$ in the functional integral [49]. This term is of higher order in the couplings and expected to be subdominant for not too large couplings. Finally, we obtain

$$\begin{aligned}\partial_k\Gamma_k[\chi_k]\big|_{\chi_k} &= \partial_k\Gamma_k[\chi_k] - \int(\partial_k\chi_{k,i})\frac{\delta\Gamma_k[\chi_k]}{\delta\chi_{k,i}} \\ &= \partial_k\Gamma_k[\chi_k] - \int\frac{\delta\Gamma_k[\chi_k]}{\delta a_{k,i}}\partial_k a_{k,i} \\ &\quad -\int\frac{\delta\Gamma_k[\chi_k]}{\delta d_k}\partial_k d_k - \int\frac{\delta\Gamma_k[\chi_k]}{\delta d_k^*}\partial_k d_k^*\,, \end{aligned} \tag{3.32}$$

where we have used $\chi_k = (\mathbf{a}_k^T, d_k, d_k^*, \psi, \psi^*)^T$. This equation is our starting point for the construction of the "perfect bosons" [55] on all scales.

Chapter 4

Competition of Antiferromagnetism and d-wave Superconductivity

In this chapter we discuss the two-dimensional Hubbard model with focus on antiferromagnetism and d-wave superconductivity as well as their mutual influence. A truncation for the effective average action is motivated which is reasonable for a study of the symmetric phase over a wide range of chemical potential. We restrict our truncation to the antiferromagnetic and the d-wave pairing channel since close to half-filling antiferromagnetic fluctuations dominate and the ground state is antiferromagnetically ordered. At moderate doping away from half-filling the system is expected to become a d-wave superconductor driven by antiferromagnetic fluctuations [5].

The main point of this chapter is the calculation of the so called "pseudo-critical" temperature T_{pc}. This temperature T_{pc} is by definition the highest temperature for which the interaction strength of the electrons diverges in the renormalization flow. In our language, this divergence of the fermionic coupling in a certain channel on a scale k_{SSB} is translated into a vanishing of the bosonic mass of the corresponding boson. The scale k_{SSB} indicates the onset of local ordering. The true critical temperature associated with a phase transition is below the pseudo-critical temperature. In chapter 5 a possible scenario for the phase transition to d-wave superconductivity is discussed within a simplified truncation. For the symmetry broken regime associated with antiferromagnetism, we refer to [25, 40].

In section 4.1 we present our truncation of the effective average action. It is formulated as a Yukawa-like theory where the fermions couple to two species of bosonic fields, the **a**-field and the d-field. The bosonic fields describe composite fermion bilinears. On the initial scale the effective average action Γ_k has to equal the microscopic action. Spontaneous symmetry breaking with respect to the **a**-field corresponds to antiferromagnetism and with respect to the d-field to superconductivity with d-wave symmetry. The regularization scheme

is introduced in section 4.2 where we discuss the regulator functions for the fermions and both bosonic fields.

A way to calculate 1-PI vertex functions to one-loop order is introduced in section 4.3. On the one hand very similar calculations have to be performed in order to derive the flow equations for the couplings. On the other hand one-loop perturbation theory to the vertex functions may be helpful in the task of finding a reliable truncation, e.g. for the momentum dependences of the vertex functions. The last point applies particularly with regard to the dependence of the inverse bosonic propagators on frequency and space-like momenta. A study of the kinetic term of the **a**-boson indicates a dominance of incommensurate antiferromagnetic fluctuations sufficiently away from half-filling rather than commensurate fluctuations which dominate at half-filling, see section 4.3.1. This directly affects the parameterization of the kinetic term of the **a**-field.

Initially, the local fermionic coupling is bosonized and we want to achieve a completely bosonized theory on all scales. However, during the renormalization flow there appear new four fermion couplings in different channels. The treatment of these newly generated couplings turns out to be crucial. We derive the responsible contributions within our truncation in section 4.3 and discuss their treatment in section 4.4. In particular the generation of a fermionic coupling in the d-wave channel triggered by antiferromagnetic fluctuations is based on rebosonization, see section 4.6. The flow equations of the couplings are derived in section 4.5. Numerical results are presented and discussed in section 4.7.

4.1 Truncation of the Effective Action

On high momentum scale the microscopic action sets the initial condition for the flow equation (3.24), or more precisely the modified flow equation (3.32). However, in the renormalization flow the effective action picks up all possible couplings which are allowed by symmetry. In order to make progress we have to truncate this set of infinitely many couplings to a finite number of couplings. The result is an Ansatz for the scale dependent action Γ_k. In summary, we consider a fermionic kinetic term $\Gamma_{F,k}$, Yukawa-like interaction terms $\Gamma^Y_{a,k}$ and $\Gamma^Y_{d,k}$ coupling the fermions to the two types of bosonic fields, and purely bosonic terms. For the fermionic quadratic part we carry the classical term forward,

$$\Gamma_{F,k} = \sum_Q \psi^\dagger(Q) P_F(Q) \psi(Q)\,, \tag{4.1}$$

with the inverse fermionic propagator

$$P_F(Q) = i\omega_Q + \xi_Q\,, \tag{4.2}$$

where

$$\omega_Q = (2n+1)\pi T\,, \quad \xi_Q = -\mu - 2t(\cos q_1 + \cos q_2) - 4t' \cos q_1 \cos q_2\,, \quad (4.3)$$

where $n \in \mathbb{Z}$. In the approximation made in this thesis, the fermion propagator is not renormalized.

In order to describe antiferromagnetic behavior we do not directly use the field $\boldsymbol{m}$ introduced via partial bosonization (2.33). It is preferable to impose a shift in the momentum variables and define

$$\mathbf{a}(Q) = \mathbf{m}(Q + \Pi)\,, \quad (4.4)$$

with $\Pi = (0, \boldsymbol{\pi} = (\pi, \pi))$. The zero mode of this field $\boldsymbol{a}(0)$ corresponds to a homogeneous antiferromagnetic spin density. See also figure 2.2 (a) and the discussion in section 2.3. One loop corrections to the inverse bosonic propagator confirm this choice, see section 4.3.1.

The Yukawa-like interaction term which couples the bosonic field to the magnetization fermion bilinear defined in (2.18) reads in terms of the **a**-field

$$\Gamma^Y_{a,k} = -\sum_{K,Q,Q'} \delta(K + \Pi - Q + Q')\bar{h}_a(K)\mathbf{a}(K) \cdot [\psi^\dagger(Q)\boldsymbol{\sigma}\psi(Q')]\,. \quad (4.5)$$

Note the Π-shift in the momentum conservation as appropriate for antiferromagnetism. The Yukawa coupling $\bar{h}_a$ depends on the scale. For the purely bosonic term we introduce a kinetic term[1] plus a local effective potential

$$\Gamma_{a,k} = \frac{1}{2}\sum_Q \mathbf{a}^T(-Q)P_a(Q)\mathbf{a}(Q) + \sum_X U_a[\mathbf{a}]\,. \quad (4.6)$$

Due to $SU(2)$ symmetry the effective potential can only depend on the rotation invariant combination

$$\alpha(K, K') = \frac{1}{2}\mathbf{a}(K) \cdot \mathbf{a}(K')\,. \quad (4.7)$$

Furthermore, we expand the effective potential in powers of the bosonic **a**-field

[1] By "kinetic term" we mean $\Gamma^{(2)}|_{\chi=0} - \Gamma^{(2)}|_{\chi=0,Q=0}$ which incorporates, according to field theoretical language, the frequency and momentum dependent part of $\Gamma^{(2)}$.

up to eighth order

$$\begin{aligned}\sum_X U_a[\mathbf{a}] = &\sum_K \bar{m}_a^2 \alpha(-K,K) \\ &+\frac{1}{2}\sum_{K_1,\cdots,K_4} \bar{\lambda}_a \delta(K_1+K_2+K_3+K_4)\alpha(K_1,K_2)\alpha(K_3,K_4) \\ &+\frac{1}{3!}\sum_{K_1,\cdots,K_6} \bar{\gamma}_a \delta(K_1+\cdots+K_6)\alpha(K_1,K_2)\alpha(K_3,K_4)\alpha(K_5,K_6) \\ &+\frac{1}{4!}\sum_{K_1,\cdots,K_8} \bar{\zeta}_a \delta(K_1+\cdots+K_8)\alpha(K_1,K_2)\alpha(K_3,K_4) \\ &\qquad\qquad \times\alpha(K_5,K_6)\alpha(K_7,K_8)\,, \end{aligned} \tag{4.8}$$

in the symmetric phase (SYM), since a study of possible discontinuous transitions into the symmetry broken regime needs a truncation beyond quartic order in the bosonic fields. We have restricted our calculations to the symmetric phase in this chapter. The parameters $\bar{m}_a^2$, $\bar{\lambda}_a$, $\bar{\gamma}_a$ and $\bar{\zeta}_a$ depend on scale and are evaluated at vanishing external momenta. Moreover, in the symmetry broken phase an expansion around the minima of the effective potential is much more suitable. Here, we show a simple truncation for the bosonic potential in the symmetry broken phase,

$$\begin{aligned}\sum_X U_a[\mathbf{a}] = &\frac{1}{2}\sum_{K_1,\cdots,K_4} \bar{\lambda}_a \delta(K_1+K_2+K_3+K_4) \\ &\times\big(\alpha(K_1,K_2)-\alpha_0\delta(K_1)\delta(K_2)\big)\big(\alpha(K_3,K_4)-\alpha_0\delta(K_3)\delta(K_4)\big), \end{aligned} \tag{4.9}$$

where we have expanded up to quartic order in the bosonic fields.

On the microscopic scale the bosonic kinetic term vanishes as well as the couplings $\bar{\lambda}_a$, $\bar{\gamma}_a$ and $\bar{\zeta}_a$. The inverse bosonic propagator is simply the scale dependent mass term $\bar{m}_a^2$. However, on lower momentum scales a nontrivial kinetic term is generated and the boson becomes dynamic. We parameterize the momentum and frequency dependence by

$$P_a(Q=(\Omega_Q,\mathbf{q})) = Z_a\Omega_Q^2 + P_a(\Omega_Q=0,[\mathbf{q}])\,, \tag{4.10}$$

where $[\mathbf{q}]$ is defined as $[\mathbf{q}]=(q_x,q_y)$ for $q_x,q_y\in[-\pi,\pi]$ and continued periodically otherwise. Close to half filling where antiferromagnetic fluctuations dominate a reasonable choice of $P_a(\Omega_Q=0,[\mathbf{q}])$ is

$$P_a(\Omega_Q=0,[\mathbf{q}]) = A_a\cdot[\mathbf{q}]^2t^2\,, \tag{4.11}$$

see [40, 25]. However, away from half filling due to a different topology of the Fermi surface the momentum dependence becomes more complicated and the

Ansatz for $P_a(\Omega_Q = 0, [\mathbf{q}])$ has to be modified appropriately. This is discussed in section 4.3.1.

The Ansatz (4.11) (or the modified Ansatz discussed in section 4.3.1) mimics the dependence of the inverse bosonic propagator on the space-like momenta. It is not a very accurate approximation for $q_x, q_y \approx \pi$. However, for k near the initial scale Λ the hole kinetic term is very small compared to the mass term. For $k \ll \Lambda$ the region $q_x, q_y \approx \pi$ gives only a small contribution.

The dependence on the Matsubara frequency is more difficult. We anticipate here on the one-loop results derived in section 4.3.1 and look at figure 4.2 (a) and (b). The mode with frequency $\Omega_Q = 0$ is changed most while the higher frequency modes retain the classical mass term without sizeable kinetic term. We choose $P_a(\Omega_Q, \mathbf{q} = 0) = Z_a \Omega_Q^2$ for the sake of simplicity, see also [25, 40]. It has the right qualitative property of suppressing the effect of high frequency modes.

A similar behavior is expected, e.g. for the quartic bosonic coupling $\bar{\lambda}_a$ which is generated by a fermionic loop [25]. The couplings with small external frequencies are supposed to be changed most while for large external frequencies the coupling is expected to stay close to zero. However, we evaluate $\bar{\lambda}_a$ at external frequency $\Omega_Q = 0$ and mimic the suppression of high frequency modes by the frequency dependence of the bosonic propagators introduced above. A similar argument also applies to $\bar{\gamma}_a$ and $\bar{\zeta}_a$.

The other bosonic field which we introduce here is the d-wave field denoted by d and introduced in (2.29). It couples to the corresponding fermion bilinear introduced in (2.31),

$$\Gamma^Y_{d,k} = -\sum_{K,Q,Q'} \delta(K-Q-Q')\bar{h}_d(Q-Q')\big(d^*(K)[\psi^T(Q)\epsilon\psi(Q')] - d(K)[\psi^\dagger(Q)\epsilon\psi^*(Q')]\big)\,, \quad (4.12)$$

where the Yukawa coupling is scale and momentum dependent

$$\bar{h}_d(Q-Q') = \bar{h}_d f_d(\mathbf{q}-\mathbf{q}') \equiv \bar{h}_d \frac{1}{2}\big(\cos\frac{q_x - q'_x}{2} - \cos\frac{q_y - q'_y}{2}\big)\,. \quad (4.13)$$

Similar as for **a**-boson there is also a purely bosonic part containing a kinetic part and a contribution to the effective potential

$$\Gamma_{d,k} = \sum_K d^*(K) P_d(K) d(K) + \sum_X U_d[d^*, d]\,. \quad (4.14)$$

For the effective potential we use an expansion up to sixth order in the bosonic

fields in the symmetric phase (SYM)

$$\begin{aligned}\sum_X U_d[d,d^*] = &\sum_K d^*(K)\,\bar{m}_d^2\,d(K)\\ &+\frac{1}{2}\sum_{K_1,\cdots,K_4}\bar{\lambda}_d\delta(K_1-K_2+K_3-K_4)d^*(K_1)d(K_2)d^*(K_3)d(K_4)\\ &+\frac{1}{3}\sum_{K_1,\cdots,K_6}\bar{\gamma}_d\delta(K_1-K_2+K_3-K_4+K_5-K_6)\\ &\qquad\times d^*(K_1)d(K_2)d^*(K_3)d(K_4)d^*(K_5)d(K_6)\,. \quad (4.15)\end{aligned}$$

In the spontaneous symmetry broken regime we again expand around the minima

$$\begin{aligned}\sum_X U_d[d,d^*] = \frac{1}{2}\sum_{K_1,\cdots,K_4}&\bar{\lambda}_d\delta(K_1-K_2+K_3-K_4)\\ &\times\big(d^*(K_1)d(K_2)-\delta_0\delta(K_1)\delta(K_2)\big)\\ &\times\big(d^*(K_3)d(K_4)-\delta_0\delta(K_3)\delta(K_4)\big)\,. \quad (4.16)\end{aligned}$$

However, it may be necessary to study the effective potential to much higher order in the expansion in powers of fields, or even discretize the effective potential in field space. In chapter 5 a possible scenario for a phase transition to d-wave superconductivity is discussed which needs a truncation beyond (4.16).

Symmetry also allows terms coupling the bosonic fields directly together such as

$$\Gamma_{ad,k} = \sum_{K_1,\ldots,K_4}\bar{\lambda}_{ad}\delta(K_1+K_2-K_3+K_4)\alpha(K_1,K_2)d^*(K_3)d(K_4)\,. \quad (4.17)$$

We have not studied such couplings so far. This is expected to be important in the regions in parameter space between antiferromagnetic and d-wave superconducting phases. For instance, if one symmetry is spontaneously broken during the flow the other channel acquires a mass-like term which may tend to stabilize or destabilize this channel.

Similar as for the **a**-boson the bosonic kinetic term vanishes on the initial scale as well as the couplings $\bar{\lambda}_d$ and $\bar{\gamma}_d$. As motivated in section 4.3.1, we describe the momentum dependence of the bosonic two-point function generated during the flow by the following Ansatz,

$$P_d(Q=(\Omega_Q,\mathbf{q})) = P_d(\Omega_Q,[\mathbf{q}]=0) + P_d(\Omega_Q=0,[\mathbf{q}])\,, \quad (4.18)$$

with the dependence on space-like momenta

$$P_d(\Omega_Q=0,[\mathbf{q}]) = A_d\cdot[\mathbf{q}]^2t^2\,. \quad (4.19)$$

The frequency part depends qualitatively on the doping of the system. Close to half filling we choose similar as for the **a**-field $P_d(\Omega_Q, [\mathbf{q}] = 0) = Z_{d,2}\Omega_Q^2$, whereas away from half filling $P_d(\Omega_Q, [\mathbf{q}] = 0) = iZ_d\Omega_Q$ may be preferable. The discussion of the frequency dependence of the inverse bosonic propagator of the **a**-boson and the corresponding bosonic couplings also applies to this case. The qualitative property of suppressing the effect of the high frequency modes is achieved by the frequency dependence of the inverse bosonic propagator rather than the bosonic couplings which are evaluated for vanishing external frequencies.

Initial Values

At the initial scale the effective average action has to equal the microscopic action. The initial conditions for the parameters occurring during the flow have to account for this fact. For sufficiently large values of the scale k one starts in the symmetric regime and the loop contributions vanish. The couplings of the **a**-boson satisfy

$$\bar{m}_a^2 = U_m, \quad \bar{h}_a = U_m, \quad \lambda_a = \gamma_a = \zeta_a = 0, \quad Z_a = A_a = 0\,, \tag{4.20}$$

where $U_m = U/3$ due to the partial bosonization, see eq. (2.26). We bosonize on initial scale the fermionic interaction completely into the antiferromagnetic channel.

On initial scale the d-boson is only introduced as auxiliary field with a finite mass term $\bar{m}_d^2$. The initial values of the couplings incorporating the d-boson are

$$\bar{h}_d = 0, \quad \lambda_d = \gamma_d = 0, \quad Z_d = A_d = 0\,. \tag{4.21}$$

The couplings to the rest of the theory, e.g. to the fermions and to the **a**-fields, are generated during the flow as discussed below.

4.2 Regularization Scheme

In addition to the truncation of the effective average action the regulator functions for the functional renormalization group approach have to be specified. At first we define the regulator functions for the different types of fields separately. We combine everything to the full regulator matrix R_k appearing in the flow equation (3.24) at the end of this section.

Our choice for the fermionic regulator is inspired by the fact that at finite temperature the fermionic propagator $P_F(Q) = 2\pi i(n_F + \frac{1}{2})T + \xi_{\mathbf{q}}$ has no zero modes. The temperature itself acts as a regulator. We put this into use by the

regulator function [25]

$$R_F^k(Q) = i\omega_Q\big(\frac{T_k}{T} - 1\big) = 2\pi i(n_F + \frac{1}{2})(T_k - T)\,, \tag{4.22}$$

with $(p > 2)$

$$T_k^p = T^p + k^p \quad \text{and} \quad \partial_k T_k = (k/T_k)^{p-1} \to \begin{cases} 1 & \text{if} \quad k \gg T \\ (k/T)^{p-1} & \text{if} \quad k \ll T \end{cases}, \tag{4.23}$$

where we choose $p = 4$ in order to integrate out the fermions very effectively. For $k \gtrsim T$ the cutoff R_F^k in the inverse fermion propagator suppresses the contribution of all fluctuations with momenta $|\mathbf{p} - \mathbf{p}_F|^2 < (\pi k)^2$, even for $T = 0$. It becomes ineffective for $k \ll T$ where no cutoff is needed anymore. Basically, the temperature T is replaced by the scale dependent "temperature" T_k – we cool the fermions down to the temperature of interest during the flow. In figure 4.6 the action of this regulator is demonstrated by means of a typical example.

For bosons the situation is different. Here, long range bosonic modes may cause infrared problems. In particular near a second order phase transition where the bosonic correlation length diverges which is the same as a vanishing bosonic mass term. We use a "linear cutoff" for the space-like momenta [57] for the **a**-boson near half filling and for the d-boson

$$R_{a,d}^k(Q) = A_{a,d} \cdot (k^2 - [\mathbf{q}]^2 t^2)\Theta(k^2 - [\mathbf{q}]^2 t^2)\,. \tag{4.24}$$

Sufficiently away from half filling the momentum dependence of the propagator of the **a**-boson is more complicated, see the one-loop calculations in the next section. However, concerning regularization the treatment is analog to the here described procedure. A more detailed discussion is postponed until the next section.

Following the flow equation scheme discussed in chapter 3 the inverse propagators of the bosonic fields are replaced by

$$P_{a,d}^k(Q) = P_{a,d}(Q) + R_{a,d}^k(Q)\,, \tag{4.25}$$

where the space-like part $P_{a,d}^k(\mathbf{q}) \equiv P_{a,d}^k(Q = (0, \mathbf{q}))$ reads

$$P_{a,d}^k(\mathbf{q}) = A_{a,d}\big([\mathbf{q}]^2 t^2 + (k^2 - [\mathbf{q}]^2 t^2)\Theta(k^2 - [\mathbf{q}]^2 t^2)\big) = A_{a,d}\mathbf{q}_k^2\,, \tag{4.26}$$

where

$$\mathbf{q}_k^2 = \begin{cases} [\mathbf{q}]^2 t^2 & \text{if} \quad [\mathbf{q}]^2 t^2 > k^2 \\ k^2 & \text{if} \quad [\mathbf{q}]^2 t^2 < k^2 \end{cases}. \tag{4.27}$$

Thus the bosonic regulator modifies only the propagation of the infrared modes with momenta $[\mathbf{q}]^2 t^2 < k^2$. A lowering of the scale k can therefore be interpreted for sufficiently small scale k as an averaging over larger and larger volume in position space. An advantage of a solely space-like regulator is that the Matsubara sums still can be performed analytically. (This is also true for the fermionic regulator.)

The often used scale derivative of the regulator functions is

$$\partial_k R^k_{a,d}(Q) = kA_{a,d}\big(2 - \eta_{a,d}(1 - \frac{[\mathbf{q}]^2 t^2}{k^2})\big)\Theta(k^2 - [\mathbf{q}]^2 t^2)\,, \tag{4.28}$$

where the anomalous dimensions are defined by $\eta_{a,d} = -\frac{\partial \ln A_{a,d}}{\partial \ln k}$. Note that the Theta-function which appears under the integral yields to considerable simplifications. In purely bosonic parts of the flow equations the integration over space-like momenta becomes trivial.

In order to combine the single cutoff functions to the full R_k we declare our definition of second functional derivatives. For instance, the second functional derivatives for Γ_k are defined by

$$\Gamma^{(2)}_{k,ab}(P_1, P_2) = \frac{\overrightarrow{\delta}}{\delta\chi^T_a(-P_1)}\Gamma_k\frac{\overleftarrow{\delta}}{\delta\chi_b(P_2)}\,, \tag{4.29}$$

with the vector notation in momentum space

$$\chi(P) \;=\; \big(\mathbf{a}^T(P), d(P), d^*(-P), \psi^T(P), \psi^{*T}(-P)\big)^T\,. \tag{4.30}$$

With these definitions the regulator matrix R_k reads

$$R_k = \begin{pmatrix} R^k_{\mathbf{a}} & & & & \\ & R^k_d & (R^k_d)^T & & \\ & & & -(R^k_F)^T & \\ & & & & R^k_F \end{pmatrix}\,, \tag{4.31}$$

with $R^k_{\mathbf{a}} = \mathrm{diag}(R^k_a, R^k_a, R^k_a)$. R_k is diagonal in momentum space.

4.3 1-PI Vertex Functions to One-loop Order

The reason why we study one-loop corrections to the 1-PI vertex functions is twofold. On the one hand the intention is to get a feeling for their momentum dependence, especially in case of the bosonic two-point functions. This is of particular interest in order to find a reasonable truncation for the bosonic

kinetic terms which covers the relevant momentum structure with a preferable small number of scale dependent parameters[2]. Additionally, a mean field phase diagram which shows the dependence of the mean field critical temperature on the doping of the system can be easily inferred from these calculations, see e.g. [44, 40, 43]. On the other hand in the derivation of the flow equations for the vertex functions the same one-loop calculations are involved. However, to see this connection we invert the order and show that one-loop perturbation theory can be immediately derived from the flow equation. Γ_k can be expanded in loops

$$\Gamma_k = S + \hbar\,\Gamma_k^{1-\text{loop}} + \mathcal{O}(\hbar^2)\,, \tag{4.32}$$

where S is the classical action. It is clear that, to one-loop order, $\Gamma_k^{(2)}$ can be replaced by $S^{(2)}$ in the rhs of (3.24). To one-loop order we obtain

$$\partial_k \Gamma_k^{1-\text{loop}} = \frac{1}{2}\text{STr}\big\{(\partial_k R_k)[S^{(2)} + R_k]^{-1}\big\} = \frac{1}{2}\partial_k \text{STr}\ln[S^{(2)} + R_k]\,. \tag{4.33}$$

An integration yields to one-loop level,

$$\Gamma^{1-\text{loop}} = S + \frac{1}{2}\text{STr}\ln S^{(2)} + \text{const.}\,, \tag{4.34}$$

which is precisely the standard one-loop effective action.

Defining the operator $\tilde{\partial}_k = (\partial_k R_k)\frac{\partial}{\partial R_k}$ we can write the flow equation in a similar form

$$\partial_k \Gamma_k = \frac{1}{2}\text{STr}\big\{\tilde{\partial}_k \ln(\Gamma_k^{(2)} + R_k)\big\}\,. \tag{4.35}$$

We split up the fields into a sum of a homogenous background field χ and a fluctuating part $\delta\hat{\chi}(Q)$ which contains the non-trivial momentum dependence,

$$\hat{\chi}(Q) = \chi\delta(Q) + \delta\hat{\chi}(Q)\,. \tag{4.36}$$

For the fermions it is $\psi^{(\dagger)} = 0$ and we set $\hat{\psi}^{(\dagger)}(Q) \equiv \delta\hat{\psi}^{(\dagger)}(Q)$. Furthermore, we decompose the fluctuation matrix $\Gamma_k^{(2)} + R_k$ into a field independent part $\mathcal{P}_k = \mathcal{P} + R_k$ which contains the inverse propagators including the background fields and the cutoff functions, and a field dependent part $\mathcal{F}$,

$$\Gamma_k^{(2)} + R_k = \mathcal{P}_k + \mathcal{F}\,. \tag{4.37}$$

Note that $\mathcal{P}_k$ contains in this way all parts which are diagonal in momentum space.

[2]We are mainly interested in fermionic one-loop corrections at finite temperature which are infrared finite.

The flow equations for the couplings introduced in our truncation for Γ_k can be obtained by projection from the flow equation (4.35). Therefor, we insert eq. (4.37) into (4.35) and perform an expansion in the number of fields,

$$\begin{aligned}\partial_k\Gamma_k &= \frac{1}{2}\mathrm{STr}\big\{\tilde{\partial}_k \ln(\mathcal{P}_k+\mathcal{F})\big\}\\ &= \frac{1}{2}\,\mathrm{STr}\,\tilde{\partial}_k \ln \mathcal{P}_k + \frac{1}{2}\,\mathrm{STr}\big\{\tilde{\partial}_k\big(\mathcal{P}_k^{-1}\mathcal{F}\big)\big\} - \frac{1}{4}\,\mathrm{STr}\big\{\tilde{\partial}_k\big(\mathcal{P}_k^{-1}\mathcal{F}\big)^2\big\}\\ &\quad + \frac{1}{6}\,\mathrm{STr}\big\{\tilde{\partial}_k\big(\mathcal{P}_k^{-1}\mathcal{F}\big)^3\big\} - \frac{1}{8}\,\mathrm{STr}\big\{\tilde{\partial}_k\big(\mathcal{P}_k^{-1}\mathcal{F}\big)^4\big\} + \cdots . \end{aligned} \tag{4.38}$$

We can reduce the calculation effort of the projection on the flow equations for the couplings considerably by splitting up the part containing the field dependence into parts containing only a single type of field

$$\mathcal{F} = F_a + F_d + F_{d^*} + F_\psi + F_{\psi^*} + G_{\mathbf{aa}} + G_{DD}\,, \tag{4.39}$$

with the short hand $D = (d, d^*)^T$. This brings about a splitting of $\mathcal{P}^{-1}\mathcal{F}$ as well,

$$\mathcal{P}_k^{-1}\mathcal{F} = N_a + N_d + N_{d^*} + N_\psi + N_{\psi^*} + M_{\mathbf{aa}} + M_{DD}\,, \tag{4.40}$$

with $\mathcal{P}_k^{-1}F_i$ for $i \in \{a, d, d^*, \psi, \psi^*, \mathbf{aa}, DD\}$. The matrices $\mathcal{P}$, $\mathcal{P}^{-1}$ and $\mathcal{F}$ are displayed explicitely in Appendix B.

The perturbative one-loop effective action (4.34) can be expanded in the same way. Alternatively, one can start from eq. (4.38), drop the scale derivative $\tilde{\partial}_k$ and the regulator terms ($\mathcal{P}_k \to \mathcal{P}$), and set the couplings on their initial values.

4.3.1 Propagators

We start with the fermionic one-loop correction to the bosonic two-point functions. In figure 4.1 some of the one-loop Feynman diagrams renormalizing the two-point functions of the bosons are displayed.

a-boson

Applying the prescriptions developed in the last section, we derive the momentum dependent one-loop correction to the propagator of the **a**-boson in the symmetric phase (SYM). We keep in the expansion of the one-loop effective action in powers of fields only the parts containing the relevant information[3],

$$\Delta\Gamma_a \supset -\frac{1}{4}\mathrm{STr}(N_a^2) = \sum_K \Delta\Gamma^{(2)}_{aa}(K)\frac{1}{2}\mathbf{a}(-K)\cdot\mathbf{a}(K)\,. \tag{4.41}$$

[3]Generally, we denote this reduction by the $\supset$ sign (e.g. in eq. (4.41)). The projection on the vertex function of interest annihilates the not displayed parts.

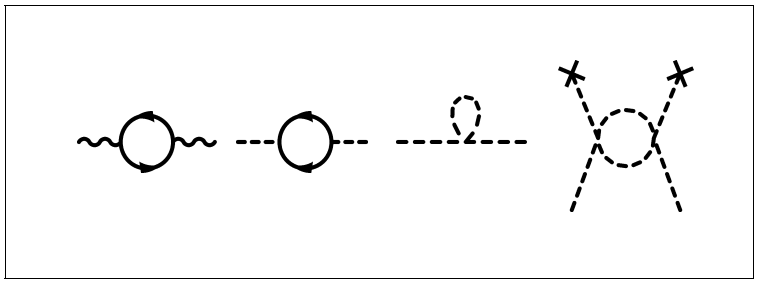

Figure 4.1: Loop corrections to the inverse propagators of the **a**- and the d-boson. The solid lines correspond to fermions, the wiggly lines to **a**-fields and the dashed lines to d-fields. The last diagram exists only in SSB.

The projection on the inverse propagator in SYM is achieved by functional derivatives

$$\Delta P_a(P_1,P_2) = \frac{\overrightarrow{\delta}}{\delta \mathbf{a}^T(-P_1)} \Delta\Gamma_a \frac{\overleftarrow{\delta}}{\delta \mathbf{a}(P_2)}\bigg|_{\mathbf{a}=0}. \tag{4.42}$$

In momentum space the propagator is diagonal and depends on one external total momentum $K = (\Omega_K, \mathbf{k})$. Here we study only the fermionic contribution,

$$\Delta P_a^F(K) = \sum_P \frac{\bar{h}_a(K)\bar{h}_a(-K)}{P_F(K+P+\Pi)P_F(P)} + (K \to -K)\,. \tag{4.43}$$

Since we consider the Yukawa coupling in our truncation independent of frequency and space-like momenta we perform the Matsubara sum over the fermionic propagators at first,

$$\begin{aligned} & \sum_{n\in Z} \frac{1}{P_F^k(P)P_F^k(K+P+\Pi)} \\ = & \sum_{n\in Z} \frac{1}{i(2n+1)\pi T_k + \xi_{\mathbf{p}}} \frac{1}{i(2n+1)\pi T_k + \xi_{\mathbf{k}+\mathbf{p}+\boldsymbol{\pi}} + i\Omega_K \frac{T_k}{T}} \\ = & -\frac{\tanh(\frac{\xi_{\mathbf{p}}}{2T_k}) - \tanh(\frac{\xi_{\mathbf{k}+\mathbf{p}+\pi}+i\Omega_K\frac{T_k}{T}}{2T_k})}{2T_k(\xi_{\mathbf{p}} - \xi_{\mathbf{k}+\mathbf{p}+\pi} - i\Omega_K\frac{T_k}{T})}\,. \end{aligned} \tag{4.44}$$

Note, that we have added the cutoff functions to the inverse of the fermionic propagators, $P_F^k(Q) = P_F(Q) + R_F^k(Q)$. Hence, on the one hand we obtain the flow equation for the two-point function by derivative with respect to the scale k in the regulator. On the other hand one gets the perturbative one-loop

result simply by setting $k = 0$ which corresponds to the replacement $T_k \to T$. For both intentions,

$$\begin{aligned}\Delta P^F_{a,k}(\Omega_K, \mathbf{k}) \;=\; & -\frac{T\bar{h}_a^2}{2T_k}\int_{-\pi}^{\pi}\frac{d^2p}{(2\pi)^2}\frac{\tanh(\frac{\xi_{\mathbf{p}}}{2T_k}) - \tanh(\frac{\xi_{\mathbf{k}+\mathbf{p}+\pi}}{2T_k} + \frac{i\Omega_K}{2T})}{\xi_{\mathbf{p}} - \xi_{\mathbf{k}+\mathbf{p}+\pi} - i\Omega_K\frac{T_k}{T}} \\ & +(K \to -K)\,, \end{aligned} \tag{4.45}$$

provides a starting point. Note the overall factor T coming from the measure (2.10) which is not replaced by T_k due to the regularization procedure.

From eq. (4.45) we derive the flow equations for the mass $\bar{m}_a^2$, the wave function renormalization Z_a and the gradient coefficient A_a wherewith the inverse propagator of the **a**-boson is described. However, the first aim of this calculation is to find a truncation for the momentum dependence of the inverse propagator. At the end the complete inverse propagator shall be approximated on all scales by the following Ansatz

$$\tilde{P}_a(K) = \bar{m}_a^2 + P_a(K)\,. \tag{4.46}$$

In the here considered parameter space the lowest value of $\Delta P^F_{a,k}(\Omega_K, \mathbf{k})$ is always reached for the Matsubara frequency $\Omega_K = 0$, see figure 4.2 (a) and (b). Now we discuss the dependence of this one-loop correction on the space-like momenta, we set $\Omega_K = 0$ for a moment and define

$$P_a(\mathbf{k}) \equiv P_a(K = (0, \mathbf{k}))\,. \tag{4.47}$$

For the dependence on space-like momenta of $P_a(\mathbf{k})$ we note two qualitatively different situations. At half filling and close to half filling for sufficiently high temperatures it looks like figure 4.2 (c) and we apply the truncation specified in eq. (4.11). We Taylor-expand around the origin up to second order in space-like momenta. On a mean field level, the mass $\bar{m}_a^2$ is defined as the mass on UV scale given by the bosonization procedure plus $\Delta P^F_{a,k}(\Omega_K = 0, \mathbf{k} = 0)$. Due to the invariance under reflections $\mathbf{k} \to -\mathbf{k}$, the linear coefficients vanish. The second order contribution can be described by only one number A_a reflecting the fact that the problem becomes isotropic in the limit of vanishing space-like momenta. Modes with very small space-like momenta do not resolve the lattice structure. Hence, the gradient coefficient A_a can be defined as

$$\begin{aligned} A_a \;&=\; \frac{1}{2}\frac{\partial^2}{\partial l^2}\Delta P^F_{a,k}(\Omega_K = 0, \mathbf{k} = l\mathbf{e}_x)\Big|_{l=0} \\ &=\; -\frac{T}{t^2T_k}\frac{1}{2}\frac{\partial^2}{\partial l^2}\bar{h}_a^2\int_{-\pi}^{\pi}\frac{d^2p}{(2\pi)^2}\frac{\tanh(\frac{\xi_{\mathbf{p}}}{2T_k}) - \tanh(\frac{\xi_{l\mathbf{e}_\mathbf{x}+\boldsymbol{\pi}+\mathbf{p}}}{2T_k})}{\xi_{\mathbf{p}} - \xi_{l\mathbf{e}_\mathbf{x}+\boldsymbol{\pi}+\mathbf{p}}}\Bigg|_{l=0}\,. \end{aligned} \tag{4.48}$$

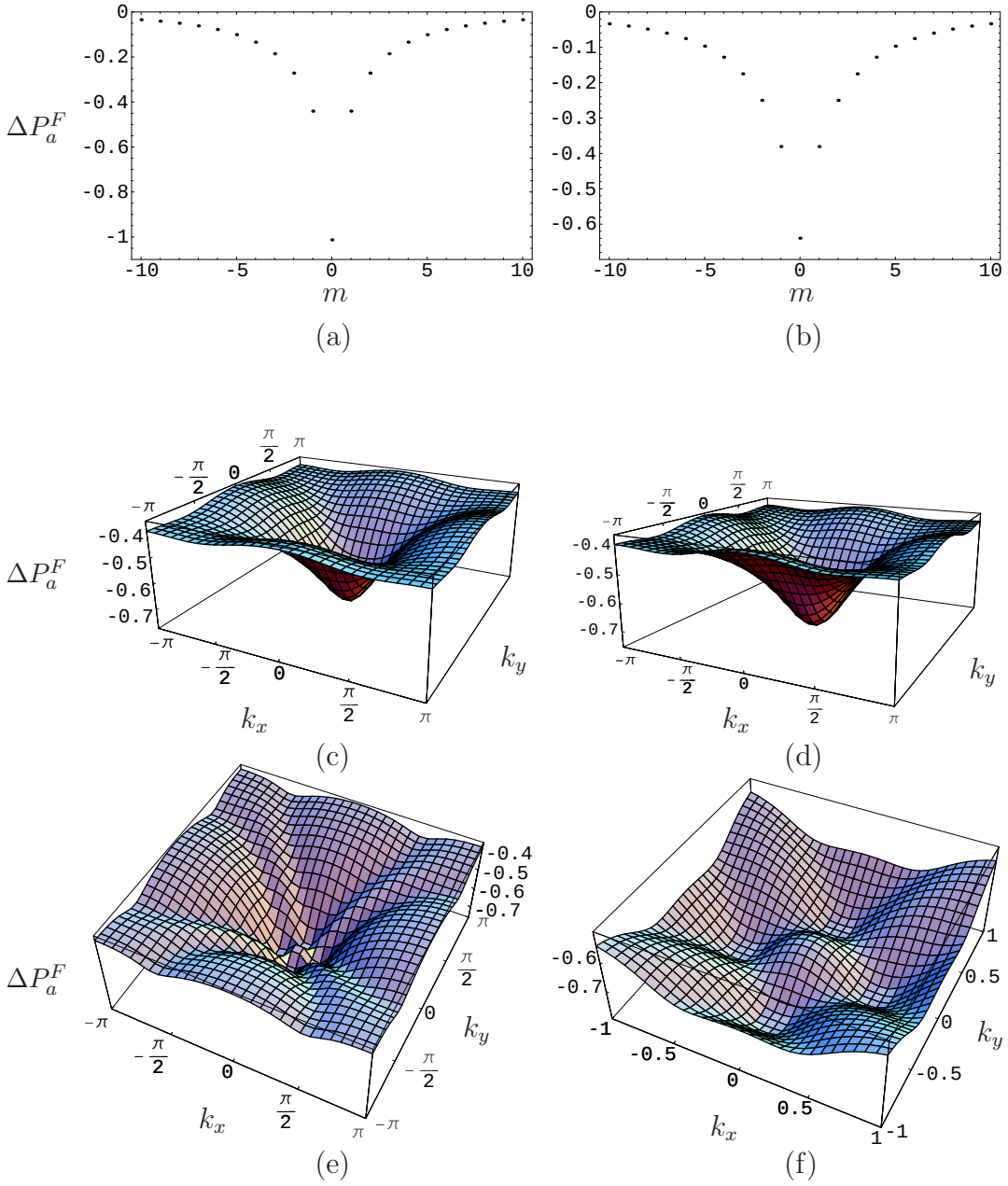

Figure 4.2: One-loop correction to the inverse propagator of the **a**-boson according to eq. (4.45) with $k = 0$ ($T_k = T$). Figure (a) and (b) show the frequency dependence ($\mathbf{k} = 0$) for (a) with $\mu = 0$, $t' = 0$ and $T/t = 0.2$ and for (b) with $\mu/t = -0.5$, $t' = 0$ and $T/t = 0.2$, respectively. In (c), (d), (e) and (f) the dependence on space-like momenta ($\Omega_K = 0$) is shown for (c) with $\mu = 0$, $t' = 0$, $T/t = 0.35$, for (d) with $\mu/t = -0.3$, $t' = 0$, $T/t = 0.3$, for (e) with $\mu/t = -0.3$, $t' = 0$, $T/t = 0.1$ and for (f) with $\mu/t = -0.5$, $t'/t = -0.05$, $T/t = 0.1$, respectively.

However, away from half filling the momentum dependence of $\Delta P^F_{a,k=0}(\Omega_K = 0, \mathbf{k})$ is different for sufficiently low temperatures, see figure 4.2 (d) and (e). In the center ($\mathbf{k} = 0$) there is a local maximum and furthermore there are four degenerated minima at the positions

$$\mathbf{k}_{1,2} = (\pm\hat{k}, 0) \quad \text{and} \quad \mathbf{k}_{3,4} = (0, \pm\hat{k})\,, \tag{4.49}$$

where $\hat{k}$ depends on the chemical potential [58]. A minimum at $\mathbf{k} = 0$ is a manifestation of the dominance of *commensurate* antiferromagnetic fluctuations. Remember that we have defined the **a**-boson with momentum shift of $\Pi = (0, \boldsymbol{\pi}) = (0, \pi, \pi)$ in momentum space, see eq. (4.4). However, a dominance of *incommensurate* antiferromagnetic fluctuations manifest itself by minima at the momenta defined in eq. (4.49). See [58] for a discussion of incommensurate antiferromagnetism in the two-dimensional Hubbard model.

In order to cope with this more complicated situation with still a small number of parameters we use a polynomial of quartic order in the space-like momenta,

$$P_a(\mathbf{k}) = c + \alpha(k_x^2 + k_y^2) + \beta(k_x^2 + k_y^2)^2 + \gamma k_x^2 k_y^2\,. \tag{4.50}$$

This simple Ansatz may qualitatively describe the dependence on space-like momenta around the minima. The corresponding modes are expected to be the most relevant modes to describe (in-)commensurate antiferromagnetic fluctuations. In this spirit we fix the coefficients c, α, β and γ with the aid of the following conditions. At first the positions of the minima are to be described correctly by the polynomial. The mass $\bar{m}_a^2$ is defined here by the sum of the classical mass plus e.g. $\Delta P^F_{a,k}(\Omega_K = 0, \mathbf{k}_1)$. This yields the conditions

$$P_a(\mathbf{k}_1) = 0\,, \quad \frac{\partial}{\partial k_x} P_a(\mathbf{k})\Big|_{\mathbf{k}=\mathbf{k}_1} = 0\,. \tag{4.51}$$

Note that due to symmetry a replacement of $\mathbf{k}_1$ by $\mathbf{k}_j$ with $j \in \{2, 3, 4\}$ yields no new constraints. This also holds for the replacement of $\frac{\partial}{\partial k_x}$ by $\frac{\partial}{\partial k_y}$. Secondly, we want to describe the curvature in the minima along the axes correctly and impose

$$\frac{\partial^2}{\partial k_x^2} P_a(\mathbf{k}_1) = \frac{\partial^2}{\partial l^2} \Delta P^F_{a,k}(\Omega_K = 0, \mathbf{k} = l\mathbf{e}_x)\Big|_{l=\hat{k}}\,. \tag{4.52}$$

So far we have fixed the coefficients c, α and β. The coefficient γ accommodates the anisotropy due to the lattice. To incorporate this anisotropy, we set

$$\frac{\partial^2}{\partial k_y^2} P_a(\mathbf{k}_1) = \frac{\partial^2}{\partial k_x^2} P_a(\mathbf{k}_1)\,. \tag{4.53}$$

Symmetry considerations on the basis of (4.50) show

$$\frac{\partial^2}{\partial k_x^2} P_a(\mathbf{k}_i) = \frac{\partial^2}{\partial k_y^2} P_a(\mathbf{k}_j) \quad \text{and} \quad \frac{\partial^2}{\partial k_x \partial k_y} P_a(\mathbf{k}_i) = 0\,, \tag{4.54}$$

for $i, j \in \{1, \ldots, 4\}$, which is an approximation. The constraints (4.51), (4.52) and (4.53) fix the coefficients c, α, β and γ in eq. (4.50) and we obtain

$$P_a(\mathbf{k}) = \hat{A}_a \frac{1}{2}\big(\frac{\hat{k}^2}{2} - (k_x^2 + k_y^2) + \frac{1}{2\hat{k}^2}(k_x^2 + k_y^2)^2 + \frac{2}{\hat{k}^2} k_x^2 k_y^2\big)\,, \tag{4.55}$$

where the gradient coefficient $\hat{A}_a$ at the momenta $\mathbf{k}_i$ is defined by

$$\begin{aligned} \hat{A}_a &= \frac{1}{2}\frac{\partial^2}{\partial l^2} \Delta P^F_{a,k}(\Omega_K = 0, \mathbf{k} = l\mathbf{e}_x)\Big|_{l=\hat{k}} \\ &= -\frac{T}{t^2 T_k}\frac{1}{2}\frac{\partial^2}{\partial l^2}\bar{h}_a^2 \int_{-\pi}^{\pi} \frac{d^2p}{(2\pi)^2} \frac{\tanh(\frac{\xi_{\mathbf{p}}}{2T_k}) - \tanh(\frac{\xi_{l\mathbf{e_x}+\boldsymbol{\pi}+\mathbf{p}}}{2T_k})}{\xi_{\mathbf{p}} - \xi_{l\mathbf{e_x}+\boldsymbol{\pi}+\mathbf{p}}}\Bigg|_{l=\hat{k}}\,. \end{aligned} \tag{4.56}$$

Note that we use the parameterization (4.55) instead of (4.11) as soon as A_a becomes zero and therewith connected the minimum leaves the position $\mathbf{k} = 0$. This is reflected by the fact that $\hat{k}$ becomes finite in (4.55). The ratio $\hat{A}_a/\hat{k}^2$ is finite everywhere.

The here used regularization scheme of the incommensurate case is analog to the scheme described above, see eq. (4.26). With the short hand notation

$$F(\mathbf{k}, \hat{k}) = \frac{1}{2}\big(\frac{\hat{k}^2}{2} - (k_x^2 + k_y^2) + \frac{1}{2\hat{k}^2}(k_x^2 + k_y^2)^2 + \frac{2}{\hat{k}^2} k_x^2 k_y^2\big)\,, \tag{4.57}$$

the space-like part ($\Omega_Q = 0$) of $P_a^k(Q) = P_a(Q) + R_a^k(Q)$ reads

$$P_a^k(\mathbf{q}) = \hat{A}_a\big(F(\mathbf{q}, \hat{k}) + (k^2 - F(\mathbf{q}, \hat{k})\Theta(k^2 - F(\mathbf{q}, \hat{k})\big)\,. \tag{4.58}$$

The flow equations for $\hat{A}_a$ and $\hat{k}$ are discussed in the next but one section.

d-boson

Now we discuss the one-loop correction to the inverse propagator of the d-boson. Similar as before we start from the corresponding one-loop contributions to the effective action. In SYM it is

$$\Delta\Gamma_d \supset -\frac{1}{2}\mathrm{STr}\big(N_{d^*} N_d\big) = \sum_K \Delta\Gamma^{(2)}_{d^* d}(K) d^*(K) d(K)\,. \tag{4.59}$$

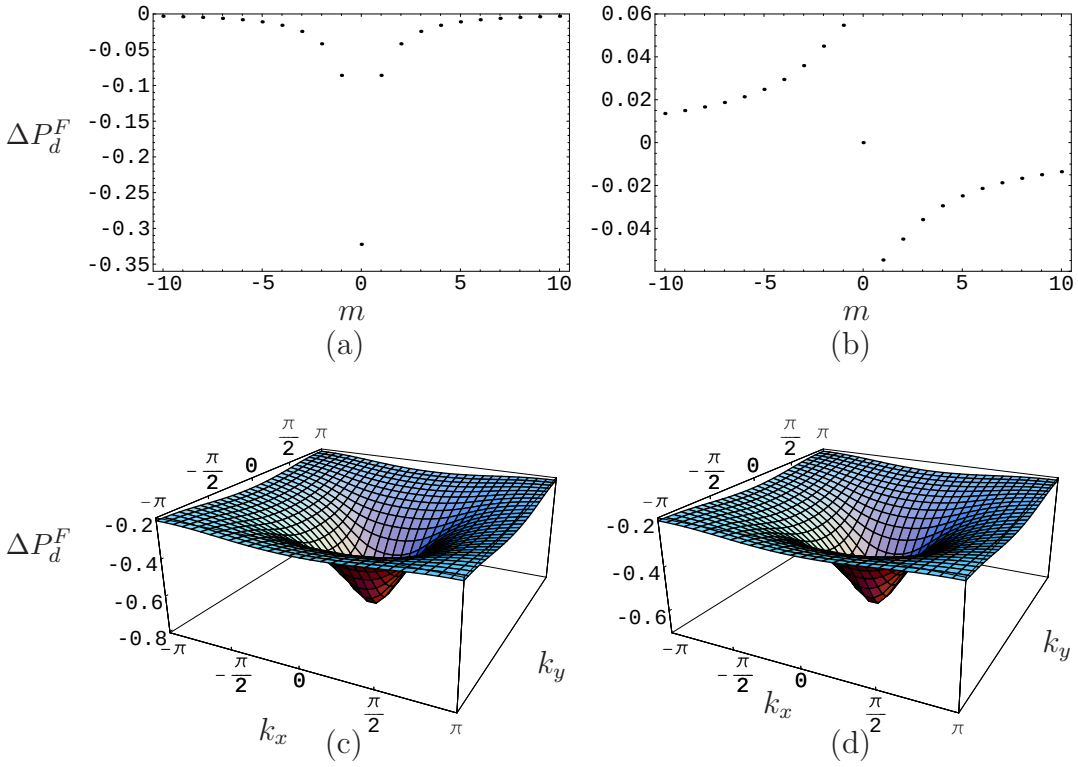

Figure 4.3: One-loop correction to the inverse propagator of the d-boson according to eq. (4.63) with $k = 0$ ($T_k = T$). Figure (a) shows the frequency dependence ($\mathbf{k} = 0$) of the real part for $\mu/t = 0$, $t' = 0$ and $T/t = 0.2$ and (b) of the imaginary part for $\mu/t = -0.5$, $t' = 0$ and $T/t = 0.2$. In (c) and (d) the dependence on space-like momenta ($\Omega_K = 0$) is shown for (c) with $\mu/t = -0.4$, $t'/t = -0.1$ and $T/t = 0.2$ and for (d) with $\mu/t = -0.5$, $t' = 0$ and $T/t = 0.2$, respectively.

Here the projection on the vertex function of interest is given by

$$\Delta P_d(P_1, P_2) = \frac{\overrightarrow{\delta}}{\delta d^*(P_1)} \Delta\Gamma_d \frac{\overleftarrow{\delta}}{\delta d(P_2)}\bigg|_{d,d^*=0} . \tag{4.60}$$

In order to find a reasonable truncation for the inverse propagator we are interested in the fermionic one-loop contribution which reads

$$\Delta P_d^F(K) = -4 \sum_P \frac{\bar{h}_d (K - 2P)^2}{P_F(P) P_F(K - P)} , \tag{4.61}$$

In our truncation the Yukawa coupling depends on space-like momenta but not on frequency, therefore we perform the Matsubara over the fermionic prop-

agators at first

$$\begin{aligned}
&\sum_n \frac{1}{P_F^k(P)P_F^k(K-P)} \\
&= -\sum_n \frac{1}{i(2n+1)\pi T_k + \xi_{\mathbf{p}}} \frac{1}{i(2n+1)\pi T_k - (\xi_{\mathbf{k}-\mathbf{p}} + i\Omega_K \frac{T_k}{T})} \\
&= \frac{\tanh(\frac{\xi_{\mathbf{p}}}{2T_k}) + \tanh(\frac{\xi_{\mathbf{k}-\mathbf{p}} + i\Omega_K \frac{T_k}{T}}{2T_k})}{2T_k(\xi_{\mathbf{p}} + \xi_{\mathbf{k}-\mathbf{p}} + i\Omega_K \frac{T_k}{T})}\,,
\end{aligned} \tag{4.62}$$

where we again have added the cutoff function to the inverse fermionic propagator. Finally we obtain

$$\Delta P^F_{d,k}(\Omega_K, \mathbf{k}) = -\frac{2T}{T_k} \int_{-\pi}^{\pi} \frac{d^2p}{(2\pi)^2} \bar{h}_d^2(2\mathbf{p}-\mathbf{k}) \frac{\tanh(\frac{\xi_{\mathbf{p}}}{2T_k}) + \tanh(\frac{\xi_{\mathbf{k}-\mathbf{p}}}{2T_k} + \frac{i\Omega_K}{2T})}{\xi_{\mathbf{p}} + \xi_{\mathbf{k}-\mathbf{p}} + i\Omega_K \frac{T_k}{T}}. \tag{4.63}$$

However, the dependence on the space-like momenta is much simpler than in the case of the **a**-boson, see figure 4.3 (c) and (d). We proceed similar as for the half filling case of the **a**-boson and use the truncation (4.18). The gradient coefficient is defined by

$$\begin{aligned}
A_d &= \frac{1}{2}\frac{\partial^2}{\partial l^2} \Delta P^F_{d,k}(\Omega_K = 0, \mathbf{k} = l\mathbf{e}_x)\Big|_{l=0} \\
&= -\frac{T}{t^2 T_k} \frac{\partial^2}{\partial l^2} \int_{-\pi}^{\pi} \frac{d^2p}{(2\pi)^2} \bar{h}_d^2(2\mathbf{p}-l\mathbf{e}_{\mathbf{x}}) \frac{\tanh(\frac{\xi_{\mathbf{p}}}{2T_k}) + \tanh(\frac{\xi_{l\mathbf{e}_{\mathbf{x}}-\mathbf{p}}}{2T_k})}{\xi_{\mathbf{p}} + \xi_{l\mathbf{e}_{\mathbf{x}}-\mathbf{p}}} \Bigg|_{l=0}.
\end{aligned} \tag{4.64}$$

Note that the Yukawa coupling of the fermions to the d-fields is momentum dependent.

4.3.2 Yukawa Couplings

In this section we derive the one-loop correction to the Yukawa couplings of both bosons in SYM. The corresponding contributions are visualized in figure 4.4. On this basis the flow equations to the Yukawa couplings are derived in the next but one section.

Within our truncation there are two contributions correcting the Yukawa coupling of the **a**-boson, namely the first two diagrams in figure 4.4. We use the decomposition (4.39) and consider only the contributing parts

$$\begin{aligned}
&\frac{1}{6}\mathrm{STr}\left\{(\mathcal{P}^{-1}\mathcal{F})^3\right\} \supset \frac{1}{6}\,\mathrm{STr}(N_a + N_\psi + N_{\psi^*})^3 \\
&\supset \frac{1}{6}\,\mathrm{STr}\big(N_a N_\psi N_{\psi^*} + N_a N_{\psi^*} N_\psi + N_\psi N_a N_{\psi^*} \\
&\qquad + N_\psi N_{\psi^*} N_a + N_{\psi^*} N_a N_\psi + N_{\psi^*} N_\psi N_a\big)\,.
\end{aligned} \tag{4.65}$$

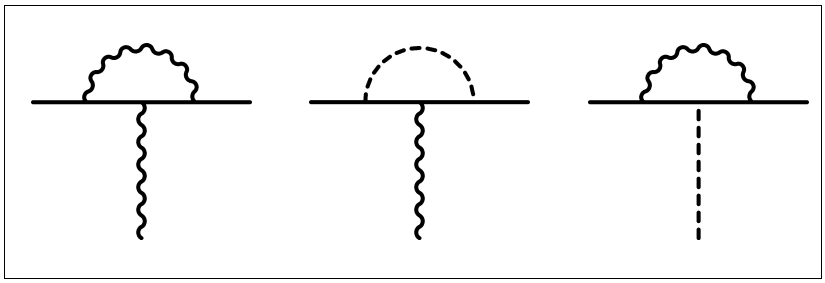

Figure 4.4: One-loop corrections in SYM to the Yukawa couplings. There are two contributions for the **a**- and one for the d-boson.

Now we use the cyclic invariance property of the super-trace STr and obtain the following contributions to the Yukawa coupling

$$\Delta\Gamma_a^Y \supset \frac{1}{2}\,\mathrm{STr}\,(N_a N_{\psi^*} N_\psi) + \frac{1}{2}\,\mathrm{STr}\,(N_a N_\psi N_{\psi^*})\ . \tag{4.66}$$

The result is a sum of a contribution exchanging an **a**-boson and a contribution exchanging a d-boson, see figure 4.4,

$$\begin{aligned}\Delta\Gamma_a^Y \;=\; \sum_{K,Q,Q'} \Big(&\Delta\Gamma^{(3)}_{a\psi^*\psi,a}(K,Q,Q') + \Delta\Gamma^{(3)}_{a\psi^*\psi,d}(K,Q,Q')\Big) \\ &\times\delta(K+\Pi-Q+Q')\mathbf{a}(K)\cdot\psi^\dagger(Q)\boldsymbol{\sigma}\psi(Q')]\,.\end{aligned} \tag{4.67}$$

Explicitely, these contributions are for the first diagram in 4.4

$$\begin{aligned}&\Delta\Gamma^{(3)}_{a\psi^*\psi,a}(K,Q,Q'=Q-K-\Pi) \\ =\;&\sum_P \frac{\bar h_a(K)\bar h_a(P)\bar h_a(-P)}{P_F(Q-K-P)P_F(Q-P-\Pi)\tilde P_a(P)}\,,\end{aligned} \tag{4.68}$$

and

$$\begin{aligned}&\Delta\Gamma^{(3)}_{a\psi^*\psi,d}(K,Q,Q'=Q-K-\Pi) \\ =\;&-4\sum_P \frac{\bar h_a(K)\bar h_d(P-2Q)\bar h_d(2Q-2K-P)}{P_F(K+P-Q+\Pi)P_F(P-Q)\tilde P_d(P)}\,,\end{aligned} \tag{4.69}$$

for the second diagram in 4.4. The inverse propagators are defined as

$$\tilde P_{a,d}(P) = P_{a,d}(P) + \bar m^2_{a,d}\,, \tag{4.70}$$

for the boson a and d, respectively. The spinor indices are examined with the aid of the relations (D.4).

For the correction to the Yukawa coupling of the d-boson (see third diagram in 4.4) we proceed analogously. The contributions are contained in

$$\frac{1}{6}\mathrm{STr}\left\{(\mathcal{P}^{-1}\mathcal{F})^3\right\} \supset \frac{1}{6}\mathrm{STr}\left(N_d + N_{\psi^*}\right)^3 \supset \frac{1}{2}\,\mathrm{STr}\left(N_d N_{\psi^*} N_{\psi^*}\right) . \tag{4.71}$$

There is only one contributions exchanging an **a**-boson, since a contribution in which a d-boson itself is exchanged is forbidden by symmetry. We obtain

$$\Delta\Gamma_d^Y = \sum_{K,Q,Q'} \Delta\Gamma^{(3)}_{d\,\psi^*\psi^*}(K,Q,Q')\delta(K-Q-Q')d(K)[\psi^\dagger(Q)\epsilon\psi^*(Q')] , \tag{4.72}$$

where

$$\begin{aligned} &\Delta\Gamma^{(3)}_{d\,\psi^*\psi^*}(K,Q,K-Q) \\ =\; &-\frac{3}{2}\sum_P \frac{\bar{h}_d(2Q+2P-K)\bar{h}_a(P)\bar{h}_a(-P)}{P_F(Q+P-\Pi)P_F(K-Q-P+\Pi)\tilde{P}_a(P)} \\ &+(Q\to K-Q) . \end{aligned} \tag{4.73}$$

4.3.3 Four Fermion Interactions

Our truncation for the effective action does not contain four fermion interactions. This was achieved by bosonization. However, even in a completely bosonized fermionic theory there are one-loop corrections to the four fermion coupling. The contributions which appear within our truncation in SYM are displayed in figure 4.5. Starting point in this case is

$$\begin{aligned} &-\frac{1}{8}\,\mathrm{STr}\left\{(\mathcal{P}^{-1}\mathcal{F})^4\right\} \supset -\frac{1}{8}\mathrm{STr}\left(N_{\psi^*}+N_\psi\right)^4 \\ \supset\; &-\frac{1}{8}\,\mathrm{STr}\left(N_{\psi^*}N_{\psi^*}N_\psi N_\psi + N_{\psi^*}N_\psi N_{\psi^*}N_\psi + N_{\psi^*}N_\psi N_\psi N_{\psi^*}\right. \\ &\qquad \left. + N_\psi N_{\psi^*}N_{\psi^*}N_\psi + N_\psi N_{\psi^*}N_\psi N_{\psi^*} + N_\psi N_\psi N_{\psi^*}N_{\psi^*}\right) \\ =\; &-\frac{1}{2}\,\mathrm{STr}\left(N_{\psi^*}N_{\psi^*}N_\psi N_\psi\right) - \frac{1}{4}\,\mathrm{STr}\left(N_{\psi^*}N_\psi N_{\psi^*}N_\psi\right) . \end{aligned} \tag{4.74}$$

Generally, we write the four fermion contributions as

$$\begin{aligned} \Delta\Gamma_F = \sum_{K_1,\ldots,K_4} &\Delta\Gamma^{(4)}_{F,\,\alpha\beta\gamma\delta}(K_1,\ldots,K_4)\delta(K_1-K_2+K_3-K_4) \\ &\times\psi^*_\alpha(K_1)\psi_\beta(K_2)\psi^*_\gamma(K_3)\psi_\delta(K_4) . \end{aligned} \tag{4.75}$$

The momentum dependence of these corrections is of special interest. This issue is discussed in detail in the next section, where we explain our general

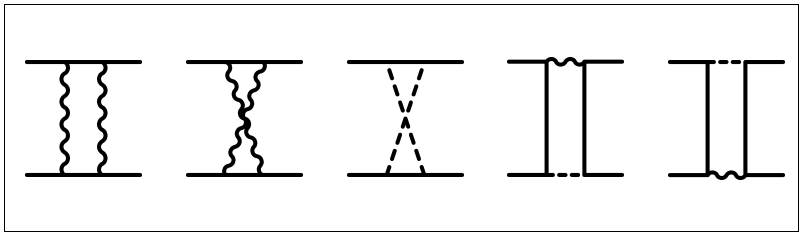

Figure 4.5: One-loop corrections (box diagrams) to the four fermion interaction in SYM.

treatment of these contributions. For instance, some of these box diagrams are crucial for the generation of a momentum dependent d-wave coupling, see section 4.5.

There are two contributions where two **a**-bosons are exchanged, see the first two diagrams in figure 4.5. We find

$$\begin{aligned}\Delta\Gamma_F^{aa} = \frac{1}{2}\sum_{K_1,\ldots,K_4}\sum_P \frac{\bar{h}_a(P)\bar{h}_a(-P)\bar{h}_a(K_3-K_2+P)\bar{h}_a(K_2-K_3-P)}{P_F(K_1-P-\Pi)\tilde{P}_a(P)\tilde{P}_a(K_3-K_2+P)} \\ \times\left\{\frac{(\sigma^i\sigma^j)_{\alpha\delta}(\sigma^i\sigma^j)_{\gamma\beta}}{P_F(K_3+P-\Pi)}+\frac{(\sigma^i\sigma^j)_{\alpha\delta}(\sigma^j\sigma^i)_{\gamma\beta}}{P_F(K_2-P+\Pi)}\right\} \\ \times\delta(K_1-K_2+K_3-K_4)\psi^*_\alpha(K_1)\psi_\beta(K_2)\psi^*_\gamma(K_3)\psi_\delta(K_4)\,. \quad (4.76)\end{aligned}$$

In the following contribution there are two d-bosons exchanged,

$$\begin{aligned}\Delta\Gamma_F^{dd} = -8\sum_{K_1,\ldots,K_4}\sum_P \delta(K_1-K_2+K_3-K_4)\delta_{\alpha\beta}\delta_{\gamma\delta} \\ \times\frac{\bar{h}_d(P-K_1)\bar{h}_d(2K_4-K_1-P)\bar{h}_d(K_2-2K_3+P)\bar{h}_d(K_2-P)}{P_F(P)\tilde{P}_d(K_1+P)P_F(K_1-K_4+P)\tilde{P}_d(K_2+P)} \\ \times\psi^*_\alpha(K_1)\psi_\beta(K_2)\psi^*_\gamma(K_3)\psi_\delta(K_4)\,, \quad (4.77)\end{aligned}$$

see the third diagram in figure 4.5. Additionally, we obtain

$$\begin{aligned}\Delta\Gamma_F^{ad} = -2\sum_{K_1,\ldots,K_4}\sum_P \delta(K_1-K_2+K_3-K_4)\big(3\delta_{\gamma\kappa}\delta_{\delta\rho}-\sigma^j_{\gamma\rho}\sigma^j_{\delta\kappa}\big) \\ \left\{\frac{\bar{h}_a(P)\bar{h}_a(-P)\bar{h}_d(K_1-K_3+P-\Pi)\bar{h}_d(K_2-K_4-P+\Pi)}{\tilde{P}_a(P)P_F(K_1+P-\Pi)\tilde{P}_d(K_1+K_3+P-\Pi)P_F(K_4+P-\Pi)}\right. \\ \left.+\frac{\bar{h}_a(P)\bar{h}_a(-P)\bar{h}_d(K_1-K_3+P-\Pi)\bar{h}_d(K_2-K_4-P+\Pi)}{\tilde{P}_d(K_1+K_3-P-\Pi)P_F(K_3-P-\Pi)\tilde{P}_a(P)P_F(K_2-P+\Pi)}\right\} \\ \times\psi^*_\gamma(K_1)\psi^*_\delta(K_3)\psi_\rho(K_2)\psi_\kappa(K_4)\,, \quad (4.78)\end{aligned}$$

where one **a**-boson and one d-boson are exchanged, see the last two diagrams in figure 4.5. However, we consider here only the first two box diagrams which exchange only **a**-bosons. They are expected to be responsible for the generation of a coupling in the d-wave channel. This is discussed in more detail in section 4.6. The remaining box diagrams vanish on initial scale within our truncation since they are proportional to the coupling $\bar{h}_d$ which is zero on initial scale.

In order to obtain the momentum dependent vertex functions we start from eq. (4.75) and set

$$\Delta\Gamma^{(4)}_{F,\,\bar{\alpha}\bar{\beta}\bar{\gamma}\bar{\delta}}(Q_1,\ldots,Q_4) = F(Q_1,Q_2,Q_3,Q_4)t_{\bar{\alpha}\bar{\beta}\bar{\gamma}\bar{\delta}}\,. \tag{4.79}$$

The projection on the momentum and spin dependent four fermion vertex function $\lambda_{\psi,\alpha\beta\gamma\delta}(K_1,\ldots,K_4)$ can be defined by

$$\begin{aligned}
&\frac{\delta^4}{\delta\psi^*_\alpha(K_1)\delta\psi_\beta(K_2)\delta\psi^*_\gamma(K_3)\delta\psi_\delta(K_4)}\Delta\Gamma_F \\
&= F(K_3,K_4,K_1,K_1+K_3-K_4)\; t_{\gamma\delta\alpha\beta} \\
&\quad -F(K_3,K_2,K_1,K_1+K_3-K_2)\; t_{\gamma\beta\alpha\delta} \\
&\quad -F(K_1,K_4,K_3,K_1+K_3-K_4)\; t_{\alpha\delta\gamma\beta} \\
&\quad +F(K_1,K_2,K_3,K_1+K_3-K_2)\; t_{\alpha\beta\gamma\delta}\,.
\end{aligned} \tag{4.80}$$

For a bosonic quartic interaction a similar formula applies. The difference is that in this case all terms on the rhs come with a plus sign and the spin indices are replaced by vector indices.

4.4 Rebosonization of Fermionic Interactions

Within our truncation a momentum dependent four fermion coupling is generated during the flow to lower momentum scales. The responsible contributions have been derived in the last section. However, if this newly generated contributions are taken into account as four fermion couplings, the most important advantages of the bosonization, depicted in section 2.4, are lost. Therefore, our aim is to take these four fermion contribution into account but at the same time keep the fermionic coupling equal to zero on all scales. This can be achieved approximately by the method of *rebosonization* [55, 49, 56]. We redefine the bosonic fields on each scale by the method of scale-dependent field transformations discussed in section 3.3. This scale dependence of the bosonic fields allows to "rebosonize" the four fermion interaction approximately on all scales.

Technically, the modified flow equation for the effective average action (3.32) is the starting point. At first we derive the modified flow equations for the

Yukawa couplings and the newly generated four fermion interaction. We split up the parts of the equation for the four fermion coupling which arise due to the box diagrams into the specific channels, namely the **a**- and the d-channel, plus a rest. Now, the scale-dependent transformations of the bosonic fields are adjusted in a way that the newly generated contributions in the **a**- and the d-channel can be bosonized. The rest is beyond our truncation and neglected here. Thus, as we discuss in short, the fermionic coupling in the **a**- and the d-channel vanish on all scales. Eventually we have constructed the "perfect bosons" on all scales. However, this procedure is exact only for very special cases. In general, the momentum and spin dependence of the four fermion vertex function have to be restricted appropriately. The task is to identify the contributions which can be absorbed by a particular boson by means of their momentum and spin dependence.

This section is organized as the following. At first we address the question which four fermion contribution can be absorbed by which boson. Therefor we invert the order and ask which momentum and spin structure can be absorbed by the boson on hand exactly. Subsequently, the modified flow equations for the Yukawa couplings, which account for parts of the newly generated four fermion interaction, are set up.

In case of the **a**-boson the quadratic and the Yukawa term look like

$$\begin{aligned}\Gamma_{a,Y} = &\frac{1}{2}\sum_{Q_1,Q_2}\delta(Q_1+Q_2)\mathbf{a}^T(Q_1)\tilde{P}_{\mathbf{a}}(Q_1)\mathbf{a}(Q_2)\\ &-\sum_{Q_1,Q_2}\delta(Q_1+Q_2)\bar{h}_a(Q_1)\mathbf{a}(Q_1)\cdot\sum_P[\psi^\dagger(P)\boldsymbol{\sigma}\psi(P-\Pi+Q_2)]. \quad (4.81)\end{aligned}$$

In order to simplify notation we introduce the scale dependent bilinear

$$\tilde{\mathbf{a}}_k(Q) = \bar{h}_a(-Q)\sum_P \psi^\dagger(P)\boldsymbol{\sigma}\psi(P-\Pi+Q)\,. \quad (4.82)$$

Hereby eq. (4.81) can be written as

$$\begin{aligned}\Gamma_{a,Y} &= \frac{1}{2}\sum_{Q_1,Q_2}\delta(Q_1+Q_2)\tilde{P}_a(Q_1)\big\{\mathbf{a}(Q_1)\cdot\mathbf{a}(Q_2)-\frac{2}{\tilde{P}_a(Q_1)}\mathbf{a}(Q_1)\cdot\tilde{\mathbf{a}}_k(Q_2)\big\}\\ &= \frac{1}{2}\sum_{Q_1,Q_2}\delta(Q_1+Q_2)\tilde{P}_a(Q_1)\Big(\mathbf{a}(Q_1)-\frac{1}{\tilde{P}_a(-Q_1)}\tilde{\mathbf{a}}_k(Q_1)\Big)\\ &\qquad\qquad\cdot\Big(\mathbf{a}(Q_2)-\frac{1}{\tilde{P}_a(-Q_2)}\tilde{\mathbf{a}}_k(Q_2)\Big)\\ &\quad-\frac{1}{2}\sum_{Q_1,Q_2}\delta(Q_1+Q_2)\tilde{P}_a(Q_1)\frac{1}{\tilde{P}_a(-Q_1)\tilde{P}_a(-Q_2)}\tilde{\mathbf{a}}_k(Q_1)\cdot\tilde{\mathbf{a}}_k(Q_2)\,. \quad (4.83)\end{aligned}$$

Hence, the last operator can be absorbed exactly by the **a**-boson. It can be written as

$$\Delta\Gamma_F^a = \frac{1}{2}\sum_{K_1,\cdots,K_4} \lambda_\psi^a(K_1,K_2,K_3,K_4)[\psi^\dagger(K_1)\boldsymbol{\sigma}\psi(K_2)] \cdot[\psi^\dagger(K_3)\boldsymbol{\sigma}\psi(K_4)]\,, \tag{4.84}$$

where

$$\lambda_\psi^a(K_1,K_2,K_3,K_4) = -\frac{\bar{h}_a(K_1-K_2-\Pi)\bar{h}_a(K_2-K_1+\Pi)}{\tilde{P}_a(K_1-K_2-\Pi)} \times\delta(K_1-K_2+K_3-K_4)\,. \tag{4.85}$$

We repeat the same steps for the d-boson. The quadratic and the Yukawa term are in this case

$$\begin{aligned}\Gamma_{d,Y} = &\sum_{Q_1,Q_2}\delta(Q_1-Q_2)d^*(Q_1)\tilde{P}_d(Q_1)d(Q_2)\\ &-\sum_{Q,P}\bar{h}_d(2P-Q)\big\{d^*(Q)[\psi^T(P)\epsilon\psi(Q-P)]\\ &\qquad -d(Q)[\psi^\dagger(P)\epsilon\psi^*(Q-P)]\big\}\,.\end{aligned} \tag{4.86}$$

The corresponding scale dependent bilinear is defined by

$$\tilde{d}_k(Q) = \sum_P \bar{h}_d(2P-Q)[\psi^T(P)\epsilon\psi(Q-P)]\,, \tag{4.87}$$

and we rewrite eq. (4.86) as

$$\begin{aligned}\Gamma_{d,Y} = &\sum_{Q_1,Q_2}\delta(Q_1-Q_2)\tilde{P}_d(Q_1)(d^*(Q_1)-\frac{1}{\tilde{P}_d(Q_1)}\tilde{d}_k^*(Q_1))\\ &\qquad\times(d(Q_2)-\frac{1}{\tilde{P}_d(Q_2)}\tilde{d}_k(Q_2)) \qquad (4.88)\\ &-\sum_{Q_1,Q_2}\delta(Q_1-Q_2)\tilde{P}_d(Q_1)\frac{1}{\tilde{P}_d(Q_1)\tilde{P}_d(Q_2)}\tilde{d}_k^*(Q_1)\tilde{d}_k(Q_2)\,. \qquad (4.89)\end{aligned}$$

Again the last operator can be absorbed exactly by the d-boson. It can be written as

$$\Delta\Gamma_F^d = \sum_{K_1,\cdots,K_4}\lambda_\psi^d(K_1,K_2,K_3,K_4)[\psi^\dagger(K_1)\epsilon\psi^*(K_3)][\psi^T(K_2)\epsilon\psi(K_4)]\,, \tag{4.90}$$

where

$$\lambda_\psi^d(K_1,K_2,K_3,K_4) = \frac{\bar{h}_d(K_1-K_3)\bar{h}_d(K_2-K_4)}{\tilde{P}_d(K_1+K_3)}\delta(K_1-K_2+K_3-K_4). \quad (4.91)$$

The general strategy is to compare the momentum dependence of the contributions generated during the flow (4.76), (4.77) and (4.78) with the terms which can be rebosonized exactly, namely eqs. (4.84) and (4.90). On this basis we decide which contribution should be rebosonized into which channel.

Now we accomplish the procedure described above and derive the modified flow equations for the four fermion couplings in the separate channels and the Yukawa couplings. We introduce a short hand notation for the bosonic fields,

$$B_k = (\mathbf{a}_k^T, d_k, d_k^*)^T\,, \quad (4.92)$$

and start from the modified flow equation (3.32)[4]

$$\begin{aligned}\partial_k\Gamma_k[\psi,\psi^*,B_k] = {}& \partial_k\Gamma_k[\psi,\psi^*,B_k]\big|_{B_k} \\ &+\sum_P\Big(\frac{\delta}{\delta\mathbf{a}_k(P)}\Gamma_k[\psi,\psi^*,B_k]\Big)\partial_k\mathbf{a}_k(P) \\ &+\sum_P\Big(\frac{\delta}{\delta d_k(P)}\Gamma_k[\psi,\psi^*,B_k]\Big)\partial_k d_k(P) \\ &+\sum_P\Big(\frac{\delta}{\delta d_k^*(P)}\Gamma_k[\psi,\psi^*,B_k]\Big)\partial_k d_k^*(P)\,. \end{aligned} \quad (4.93)$$

The derivative of the scale dependent bosonic fields with respect to the scale reads with initially arbitrary functions $\alpha_k^a(K)$ and $\alpha_k^d(K)$

$$\begin{aligned}\partial_k\mathbf{a}_k(K) &= -\partial_k\alpha_k^a(K)\tilde{\mathbf{a}}_k(K), \\ \partial_k d_k(K) &= -\partial_k\alpha_k^d(K)\tilde{d}_k(K), \\ \partial_k d_k^*(K) &= -\partial_k\alpha_k^d(K)\tilde{d}_k^*(K)\,. \end{aligned} \quad (4.94)$$

We apply eq. (4.93) up to the following level of truncation,

$$\begin{aligned}\partial_k\Gamma_k = {}& \partial_k\Gamma_k\big|_{B_k} - \sum_P \partial_k\alpha_k^a(P)\tilde{P}_a(P)\mathbf{a}_k(-P)\cdot\tilde{\mathbf{a}}_k(P) \\ &-\sum_P \partial_k\alpha_k^d(P)\tilde{P}_d(P)\Big\{d_k^*(P)\tilde{d}_k(P) - d_k(P)\tilde{d}_k^*(P)\Big\} \\ &+\sum_P \partial_k\alpha_k^a(P)\tilde{\mathbf{a}}_k(P)\cdot\tilde{\mathbf{a}}_k(-P) - 2\sum_P \partial_k\alpha_k^d(P)\tilde{d}_k^*(P)\tilde{d}_k(P). \end{aligned} \quad (4.95)$$

[4]The second term on the rhs of eq. (3.31) yields a further modification of the flow equation. In our application it is: $\partial_k\Gamma_k = \frac{1}{2}\mathrm{STr}\big[\big(\Gamma_k^{(2)}+R_k\big)^{-1}\{\partial_k R_k + A_k\}\big]$, with $A_k = 2\,\mathrm{diag}\big[\frac{\partial_k\bar{h}_a}{h_a}R_{\mathbf{a}}^k, \frac{\partial_k\bar{h}_d}{h_d}\begin{pmatrix}0 & (R_d^k)^T\\ R_d^k & 0\end{pmatrix}, 0\big]$. We neglect the renormalization group improvement term A_k in a first step, it will be included for quantitative precision.

The modified flow equations for the Yukawa coupling and the fermionic coupling of the **a**-boson are

$$\begin{aligned}\partial_k \bar{h}_a(K) &= \partial_k \bar{h}_a(K)\big|_{B_k} + \partial_k \alpha_k^a(K)\bar{h}_a(K)\tilde{P}_a(K)\,,\\ 0 \equiv \partial_k \lambda_\psi^a(K_1,\ldots,K_4)\big|_{K_1+K_3=K_2+K_4} &= \partial_k \lambda_\psi^a\big|_{B_k}(K_1,\ldots,K_4)\big|_{K_1+K_3=K_2+K_4}\\ &\quad +\bar{h}_a(K_2-K_1+\Pi)\bar{h}_a(K_1-K_2-\Pi)\\ &\quad \times\partial_k\alpha_k^a(K_2-K_1-\Pi)\,, \qquad (4.96)\end{aligned}$$

and similar for the d-boson

$$\begin{aligned}\partial_k \bar{h}_d(2Q-K) &= \partial_k \bar{h}_d(2Q-K)\big|_{B_k}\\ &\quad +\partial_k\alpha_k^d(K)\bar{h}_d(2Q-K)\tilde{P}_d(K)\,,\\ 0 \equiv \partial_k \lambda_\psi^d(K_1,\ldots,K_4)\big|_{K_1+K_3=K_2+K_4} &= \partial_k \lambda_\psi^d\big|_{B_k}(K_1,\ldots,K_4)\big|_{K_1+K_3=K_2+K_4}\\ &\quad -2\bar{h}_d(K_1-K_3)\bar{h}_d(K_2-K_4)\\ &\quad \times\partial_k\alpha_k^d(K_1+K_3)\,. \qquad (4.97)\end{aligned}$$

The functions $\alpha_k^a(K)$ and $\alpha_k^d(K)$ appear in both flow equations in eqs. (4.96) and (4.97), respectively. The fact that we keep the fermionic couplings equal to zero fixes these firstly arbitrary functions. Thereby we obtain the modified flow equations for the Yukawa couplings,

$$\begin{aligned}\partial_k \bar{h}_a(K) &= \partial_k \bar{h}_a(K)\big|_{B_k}\\ &\quad -\frac{\tilde{P}_a(K)}{\bar{h}_a(K)}\partial_k\lambda_\psi^a\big|_{B_k}(K_1,\ldots,K_4)\big|_{K=K_2-K_1-\Pi=K_3-K_4-\Pi}\,, \qquad (4.98)\end{aligned}$$

for the **a**-boson, and

$$\begin{aligned}\partial_k \bar{h}_d(2Q-K) &= \partial_k \bar{h}_d(2Q-K)\big|_{B_k}\\ &\quad +\frac{1}{2}\frac{\bar{h}_d(2Q-K)\tilde{P}_d(K)}{\bar{h}_d(K_1-K_3)\bar{h}_d(K_2-K_4)}\\ &\quad \times\partial_k\lambda_\psi^d\big|_{B_k}(K_1,\ldots,K_4)\Big|_{K=K_1+K_3=K_2+K_4}\,, \qquad (4.99)\end{aligned}$$

for the d-boson. The first contributions on the rhs of eqs. (4.98) and (4.99) are the regular parts coming from the one-loop corrections displayed in figure 4.4. We refer to it as direct contribution $(\partial_k \bar{h}_a)^d$ and $(\partial_k \bar{h}_d)^d$. The second parts account for rebosonization and we refer to it as $(\partial_k \bar{h}_a)^{rb}$ and $(\partial_k \bar{h}_d)^{rb}$.

4.5 Flow Equations

At the beginning of this chapter a truncation of the effective average action Γ_k is introduced. Γ_k is formulated in terms of fermionic fields coupled to two species of bosonic fields, the **a**- and the d-fields. It is discussed that the initial values (4.20) and (4.21) ensure the equivalence of our truncation to the action of the Hubbard model on the initial (high momentum) scale. Furthermore, a regularization scheme both for fermions and bosons is allocated. Hence, the task is now to derive the flow equations for all introduced couplings within our truncation. At first we study the flow of the effective potential, or more precisely the coefficients of an expansion in powers of fields of the effective potential. We discuss two possible ways to obtain these flow equations. All flow equations are specified independently of the regulators, the explicit results are given in the appendix C.

Initially, there are no kinetic terms of both bosonic fields since the interaction between the fermions is still local on high momentum scales. Remember that the meaning of partial bosonization is therefore simply a replacement of a fermionic coupling in a certain channel (denoted by ϕ), $\lambda_\psi^\phi \to \bar{h}_\phi^2/\bar{m}_\phi^2$. The fact that the interaction becomes non-local on lower momentum scales mirrors in the generation of kinetic terms of the bosonic fields mediating the interaction between the fermions, $\bar{h}_\phi^2/\bar{m}_\phi^2 \to \bar{h}_\phi^2/(\bar{m}_\phi^2 + P_\phi(Q))$. The flow equations for the wave function renormalizations and the gradient coefficients which parameterize these kinetic terms are derived in the second subsection.

In the subsequent subsection the flow of the Yukawa couplings is discussed. At first there are the direct contributions. However, a crucial point is the improvement of the truncation with the aid of rebosonization. This way we account for the four fermion interactions in the **a**- and the d-channel which are newly generated during the flow. For this purpose we use eqs. (4.98) and (4.99) as starting point.

4.5.1 Effective Potential

In homogeneous situations the full flow equation of the effective average action (4.38) reduces to a flow equation for the effective potential

$$\partial_k U = \frac{1}{2}\,\mathrm{STr}\,\tilde{\partial}_k \ln \mathcal{P}_k\,, \tag{4.100}$$

where $\mathcal{P}_k$ is given in the appendix, see eq. (B.5). Within our truncation the flow equation of the effective potential (4.100) can be decomposed into a sum over a bosonic and a fermionic part. In the case of neglected couplings of the type $\bar{\lambda}_{ad}$ (see eq. (4.17)) the bosonic part can be further decomposed into a

sum of contributions corresponding to different bosons. It follows

$$\partial_k U(\alpha,\delta) = \partial_k U_a(\alpha) + \partial_k U_d(\delta) + \partial_k U_F(\alpha,\delta)\,. \tag{4.101}$$

The part of the **a**-boson is the same as for an O(3)-model,

$$\partial_k U_a(\alpha) = \frac{1}{2}\sum_{P,i} \tilde{\partial}_k \ln\left[P_a(P) + \hat{M}_i^2(\alpha) + R_a^k(P)\right], \tag{4.102}$$

where $\hat{M}_i^2(\alpha)$ is defined with $i \in \{1,2,3\}$ in SYM as

$$\hat{M}_i^2(\alpha) = \begin{cases} \bar{m}_a^2 + 3\bar{\lambda}_a\alpha + \frac{5}{2}\bar{\gamma}_a\alpha^2 + \frac{7}{6}\bar{\zeta}_a\alpha^3\,, & i=1 \\ \bar{m}_a^2 + \bar{\lambda}_a\alpha + \frac{1}{2}\bar{\gamma}_a\alpha^2 + \frac{1}{6}\bar{\zeta}_a\alpha^3\,, & i=2,3 \end{cases}. \tag{4.103}$$

For the flow equations in SSB one simply has to replace the mass eigenvalues by

$$\hat{M}_i^2(\alpha) = \bar{\lambda}_a(3\alpha-\alpha_0, \alpha-\alpha_0, \alpha-\alpha_0)_i\,. \tag{4.104}$$

The part of the d-boson in SYM is

$$\begin{aligned} &\partial_k U_d(\delta) \\ &= \sum_P \frac{(\partial_k R_d^k(P))(P_d^k(-P) + \hat{M}_d^2(\delta))}{[P_d^k(P) + \hat{M}_d^2(\delta)][P_d^k(-P) + \hat{M}_d^2(\delta)] - (\bar{\lambda}_d + \bar{\gamma}_d\delta)^2\delta^2}, \end{aligned} \tag{4.105}$$

where $\hat{M}_d^2(\delta) = \bar{m}_d^2 + 2\bar{\lambda}_d\delta + \frac{3}{2}\bar{\gamma}_d\delta^2$. Note that $P_d^k(-P) \neq P_d^k(P)$, in general. The broken regime is discussed in chapter 5. The fermionic part can be written with our temperature-like regulator as

$$\partial_k U_F(\alpha,\delta) = \frac{T(\partial_k T_k)}{T_k}\int_{-\pi}^{\pi}\frac{d^2p}{(2\pi)^2}\sum_{\epsilon=\pm1}\gamma_\epsilon(\alpha,\delta)\tanh\gamma_\epsilon(\alpha,\delta)\,, \tag{4.106}$$

where $\gamma_\epsilon(\alpha,\delta)$ is defined in the appendix, see eq. (D.25). The flow equations of the couplings at zero external momenta can be derived by appropriate derivatives with respect to α and δ on both sides of eq. (4.101). This yields in SYM

$$\begin{aligned} \partial_k\bar{m}_a^2 &= \frac{\partial}{\partial\alpha}\partial_k U(\alpha,\delta)\big|_{\alpha=0}\,, \quad \partial_k\bar{\lambda}_a = \frac{\partial^2}{\partial\alpha^2}\partial_k U(\alpha,\delta)\big|_{\alpha=0}\,, \\ \partial_k\bar{\gamma}_a &= \frac{\partial^3}{\partial\alpha^3}\partial_k U(\alpha,\delta)\big|_{\alpha=0}\,, \quad \partial_k\bar{\zeta}_a = \frac{\partial^4}{\partial\alpha^4}\partial_k U(\alpha,\delta)\big|_{\alpha=0}, \end{aligned} \tag{4.107}$$

for the **a**-boson, where $\delta = 0$ if the phase is also symmetric with respect to δ. Otherwise set $\delta = \delta_0$. For the analog couplings of the d-boson simply exchange the role of α and δ in an obvious way.

In the broken phase we describe the bosonic potential by

$$\partial_k \alpha_0 = -\frac{1}{\bar{\lambda}_a}\frac{\partial}{\partial\alpha}\partial_k U(\alpha,\delta)\big|_{\alpha=\alpha_0} \quad \text{and} \quad \partial_k \bar{\lambda}_a = \frac{\partial^2}{\partial\alpha^2}\partial_k U(\alpha,\delta)\big|_{\alpha=\alpha_0}\,, \tag{4.108}$$

repeatedly with $\delta = 0$ or $\delta = \delta_0$ depending on whether the phase is symmetric with respect to δ or not. However, we have not studied the phase with $\alpha \neq 0$ here. For a discussion see [25].

The advantage of this method is that the derivation of the flow equations for the couplings of the effective potential is relatively straightforward. Furthermore, the generalization to spontaneous symmetry breaking is possible. For the d-boson this is discussed in the next chapter and for the **a**-boson in [25, 40]. There have been many approximation schemes developed and applied to various systems, see [48]. For instance, one can go to higher order in an expansion in powers of fields simply by increasing the number of derivatives. However, this method of projection is restricted to zero external momenta of the couplings. For instance, the momentum dependence is needed to regard kinetic terms for the bosons. Moreover, a derivation of flow equations for the Yukawa couplings is not possible in this way. All these issues can be addressed on the basis of (4.38) as explained in section 4.3.

Now we discuss the flow equations for the couplings of the effective potential. In order to be flexible in the choice of the cutoff functions we present it in a cutoff independent form. In appendix C these equations are given more explicitely based on our cutoff scheme. The flow equation for the mass parameter of the **a**-boson reads

$$\begin{aligned} k\partial_k \bar{m}_a^2 = {} & 2\bar{h}_a^2 \sum_P k\tilde{\partial}_k \frac{1}{P_F^k(P) P_F^k(K+P+\Pi)} \\ & -\frac{5}{2}\bar{\lambda}_a \sum_P \frac{k\partial_k R_a^k(P)}{(P_a^k(P)+\bar{m}_a^2)^2}\,, \end{aligned} \tag{4.109}$$

where it is $K = (0, \mathbf{k} = (\hat{k}, 0))$, as discussed in section 4.3.1. Eq. (4.109) consists of a sum over a purely fermionic and a purely bosonic contribution. For finite $\hat{k}$ the fermionic contribution is obtained from eq. (4.45). However, for $\hat{k} = 0$ the fermionic part can be obtained either from eq. (4.107) or from eq. (4.45) by specializing to $K = 0$. The Π-shift in the fermionic propagator is due to the corresponding shift in the definition of the **a**-fields, see eq. (4.4). For the quartic coupling of the **a**-boson it is

$$\begin{aligned} k\partial_k \bar{\lambda}_a = {} & 4\bar{h}_a^4 \sum_P k\tilde{\partial}_k \frac{1}{(P_F^k(P) P_F^k(P+\Pi))^2} \\ & +11\bar{\lambda}_a^2 \sum_P \frac{k\partial_k R_a^k(P)}{(P_a^k(P)+\bar{m}_a^2)^3} - 7\bar{\gamma}_a \sum_P \frac{k\partial_k R_a^k(P)}{(P_a^k(P)+\bar{m}_a^2)^2}\,. \end{aligned} \tag{4.110}$$

Similarly, the flow equations for the couplings of higher orders are

$$\begin{aligned} k\partial_k \bar{\gamma}_a = {} & 8\bar{h}_a^6 \sum_P k\tilde{\partial}_k \frac{1}{(P_F^k(P) P_F^k(P+\Pi))^3} \\ & -27\bar{\zeta}_a \sum_P \frac{k\partial_k R_a^k(P)}{(P_a^k(P)+\bar{m}_a^2)^2} + 102\bar{\lambda}_a\bar{\gamma}_a \sum_P \frac{k\partial_k R_a^k(P)}{(P_a^k(P)+\bar{m}_a^2)^3} \\ & -87\bar{\lambda}_a^3 \sum_P \frac{k\partial_k R_a^k(P)}{(P_a^k(P)+\bar{m}_a^2)^4}\,, \end{aligned} \tag{4.111}$$

and

$$(k\partial_k \bar{\zeta}_a)^F = 16\bar{h}_a^8 \sum_P k\tilde{\partial}_k \frac{1}{(P_F^k(P) P_F^k(P+\Pi))^4}\,. \tag{4.112}$$

In the flow equation to the highest coupling $\bar{\zeta}_a$ we neglect the bosonic contribution.

The flow equations for the couplings of the part of the effective potential which contains the d-fields are derived similar. For the mass term we obtain

$$k\partial_k \bar{m}_d^2 = -4 \sum_P k\tilde{\partial}_k \frac{\bar{h}_d (2P)^2}{P_F^k(P) P_F^k(-P)} - 2\bar{\lambda}_d \sum_P \frac{k\partial_k R_d^k(P)}{(P_d^k(P)+\bar{m}_d^2)^2}\,. \tag{4.113}$$

Again the fermionic term can be derived either on the basis of eq. (4.45) by specializing to $K = 0$ or from the analog of eq. (4.107). Note that the momentum structure in the fermionic propagators differs from the accordant term for the mass of the **a**-boson. For the bosonic contribution the same two possibilities apply, of course. The flow equation for the quartic coupling reads

$$\begin{aligned} k\partial_k \bar{\lambda}_d = {} & 16 \sum_P k\tilde{\partial}_k \frac{\bar{h}_d (2P)^4}{(P_F^k(P) P_F^k(-P))^2} \\ & +2\bar{\lambda}_d^2 \sum_P \left\{ \frac{4\, k\partial_k R_d^k(P)}{(\tilde{P}_d^k(P)+\bar{m}_d^2)^3} + \frac{k\partial_k R_d^k(P)}{(\tilde{P}_d^k(P)+\bar{m}_d^2)^2 (\tilde{P}_d^k(-P)+\bar{m}_d^2)} \right\} \\ & -6\bar{\gamma}_d \sum_P \frac{k\partial_k R_d^k(P)}{(\tilde{P}_d^k(P)+\bar{m}_d^2)^2}\,. \end{aligned} \tag{4.114}$$

Similar as for the **a**-boson we restrict the flow equation for the coupling of highest order to the fermionic contribution

$$(k\partial_k \bar{\gamma}_d)^F = -32 \sum_P k\tilde{\partial}_k \frac{\bar{h}_d (2P)^6}{(P_F^k(P) P_F^k(-P))^3}\,. \tag{4.115}$$

In figure 4.6 the action of the fermionic regulator is shown.

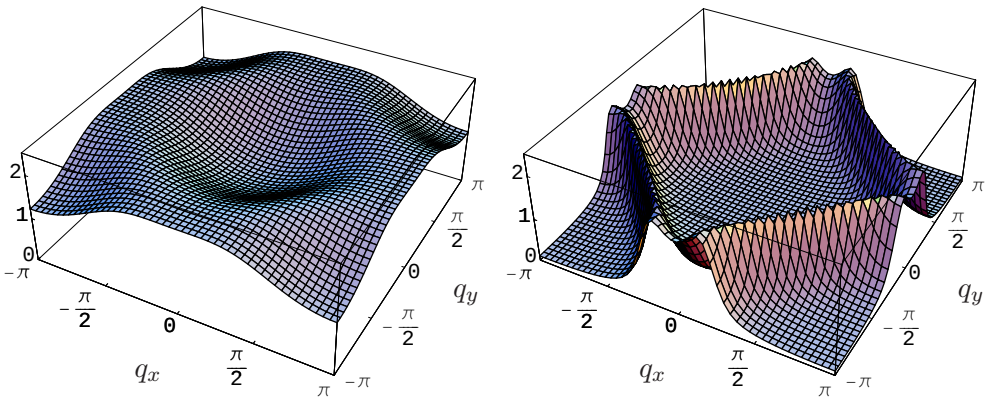

Figure 4.6: Action of the fermionic regulator. A typical integrand on the rhs of the flow equations is $\sim F_1(\frac{0.2+2(\cos q_x+\cos q_y)}{2T_k/t})$ which is plotted in (a) for $T_k/t = 2$ and in (b) for $T_k/t = 0.2$. For definition of F_1 see appendix D. Lower T_k corresponds to lower scale k and modes with momenta in the vicinity of the Fermi surface are more pronounced at lower scales as it is required.

4.5.2 Kinetic Terms of the Bosons

At the initial scale the bosonic fields introduced by partial bosonization have no kinetic terms. However, during the flow to lower momentum scales these bosonic fields become dynamic and finite kinetic terms are generated. In the symmetric phase we consider for both bosons only the fermionic contributions, see the first and second diagram in figure 4.1. The bosonic contributions, see e.g. the last but one diagram in figure 4.1, do not contribute since we consider the quartic couplings independent on momenta within our truncation.

For the kinetic term of the **a**-field we have to account for the two qualitatively different situations discussed in section 4.3.1. The flow equation for the gradient coefficient A_a evaluated at vanishing momenta, defined in eq. (4.48), reads

$$k\partial_k A_a = -\frac{T}{t^2}(k\partial_k T_k)\bar{h}_a^2 \int_{-\pi}^{\pi} \frac{d^2p}{(2\pi)^2} \frac{\partial}{\partial T_k}\frac{\partial^2}{\partial l^2} \times \frac{\tanh(\frac{\xi_{\mathbf{p}}}{2T_k}) - \tanh(\frac{\xi_{\mathbf{le_x}+\boldsymbol{\pi}+\mathbf{p}}}{2T_k})}{2T_k(\xi_{\mathbf{p}} - \xi_{\mathbf{le_x}+\boldsymbol{\pi}+\mathbf{p}})}\bigg|_{l=0} . \quad (4.116)$$

On high momentum scales A_a grows from initially zero to positive values and in the commensurate case A_a stays positive on all scales, see figure 4.7 (a). However, sufficiently away from half-filling A_a decreases and becomes negative

on lower momentum scales, see figure 4.7 (b). This indicates the formation of the four minima at the positions $\mathbf{k}_{1,2} = (\pm\hat{k}, 0)$ and $\mathbf{k}_{3,4} = (0, \pm\hat{k})$, as described in section 4.3.1. A flow equation for $\hat{k}$ can be derived from the condition

$$\frac{d}{dk}\frac{\partial \Delta P^F_{a,k}(\Omega_K = 0, \mathbf{k} = (k_x, k_y = 0))}{\partial k_x}\bigg|_{k_x=\hat{k}} = 0\,. \tag{4.117}$$

which can be simplified for momentum independent Yukawa coupling $\bar{h}_a$ to

$$\frac{d}{dk} f(T_k, \hat{k}) = 0\,, \tag{4.118}$$

where

$$\begin{aligned} f(T_k, \hat{k}) = &\int_{-\pi}^{\pi} \frac{d^2p}{(2\pi)^2}(t - 2t'\cos p_y)\sin(p_x + \hat{k}) \\ &\times\left\{\frac{\tanh\Xi_1 - \tanh\Xi_2}{(\Xi_1 - \Xi_2)^2} - \frac{1}{(\Xi_1 - \Xi_2)\cosh^2\Xi_2}\right\}\bigg|_{\mathbf{k}=(\hat{k},0)^T}, \end{aligned} \tag{4.119}$$

with $\Xi_1 = \frac{\xi_{\mathbf{p}}}{2T_k}$ and $\Xi_2 = \frac{\xi_{\mathbf{p}+\mathbf{k}+\boldsymbol{\pi}}}{2T_k}$. This yields for the flow equation of $\hat{k}$

$$(k\partial_k\hat{k})\frac{\partial}{\partial\hat{k}} f(T_k, \hat{k}) = -(k\partial_k T_k)\frac{\partial}{\partial T_k} f(T_k, \hat{k})\,. \tag{4.120}$$

The initial scale for the flow of $\hat{k}$ is defined by the scale at which A_a becomes zero, see figure 4.7 (b). We start the flow with the initial value $\hat{k} = 0$ on this scale. Eventually, there are regions in the parameter space where the flow of $\hat{k}$ is discontinuous at the initial scale. In this case one should rather start with a finite initial value of $\hat{k}$ as appropriate for a discontinuous transition. The final value for $\hat{k}$ becomes larger for increasing chemical potential μ.

The flow equation for the gradient coefficient $\hat{A}_a$ evaluated in the minima, defined in eq. (4.56), is

$$\begin{aligned} k\partial_k\hat{A}_a = &-\frac{T}{t^2}(k\partial_k T_k)\bar{h}_a^2\int_{-\pi}^{\pi}\frac{d^2p}{(2\pi)^2}\frac{\partial}{\partial T_k}\frac{\partial^2}{\partial l^2} \\ &\qquad\times\frac{\tanh(\frac{\xi_{\mathbf{p}}}{2T_k}) - \tanh(\frac{\xi_{\mathbf{le_x}+\boldsymbol{\pi}+\mathbf{p}}}{2T_k})}{2T_k(\xi_{\mathbf{p}} - \xi_{\mathbf{le_x}+\boldsymbol{\pi}+\mathbf{p}})}\bigg|_{l=\hat{k}} \\ &-\frac{T}{t^2}(k\partial_k\hat{k})\bar{h}_a^2\int_{-\pi}^{\pi}\frac{d^2p}{(2\pi)^2}\frac{\partial}{\partial\hat{k}}\frac{\partial^2}{\partial l^2} \\ &\qquad\times\frac{\tanh(\frac{\xi_{\mathbf{p}}}{2T_k}) - \tanh(\frac{\xi_{\mathbf{le_x}+\boldsymbol{\pi}+\mathbf{p}}}{2T_k})}{2T_k(\xi_{\mathbf{p}} - \xi_{\mathbf{le_x}+\boldsymbol{\pi}+\mathbf{p}})}\bigg|_{l=\hat{k}}. \end{aligned} \tag{4.121}$$

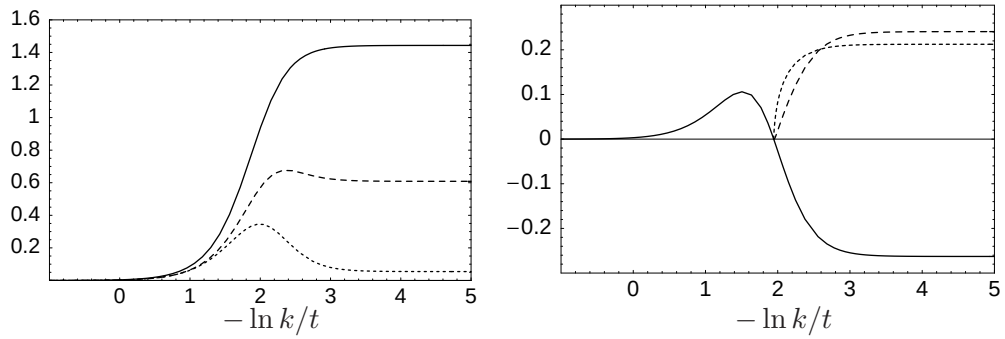

Figure 4.7: Numerical results to the flow equation. In (a) A_a is presented, the solid line corresponds to $\mu/t = -0.1$, $T/t = 0.1367$, the long-dashed line to $\mu/t = -0.16$, $T/t = 0.105$, and the short-dashed line to $\mu/t = -0.2$, $T/t = -0.11$. In (b) it is $\mu/t = -0.3$, $T/t = 0.1225$ and the solid line shows A_a which becomes negative, the short-dashed line shows $\hat{k}$ and the long-dashed line shows $\hat{A}_a$.

For the frequency dependence we set $Z_a = A_a$ as in [25] in parameter regions where A_a stays positive on all scales. In the other case we simply use

$$k\partial_k Z_a = \frac{(k\partial_k T_k)}{(2\pi T)^2}\frac{\partial}{\partial T_k}(P_a^k(\Omega_Q = 2\pi T, \mathbf{q} = 0) - P_a^k(\Omega_Q = 0, \mathbf{q} = 0))\,. \quad (4.122)$$

This completes our discussion of the kinetic term of the **a**-boson. For the gradient coefficient of the d-boson the flow equation is

$$k\partial_k A_d = -\frac{T}{t^2}(k\partial_k T_k)\int_{-\pi}^{\pi}\frac{d^2p}{(2\pi)^2}\frac{\partial}{\partial T_k}\frac{\partial^2}{\partial l^2}\bar{h}_d^2(2\mathbf{p}-l\mathbf{e_x}) \times\frac{\tanh(\frac{\xi_{\mathbf{p}}}{2T_k})+\tanh(\frac{\xi_{l\mathbf{e_x}-\mathbf{p}}}{2T_k})}{T_k(\xi_{\mathbf{p}}+\xi_{l\mathbf{e_x}-\mathbf{p}})}\Bigg|_{l=0}\,. \quad (4.123)$$

The flow equation for the wave function renormalization Z_d reads

$$k\partial_k Z_d = -T(k\partial_k T_k)\int_{-\pi}^{\pi}\frac{d^2p}{(2\pi)^2}\bar{h}_d^2(2\mathbf{p})\frac{\partial}{\partial T_k}\frac{\partial}{i\partial\Omega} \times\frac{\tanh(\frac{\xi_{\mathbf{p}}}{2T_k})+\tanh(\frac{\xi_{\mathbf{p}}}{2T_k}+\frac{i\Omega}{2T})}{T_k(\xi_{\mathbf{p}}+i\Omega\frac{T_k}{2T})}\Bigg|_{\Omega=0}\,. \quad (4.124)$$

However, close to half-filling the linear frequency dependence $\sim iZ_d\Omega_Q$ is suppressed by symmetry and we describe the frequency dependence by $P_d(\Omega_Q, \mathbf{q} = 0) = Z_{d,2}\Omega_Q^2$. For simplicity and since it shows the right qualitative behavior we set $Z_{d,2} = A_d$.

4.5.3 Yukawa Couplings

According to eqs. (4.98) and (4.99) the modified flow equations for the Yukawa couplings are composed of two additive contributions. It is about a direct contribution and a contribution due to rebosonization,

$$k\partial_k \bar{h}_a = \beta^d_{\bar{h}_a} + \beta^{rb}_{\bar{h}_a} \quad \text{and} \quad k\partial_k \bar{h}_d = \beta^d_{\bar{h}_d} + \beta^{rb}_{\bar{h}_d}\,. \tag{4.125}$$

Based on the one-loop calculations performed in sections 4.3.2 we obtain for the direct contributions

$$\begin{aligned}\beta^d_{\bar{h}_a} = &-\bar{h}_a^3 \sum_P k\tilde{\partial}_k \frac{1}{P_F^k(P)P_F^k(P+\Pi)(P_a^k(P)+\bar{m}_a^2)} \\ &+4\bar{h}_a \sum_P k\tilde{\partial}_k \frac{\bar{h}_d(P)^2}{P_F^k(P)P_F^k(P+\Pi)(P_d^k(P)+\bar{m}_d^2)}\,,\end{aligned} \tag{4.126}$$

for the **a**-boson with external momenta equal to zero, and

$$\begin{aligned}&\beta^d_{\bar{h}_d}(2Q-K) \\ &= -\frac{3}{2}\bar{h}_a^2 \sum_P k\tilde{\partial}_k \frac{\bar{h}_d(2Q+2P-K)}{P_F(Q+P-\Pi)P_F^k(K-Q-P+\Pi)(P_a^k(P)+\bar{m}_a^2)} \\ &\quad +(Q \to K-Q)\,,\end{aligned} \tag{4.127}$$

for the d-boson. For the contributions from rebosonization we proceed as described in section 4.5. Starting point to derive the contribution for the **a**-boson are on the one hand the one-loop contributions (4.76). On the other hand we learn from eq. (4.84) how to restrict the external momenta. Finally, we find in agreement with [40, 25]

$$\begin{aligned}\beta^{rb}_{\bar{h}_a} = \bar{h}_a^3 \bar{m}_a^2 \sum_P k\tilde{\partial}_k &\frac{1}{(P_a^k(P)+\bar{m}_a^2)(P_a^k(\Pi-P)+\bar{m}_a^2)P_F^k(-P)} \\ &\times\left\{\frac{1}{P_F^k(\Pi-P)} - \frac{1}{P_F^k(P)}\right\}.\end{aligned} \tag{4.128}$$

The explicit formulae for the β-functions of the Yukawa couplings within our regularization scheme are presented in appendix C. There exists a rebosonization contribution to the Yukawa coupling of the d-boson as well, we postpone the discussion hereof to the next section.

In the contributions which involve both fermionic and bosonic internal lines we have neglected the frequency dependence of the bosonic propagators. On high momentum scales this is justified since the kinetic terms of the bosons are anyway small compared to the bosonic masses. However, on low momentum

scales the mode with lowest frequency dominates while higher modes are suppressed. If we neglect the frequency dependence of the bosonic propagators the suppression of the higher frequency modes is only due to the fermionic propagators and therefore weakened.

4.6 Generation of a Coupling in the d-wave Channel

In this section we discuss how a coupling in the d-wave channel can be generated by the exchange of spin waves. This mechanism was suggested e.g. by [5, 15]. On initial scale we have bosonized the fermionic coupling into the antiferromagnetic channel. The fermionic couplings in all other channels vanish for this reason and the interaction between the electrons is firstly repulsive. However, even in the case of purely repulsive forces between the electrons the system may become unstable against Cooper-pair formation [59].

At first, we address the question what is the origin of a fermionic coupling in the d-wave channel which becomes critical in an appropriate parameter region. Subsequently, it is discussed how we can deal with this d-wave coupling by the method of rebosonization.

Within our truncation there remains only one possible origin of the fermionic d-wave coupling, namely the box diagrams exchanging only **a**-bosons. See the first two diagrams in figure 4.5 and formula (4.76). The other box diagrams are proportional to powers of the Yukawa coupling $\bar{h}_d$ which is zero on initial scale. At first we discuss the flow equation for the fermionic coupling in the d-wave channel. The strategy is the following. We start from eq. (4.76), follow the discussion of section 4.4 and use eq. (4.90) to restrict the external momenta appropriately. In this way we obtain a flow equation for the four fermion coupling which is a function of the restricted external momenta. However, it still contains contributions also from other channels and one has to project onto the contribution of the d-wave channel. For a first estimate, we apply here a very simple prescription which uses the fact that the d-wave coupling changes its sign under rotation of 90 degrees. Further, we project on spin singlets for the fermion bilinears. More concretely, we choose $K_1 = -K_3 \equiv L$ and $K_2 = -K_4 \equiv L'$ and apply

$$\begin{aligned} & k\partial_k \lambda_\psi^d\big|_{B_k}(L, L', -L, -L') \\ = \; & \frac{1}{2}\big\{\Delta\dot{\Gamma}_F^{aa(4)}(L = (\pi m T_k, \mathbf{l}), L' = (\pi m' T_k, \mathbf{l}')) \\ & -\Delta\dot{\Gamma}_F^{aa(4)}(L = (\pi m T_k, D(\mathbf{l}; \frac{\pi}{2})), L' = (\pi m' T_k, \mathbf{l}'))\big\}\,. \end{aligned} \tag{4.129}$$

The $\dot{}$ on $\Delta\Gamma_F^{aa(4)}$ denotes the insertion of $k\tilde{\partial}_k$ under the measure and $D(\mathbf{l}; \alpha)$ denotes a rotation of $\mathbf{l}$ by the angle α. In eq. (4.129) we have kept L' fixed

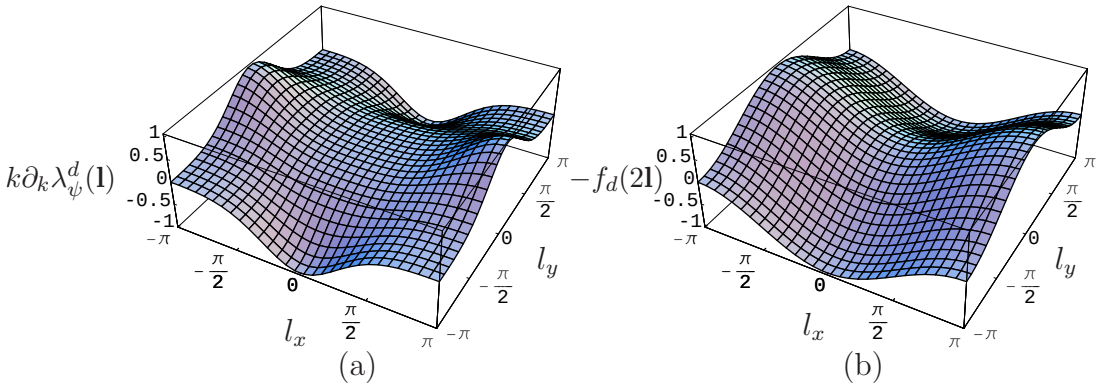

Figure 4.8: In (a) the normalized momentum dependence of the rhs of the flow equation for the fermionic coupling for $\mu/t = -0.4$, $t' = 0$ and $T/t = 0.5$ is shown. The normalized d-wave form factor is shown in (b).

and subtracted the same contribution after a rotation of 90 degrees of the space-like components of L. For instance, the antiferromagnetic channel is subtracted in this way. In figure 4.8 (a) the rhs of eq. (4.129) is presented on the initial scale as a function of $\mathbf{l}$ where we set $\mathbf{l}' = (0, \pi)$. There is a good qualitative agreement with the d-wave form factor displayed in figure 4.8 (b). Therefore, we describe the momentum dependence of the rhs of eq. (4.129) by a product of two d-wave form factors $f_d(2\mathbf{l}) f_d(2\mathbf{l}')$ multiplied by a single fermionic coupling. We fix the momenta $\mathbf{l}$ and $\mathbf{l}'$ and derive a flow equation for this single fermionic coupling which is independent of the external momenta. The effect of the other box-diagrams, see figure 4.5, is neglected in this first estimate.

The flow of this d-wave channel fermionic coupling can now be treated by the method of rebosonization. It enters the modified flow equation for the Yukawa coupling (4.99) of the d-boson. For the rebosonization contribution of the Yukawa coupling of the d-boson we finally obtain with the above declared choice of external momenta ($K_1 = -K_3 \equiv L$ and $K_2 = -K_4 \equiv L'$)

$$(k\partial_k \bar{h}_d^2)^{rb} = \bar{m}_d^2 \frac{k\partial_k \lambda_\psi^d\big|_{B_k}(L, L', -L, -L')}{f_d(2\mathbf{l}) f_d(2\mathbf{l}')}\,, \tag{4.130}$$

where the momentum dependence of the fraction cancels approximately as it should. Here we choose $\mathbf{l} = (\pi, 0)$ and $\mathbf{l}' = (0, \pi)$ and the explicit result is presented in appendix C.

4.7 Numerical Results

We now turn to the numerical analysis of the flow equations we have derived above. The differential equations were integrated with the program *Serge*[5] which is built on a standard, adaptive Runge-Kutta-like routine [60]. We have studied our truncation over a wide range of the chemical potential μ. In the following, until stated otherwise, we set the initial coupling of the Hubbard model $U/t = 3$.

At first we have considered a simpler truncation where we have neglected fluctuations in the d-wave channel and also have neglected the flow of $\bar{\gamma}_a$ and $\bar{\zeta}_a$. In figure 4.9 the pseudo-critical temperature T_{pc} of antiferromagnetism is displayed as a function of the chemical potential μ, whereas we have set in (a) $t' = 0$ and in (b) $t'/t = -0.1$. As expected for a bipartite lattice, see the discussion in section 2.3 and eq. (2.15), the pseudo-critical temperature in (a) depends only on the absolute value of the chemical potential. The value of T_{pc} is well below a mean field critical temperature, see [40, 41, 44, 43]. The endpoints of the solid line in figure 4.9 (a) are defined by the fact that for larger values of $|\mu|$ the bosonic quartic coupling becomes zero or negative in the renormalization flow before the bosonic mass vanishes. In case of a negative bosonic quartic coupling a transition to the symmetry broken regime is discontinuous and the expectation value of corresponding bosonic field jumps discontinuously to a finite value in the renormalization flow. However, the bosonic potential is not stable anymore in our truncation and one has to extend the truncation. For a discussion of the broken phase at half-filling, see [25, 40]. In figure 4.9 (b), where $t'/t = -0.1$, the lattice is not bipartite anymore and the solid line is not symmetric with respect to reflections $\mu \to -\mu$. Particularly, the maximum of the curve is shifted towards a finite value of μ and furthermore, it is not symmetric about this maximum. The endpoints of the solid line are defined analogously as in 4.9 (a). Moreover, T_{pc} is lower for a finite t' as in the case of vanishing t'. A finite t' lowers the ratio of the fermionic interaction term to the fermionic kinetic term which gives rise to a lower value of T_{pc}.

Figure 4.10 is based on both antiferromagnetic fluctuations and fluctuations in the d-wave channel. We set $t' = 0$ in the following and the resulting picture again is symmetric under the transformation $\mu \to -\mu$. The solid line near $\mu = 0$ shows the pseudo-critical temperature T_{pc} of antiferromagnetism, the dashed line at larger values of $|\mu|$ shows T_{pc} of d-wave superconductivity. In the region of the solid line we have neglected the flow of $\bar{\gamma}_a$ and $\bar{\zeta}_a$. The inclusion of fluctuations in the d-wave channel reduces T_{pc} of antiferromagnetism and this effect becomes stronger for increasing absolute values of the chemical potential

[5]The computer code *Serge* was written by E. Bick, D. Föthke, F. Höfling and C. Nowak in Heidelberg.

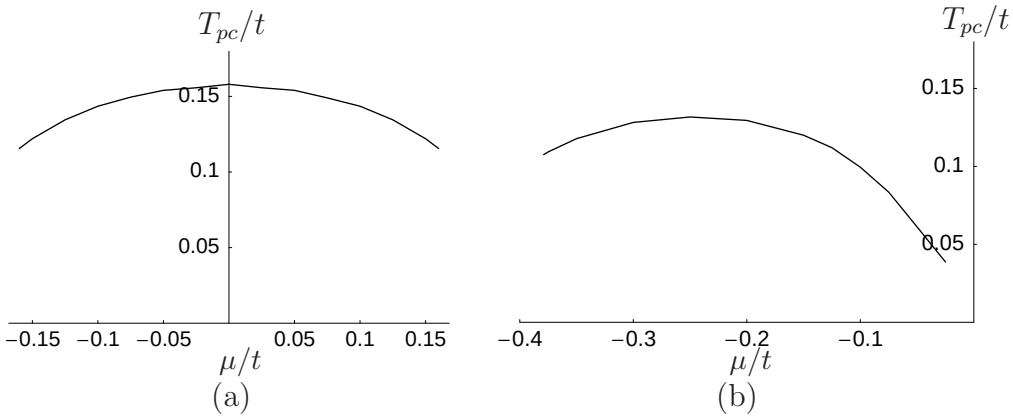

Figure 4.9: Pseudo-critical temperature T_{pc}/t with neglected d-wave fluctuations. In (a) it is $t' = 0$, note the symmetry with respect to the transformation $\mu \to -\mu$ as expected on a bipartite lattice. In (b) it is $t'/t = -0.1$.

$|\mu|$, compare with 4.9. The endpoint of the solid line at finite μ indicates the end of the region where the transition to the symmetry broken region is continuous in the renormalization flow. Again this is reflected by a negative quartic bosonic coupling $\bar{\lambda}_a$ in the renormalization flow whereas the mass of the **a**-boson stays positive. In figure 4.11 (a) a typical flow of several couplings for $\mu/t = -0.1$ and $T/t = 0.1367$ is presented. It defines one point in the solid line of figure 4.10. The mass parameter of the **a**-field decreases and hits zero on a finite scale k_{SSB}. On lower scales $k < k_{SSB}$ it increases slightly driven by the bosonic contribution to the flow. A better truncation for the bosonic potential enlarges this effect. The mass parameter of the d-boson stays finite. In addition the flow of the quartic coupling and the Yukawa coupling of the **a**-boson are displayed. Here, the quartic coupling $\bar{\lambda}_a$ stays positive at low momentum scales. The flow of the Yukawa coupling $\bar{h}_a$ is rather weak but its influence makes the largest part of the difference between a mean field critical temperature [40, 41, 44, 43] and T_{pc}. However, for larger values of $|\mu|$ the coupling $\bar{h}_a$ flows to considerably lower values. In figure 4.11 (b) the situation is reversed and one point in the dashed line of 4.10 is exposed. Here, the mass of the d-boson decreases and hits zero on a finite momentum scale k_{SSB}. Subsequently it increases slightly in the renormalization flow also driven by bosonic contribution to the flow. In this case, the mass of the **a**-boson stays positive. Furthermore, one sees very clearly that at first antiferromagnetic spin fluctuations generate a finite coupling $\bar{h}_d$ and particularly, this finite coupling $\bar{h}_d$ drives the flow of e.g. $\bar{m}_d^2$ and $\bar{\lambda}_d$. The quartic coupling $\bar{\lambda}_d$ of the d-boson stays non-negative which also holds for arbitrary μ.

The just now described picture can be viewed as a competition between

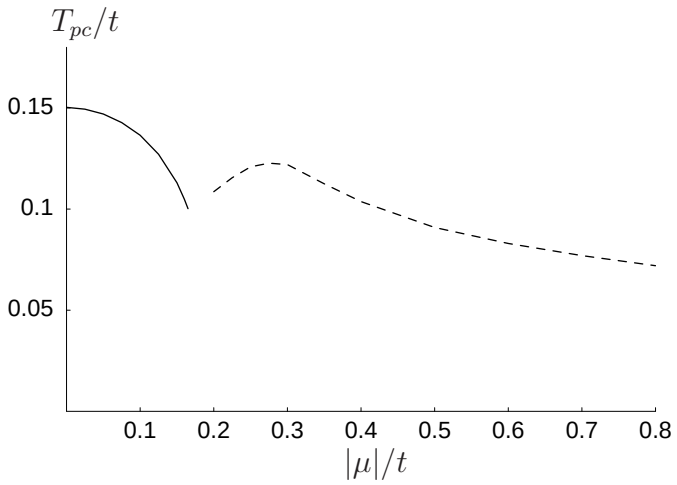

Figure 4.10: Pseudo-critical temperature as a function of the chemical potential μ for antiferromagnetism (solid line) and d-wave superconductivity (dashed line).

the two different instabilities, the tendency towards antiferromagnetism or d-wave superconductivity. Close to $\mu = 0$, and indicated by the solid line, antiferromagnetic fluctuations prevail and the system becomes unstable in the antiferromagnetic channel. Whereas, for sufficiently large chemical potential the system becomes unstable in the d-wave channel. The pseudo-critical temperature of d-wave superconductivity has a maximum at $|\mu|/t \approx 0.28$, see the dashed line. For larger values of $|\mu|$ the dashed line decreases since the fluctuations are suppressed by the chemical potential. This is seen qualitatively

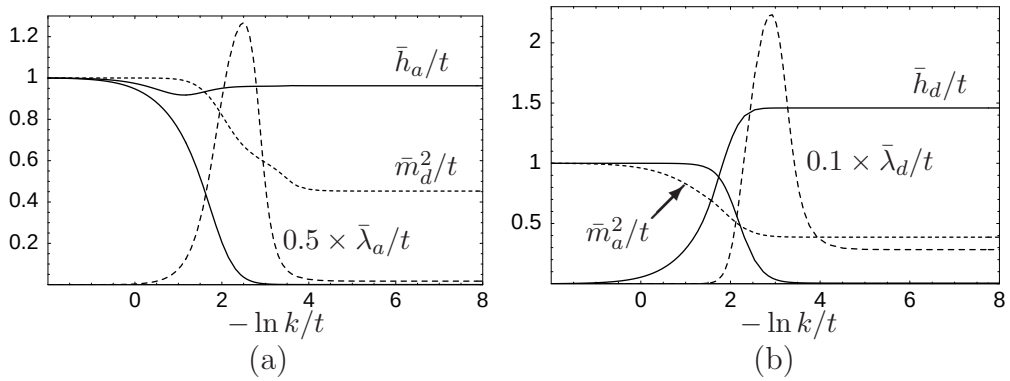

Figure 4.11: In (a) it is $\mu/t = -0.1$ and $T/t = 0.1367$, the decreasing solid line displays $\bar{m}_a^2$ which hits zero while $\bar{m}_d^2$ stays much larger. In (b) with $\mu/t = -0.4$ and $T/t = 0.104$, the situation is reversed. $\bar{m}_d^2$ indicated by the solid line hits zero whereas $\bar{m}_a^2$ stays much larger.

already in a mean field calculation, see e.g. [40, 41]. However, the increase of T_{pc} in the d-wave channel up to $|\mu|/t \approx 0.28$ is remarkable. In this range antiferromagnetic fluctuation generate a strong coupling in the d-wave channel and the corresponding Cooper instability still prevails. The coupling in the antiferromagnetic channel is also large, indicated by the fact that the mass of the $\mathbf{a}$-field decreases to small values. In this intermediate regime the system decides at comparatively low temperatures which instability prevails. However, a better treatment of the frequency dependence of the bosonic popagator is expected to lower the value of T_{pc}. Between the solid and the dashed line we have omitted a small region of chemical potential. In this region one has to extend the truncation since on this level of truncation it is not clear whether a continuous transition into the symmetry broken regime of d-wave superconductivity or a discontinuous transition into the symmetry broken regime of antiferromagnetism comes first in the renormalization flow. This issue may be clarified by the inclusion of further higher fermionic operators which correspond to bosonic interactions in our language. For instance, a term $\sim \mathbf{a}\cdot\mathbf{a}\, d^* d$, see eq. (4.17), couples the two species of bosonic fields and is expected to be important in this intermediate regime.

Moreover, the location of this intermediate region depends on the value of the coupling U of the Hubbard model. If we set $U/t = 2$ this region is shifted to $|\mu|/t \approx 0.06$ which is considerably lower as for $U/t = 3$, compare with figure 4.10. The tendency, that a decreasing value of U shifts the boundary between the antiferromagnetic and the d-wave superconducting instabilities to lower values for $|\mu|$, has also been found in [15].

Chapter 5

Kosterlitz-Thouless Transition to d-wave Superconductivity

In chapter 4 we have demonstrated how a coupling in the d-wave channel is generated by antiferromagnetic (spin wave) fluctuations in the two-dimensional Hubbard model within our bosonized functional renormalization group framework. Particularly, the competition between fluctuations in the antiferromagnetic and the d-wave pairing channel has been studied. Close to half-filling, which here corresponds to vanishing chemical potential, the antiferromagnetic channel becomes critical. Sufficiently away from half-filling the different topology of the Fermi surface does not promote antiferromagnetic fluctuations and the antiferromagnetic channel is far from being critical. However, these fluctuations are still present and cause the creation of a coupling in the d-wave channel. Once such a coupling in a Cooper-pair channel has been created, and in addition there are no other instable channels, there is a temperature (pseudo-critical temperature T_{pc}) below which the fermionic coupling in the Cooper-pairing channel diverges in the renormalization flow. Concretely, we have detected this divergence by a vanishing of the mass parameter of the d-boson on a finite scale in the renormalization flow. The resulting pseudo-critical temperature T_{pc} is displayed over a wide range of chemical potential in figure 4.10.

This chapter is devoted to a study of the phase transition to d-wave superconductivity within a simplified model which is characterized by the presence of a coupling solely in the d-wave pairing channel. The emergence of such an effective model on lower scales in context of the Hubbard model is well motivated by the results presented in chapter 4. Here, we concentrate on the temperature dependence of d-wave superconducting order by means of the functional renormalization group with partial bosonization. In particular, the phase transition from the high temperature "symmetric phase" to the low temperature superconducting phase is studied. As characteristic features we find (i) essential scaling as the critical temperature T_c is approached from above, (ii) a massless Goldstone mode for $T < T_c$ leading to superfluidity, (iii) a tem-

perature dependent anomalous dimension η for $T < T_c$, (iv) a jump in the renormalized superfluid density at T_c and (v) a gap in the electron propagator for $T < T_c$ which vanishes non-analytically as $T \to T_c$ [26].

The features (i)-(iv) are characteristic for a Kosterlitz-Thouless (KT) phase transition [61, 62, 63] which is a natural candidate for a universality class with a global $U(1)$ symmetry. Actually, while in the infinite volume limit the "bare" order parameter vanishes in accordance with the Mermin-Wagner theorem [64], a renormalized order parameter [65] spontaneously breaks the $U(1)$ symmetry for $T < T_c$, leading to an infinite correlation length for the Goldstone mode. Vortices arise as topological defects for $T < T_c$. In the Hubbard model the fermionic excitations (single electrons or holes) are an important ingredient for driving the transition. Finally, coupling our model to electromagnetic fields the photon acquires a mass through the Higgs mechanism while the Goldstone mode disappears from the spectrum, being a gauge degree of freedom. Superfluidity is replaced by superconductivity. Recently, various experimental data have been interpreted as signatures of KT phase fluctuations [66, 67, 68, 69]. The direct relation between real high temperature superconductors and the two-dimensional Hubbard model is difficult, however.

5.1 Effective Model for d-wave Superconductivity

The problem of d-wave superconductivity in the Hubbard model can be separated into two qualitative steps in the renormalization flow. In the first step the fluctuations with momenta $|\mathbf{p}^2 - \mathbf{p}_F^2| > \Lambda^2$ (with $\mathbf{p}_F$ on the Fermi-surface) have to generate a strong effective interaction in the d-wave channel. This phenomenon has been discussed in chapter 4. It has also been observed in other renormalization group studies [15, 18], the d-wave coupling also being triggered by spin wave fluctuations and in various other approaches, see e.g. [70, 71, 72], too. The second step, involving momenta $|\mathbf{p}^2 - \mathbf{p}_F^2| < \Lambda^2$ for the fermions and $\mathbf{p}^2 < \Lambda^2$ for bosonic bound states, has to deal with a situation where the d-wave channel coupling dominates. We only address here the second step. We find that the universal behavior in the vicinity of the critical temperature is dominated by effective bosonic fluctuations and becomes independent of the microscopic details. This justifies our approach with a single coupling λ_ψ^d at the scale Λ in the d-wave channel, even though this remains, of course, only an approximation. The prize to pay is that λ_ψ^d is only an effective coupling – its relation to the parameters t and U of the Hubbard model is expected to depend on T and the chemical potential μ.

We emphasize that we obtain a KT-like phase transition within a purely fermionic model. The effective bosonic degrees of freedom arise as composite

fields – we do not start from a bosonic effective theory. The transition from a fermionic to a bosonic description is a result of the renormalization flow. The complete decoupling of the fermionic degrees of freedom for the description of the critical behavior is a non-trivial result which only holds for a sufficiently large critical temperature T_c. For $T_c \to 0$ interesting modifications reflect the different universality class of a quantum phase transition [73, 74, 75, 76, 77]. Several new features are directly related to the dominance of fermionic fluctuations sufficiently away from the critical region: We find that the critical temperature T_c is below the pseudo-critical temperature T_{pc} where the effective interaction strength for the electrons diverges. On the other hand, the temperature range $T_c < T < T_{pc}$ is strongly affected by fluctuations of composite bosons. For the transition to d-wave superconductivity we find that T_c is actually rather near to T_{pc}. This contrasts to the transition to antiferromagnetism for $\mu = 0$ where T_c has been found substantially below T_{pc} [25]. Other fermionic aspects concern the relation between the gap in the electron propagator and the superfluid order. We also find a quantitatively important finite size effect which modifies the essential scaling for $T \to T_c$. Again it is dominated by the fermionic fluctuations.

Our starting point is an action with nearest and next-nearest neighbor hopping on a two dimensional square lattice with an attractive interaction in the d-wave channel

$$\begin{aligned}\Gamma_\Lambda^F[\psi] = &\sum_Q \psi^\dagger(Q)(i\omega_Q + \epsilon_{\mathbf{q}} - \mu)\psi(Q) \\ &-\lambda_\psi^d \sum_{K_1,\ldots,K_4} \delta_{K_1+K_2,K_3+K_4} 2f_d(\mathbf{k_1}-\mathbf{k_2}) \\ &\quad\times 2f_d(\mathbf{k_3}-\mathbf{k_4})\psi_\downarrow^*(K_3)\psi_\uparrow^*(K_4)\psi_\uparrow(K_2)\psi_\downarrow(K_1)\,. \end{aligned} \tag{5.1}$$

We apply the concept of partial bosonization and employ the following truncation for the effective average action[1]

$$\begin{aligned}\Gamma_k = &\sum_Q \psi^\dagger(Q)(i\omega_Q + \epsilon_{\mathbf{q}} - \mu)\psi(Q) \\ &+\sum_Q d^*(Q)(iZ\Omega_Q + A\,[\mathbf{q}]^2 t^2)d(Q) + \sum_X U(d) \\ &-\sum_{K,Q,Q'} \delta_{K,Q+Q'} 2f_d(\mathbf{q}-\mathbf{q}') \\ &\quad\times\left(d^*(K)\psi_\uparrow(Q)\psi_\downarrow(Q') - d(K)\psi_\uparrow^*(Q)\psi_\downarrow^*(Q')\right), \end{aligned} \tag{5.2}$$

[1] In this chapter we drop the subscript d in some parameters, e.g. $\bar{m}^2$, A, Z, η. There should be no reason for confusion since there is only one type of bosonic field present.

We approximate the effective potential by a quartic polynomial

$$U(d) = \begin{cases} \bar{m}^2\delta + \frac{\bar{\lambda}_d}{2}\delta^2 & \text{(SYM)} \\ \frac{\bar{\lambda}_d}{2}(\delta - \delta_0)^2 & \text{(SSB)} \end{cases}, \tag{5.3}$$

with $\delta = d^*d$. Here (SYM) is used as long as the minimum of U is located at $\phi = 0$, while the regime with spontaneous symmetry breaking (SSB) is characterized by non vanishing $\delta_0 = d_0^* d_0$. The order parameter d_0 determines the size of the gap in the fermion propagator $\Delta(\mathbf{q}) = |2f_d(2\mathbf{q})d_0|$. The generalized couplings Z, A, $\bar{m}^2$, δ_0 and $\bar{\lambda}_d$ depend on k. At the scale Λ our truncation is equivalent to the fermionic action (5.1) provided

$$\bar{m}^2/t = \frac{1}{\lambda_\psi^d/t}\,, \quad \bar{\lambda}_\phi = 0\,, \quad Z = A = 0\,, \tag{5.4}$$

as can be seen by solving for d as a functional of ψ.

We use the same regularization scheme as in chapter 4, see section 4.2, and will follow the flow until a physical scale k_{ph} where k_{ph}^{-1} corresponds to the macroscopic size of the experimental probe. (In practice, our choice $k_{ph}/t = 10^{-9} = e^{-20.723}$ corresponds to a probe size of roughly 1 cm.) For $T < T_c$ we find a non vanishing superfluid density $\delta_0(k_{ph})$ and therefore a non-vanishing gap Δ, while $\delta_0(k_{ph} \to 0) = 0$.

The flow equations for the couplings are already derived in section 4.5. Nevertheless we shortly present the flow equation for the effective potential. Similar as in eqs. (4.105) and (4.106) with eq. (D.25) for $\alpha = 0$ the effective potential in (SYM) flows as

$$\begin{aligned} \partial_k U_k(\delta) \;=\; & \frac{2T(\partial_k T_k)}{T_k} \int_{-\pi}^{\pi} \frac{d^2q}{(2\pi)^2} \gamma_\delta \tanh\gamma_\delta \\ & + \sum_Q \frac{\partial_k R_d^k(Q)[P_d^k(-Q) + \bar{m}^2 + 2\bar{\lambda}_d\delta]}{[P_d^k(Q) + \bar{m}^2 + 2\bar{\lambda}_d\delta][P_d^k(-Q) + \bar{m}^2 + 2\bar{\lambda}_d\delta] - \bar{\lambda}_d^2\delta^2}\,, \end{aligned} \tag{5.5}$$

where

$$\begin{aligned} \gamma_\delta \;&=\; \frac{1}{2T_k}\sqrt{(\epsilon_\mathbf{q} - \mu)^2 + \Delta^2(\mathbf{q})}\,, \\ P_d^k(Q) \;&=\; iZ\omega_B + A\,[\mathbf{q}]^2 t^2 + R_d^k(Q)\,. \end{aligned} \tag{5.6}$$

For the mass parameter and the bosonic quartic coupling this yields

$$\partial_k \bar{m}^2 = \frac{\partial}{\partial\delta}\partial_k U_k(\delta)|_{\delta=0}\,, \quad \partial_k \bar{\lambda}_d = \frac{\partial^2}{\partial^2\delta}\partial_k U_k(\delta)|_{\delta=0}\,. \tag{5.7}$$

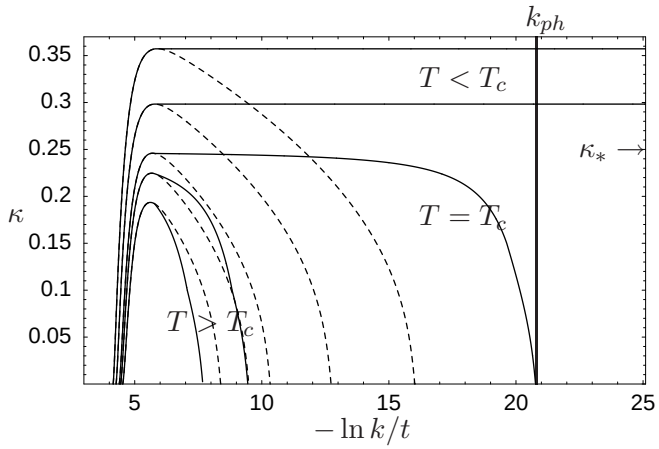

Figure 5.1: Flow of $\kappa(k)$ for T/t=(0.037 , 0.0369 ,T_c/t , 0.0365 , 0.036) with $T_c/t = 0.03681$ and $t'/t = -0.1\,, \lambda^d_\psi/t = 5/8\,,\ \mu/t = -0.6$.

The fermionic fluctuations generate frequency and gradient terms for the bound state bosons (SYM regime), see eqs. (4.124) and (4.123) respectively. There are no bosonic contributions to the flow of Z and A to this level of approximation. The flow starts in the symmetric regime (5.3) with initial values (5.4) and we choose $\Lambda/t = 0.5$. For temperatures below a pseudo-critical temperature T_{pc} the scale dependent mass term $\bar{m}^2$ vanishes at a certain critical scale k_{SSB}. This signals local ordering and indeed corresponds to a divergent effective four fermion coupling $\bar{\lambda}^d_\psi(k)$. Below k_{SSB} we use the truncation (SSB) in (5.3).

We do not consider here the region of very small T where interesting quantum critical phenomena may occur [77]. Then classical statistics dominates the flow for $k \ll T$. A typical flow in the SSB regime is depicted in figure 5.1, where we show $\kappa = t^2 A\delta_0/T$ for various values of T and $t'/t = -0.1$, $\lambda^d_\psi/t = 5/8$, $\mu/t = -0.6$. The fermionic fluctuations (first term in eq. (5.5)) first drive $\bar{m}^2(k)$ to zero and induce non vanishing $\kappa(k)$, starting from $\kappa(k_{SSB}) = 0$. For $k \ll k_{SSB}$ the effect of the fermionic fluctuations is strongly reduced due to the suppression with powers k/T from $\partial_k T_k$ and the presence of a non-vanishing gap Δ. Now the bosonic fluctuations take over and tend to reduce the value of $\kappa(k)$ as k is lowered further. For the region around and on the right of the maximum of $\kappa(k)$ in figure 5.1 we have already $k \ll T$. Then the Matsubara frequency $m = 0$ dominates the bosonic contributions and the system gets reduced to classical statistics for the $O(2)$ linear σ-model. One can see this effective reduction from 2+1 to 2 dimensions explicitly by evaluating the bosonic contribution in eq. (5.5) (the second term, denoted by $\partial_k U^B_k$). Keeping only

the $m = 0$ contribution the flow equation simplifies considerably

$$\partial_k U_k^B(\delta) \;=\; \frac{TAk}{2}\int_{-\pi}^{\pi}\frac{d^2q}{(2\pi)^2}\big(2-\eta(k)(1-\frac{\mathbf{q}^2t^2}{k^2})\big)\Theta(k^2-\mathbf{q}^2t^2\big) \times\left\{\frac{1}{Ak^2+(\delta-\delta_0)\bar{\lambda}_d}+\frac{1}{Ak^2+(3\delta-\delta_0)\bar{\lambda}_d}\right\}. \quad (5.8)$$

Here $\eta(k) = -\frac{\partial \ln A}{\partial \ln k}$ defines the anomalous dimension.

For a better understanding of the scaling behavior we introduce rescaled and renormalized quantities

$$u = \frac{t^2}{Tk^2}U\,, \quad \tilde{\delta} = \frac{t^2A}{T}\delta\,, \quad \kappa = \frac{t^2A}{T}\delta_0\,. \quad (5.9)$$

This yields for the flow of the rescaled effective potential, now at fixed $\tilde{\delta}$ instead of fixed δ,

$$k\partial_k u_k = -2u_k + \eta(k)\,\tilde{\delta}\,\frac{\partial u_k}{\partial\tilde{\delta}} + \frac{t^2}{Tk^2}k\partial_k U_k|_{\delta}\,, \quad (5.10)$$

implying for the renormalized field expectation value κ and bosonic quartic coupling λ_d

$$\partial_k\kappa = -\frac{1}{\lambda_d}\frac{\partial}{\partial\tilde{\delta}}\partial_k u_k|_{\tilde{\delta}=\kappa}\,, \quad \partial_k\lambda_d = \frac{\partial^2}{\partial^2\tilde{\delta}}\partial_k u_k|_{\tilde{\delta}=\kappa}\,. \quad (5.11)$$

The bosonic contribution to the anomalous dimension in SSB is the same as for the linear $O(2)$ model in two dimensions [65]

$$\eta(k) = \frac{1}{\pi}\frac{\lambda_d^2\kappa}{(1+2\lambda_d\kappa)^2} = \frac{1}{4\pi\kappa} + O(\kappa^{-2})\,, \quad (5.12)$$

while the fermionic contribution can be neglected.

The β-functions can be expanded in powers of $(2\lambda_d\kappa)^{-1}$. In particular, to leading order one finds

$$k\partial_k\kappa = \beta_\kappa = O(\kappa^{-1})\,, \quad k\partial_k\lambda_d = -2\lambda_d + \frac{\lambda_d^2}{2\pi} + O(\kappa^{-1})\,, \quad (5.13)$$

resulting in an infrared attractive fixed point for λ_d. The running of κ can be mapped to the running of the coupling in the non-linear σ-model for arbitrary $O(N)$-models [65, 78, 79]. For $N = 2$ also the term $\sim \kappa^{-1}$ in β_κ has to vanish, even though this is not seen in the truncation (5.2). The flow of the classical linear $O(2)$-model has already been studied with much more extended truncations [79], taking into account an arbitrary $\tilde{\delta}$-dependence of $u(\tilde{\delta})$ and

arbitrary $\tilde{\delta}$-dependent wave function renormalizations, e.g. $A(\tilde{\delta})$. All these functions flow quickly to a scaling form which depends only on one parameter κ. Evaluated for the scaling solution one finds to a very good approximation for $\kappa > \kappa_{KT}$

$$k\partial_k \kappa = \beta_\kappa = \alpha |\kappa_* - \kappa|^{\frac{3}{2}} \Theta(\kappa_* - \kappa) \tag{5.14}$$

with $\kappa_* = 0.248$ and $\alpha = 2.54$ [79]. We will use this improved truncation for β_κ for $k < T/12$ for the region $\kappa > \kappa_{KT} = 0.1$. This results in the solid lines in figure 5.1, whereas the truncation (5.2) gives the dashed lines.

We define the critical temperature T_c as the temperature for which the field expectation value κ just vanishes at the physical scale $k_{ph}/t = 10^{-9}$, see figure 5.1. For $T < T_c$ one finds a superfluid condensate in a probe of macroscopic size of roughly 1 cm. The dependence of T_c on the specific choice of k_{ph} is extremely weak. For our parameters $t = 0.3$ eV corresponds to $T_c = 128$ K while for alternative $\lambda_\psi^d/t = 1/2$, 1 we find $T_c = 58.3$, 366 K, respectively. We also note that T_c is only mildly affected by the improvement of the truncation (5.14).

5.2 Essential Scaling

A specific feature of the KT phase transition is essential scaling for the temperature dependence of the correlation length $\xi = m_R^{-1} = (\bar{m}^2/A)^{-\frac{1}{2}}$ just above T_c,

$$m_R = c \exp\Big(- \frac{b}{\sqrt{C(k_{ph}) + T - T_c}} \Big) . \tag{5.15}$$

This scaling relation is a consequence of eq. (5.14). In order to show this we start in a region where $\kappa^* > \kappa$ and integrate eq. (5.14),

$$\int_{\kappa(k)}^{\kappa(\Lambda)} \frac{d\kappa'}{(\kappa_* - \kappa')^{\frac{3}{2}}} = \alpha \int_k^\Lambda d \ln k' , \tag{5.16}$$

Performing the integrations yields

$$\kappa_* - \kappa(\Lambda) = \left[(\kappa_* - \kappa(k))^{-\frac{1}{2}} + \frac{\alpha}{2} \ln \frac{\Lambda}{k} \right]^{-2} . \tag{5.17}$$

Let $\bar{\kappa}(\Lambda)/\ \kappa(\Lambda)$be the initial value for κ which yields to $\kappa(k_{ph}) = 0/\kappa(k_{SR}) = 0$ where $(k_{SR} > k_{ph})$. $\bar{\kappa}(\Lambda)$ corresponds to T_c and $\kappa(k_{SR}) = 0$ corresponds to

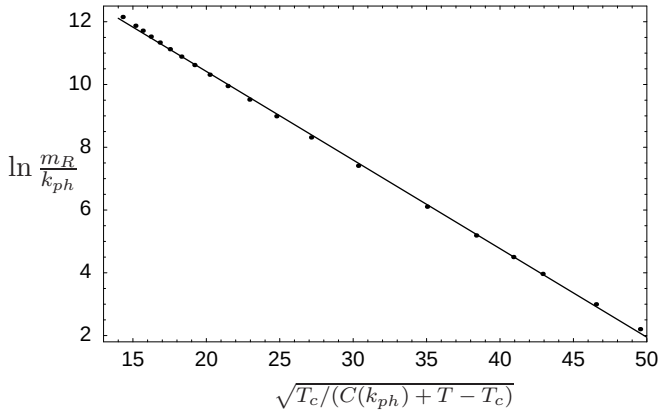

Figure 5.2: Essential scaling for $T > T_c$ with $C(k_{ph})/t = 10^{-5}$. The dots are the numerical solution to the flow equation.

$T > T_c$. (5.17) yields

$$\begin{aligned} \kappa_* - \bar{\kappa}(\Lambda) &= \kappa_* \left[1 + \frac{\alpha}{2}\kappa_*^{\frac{1}{2}} \ln \frac{\Lambda}{k_{ph}}\right]^{-2} \\ \kappa_* - \kappa(\Lambda) &= \kappa_* \left[1 + \frac{\alpha}{2}\kappa_*^{\frac{1}{2}} \ln \frac{\Lambda}{k_{SR}}\right]^{-2} . \end{aligned} \tag{5.18}$$

Now we use $\kappa(\Lambda) - \bar{\kappa}(\Lambda) = \delta\kappa_\Lambda = \gamma(T_c - T)$ where $(T > T_c)$ and find with $-\delta\kappa_\Lambda = (\kappa_* - \kappa(\Lambda)) - (\kappa_* - \bar{\kappa}(\Lambda))$

$$-\frac{\delta\kappa_\Lambda}{\kappa_*} = \left[1 + \frac{\alpha}{2}\kappa_*^{\frac{1}{2}} \ln \frac{\Lambda}{k_{SR}}\right]^{-2} - \left[1 + \frac{\alpha}{2}\kappa_*^{\frac{1}{2}} \ln \frac{\Lambda}{k_{ph}}\right]^{-2} . \tag{5.19}$$

This is equivalent to

$$\ln \frac{k_{SR}}{\Lambda} - \frac{2}{\alpha\kappa_*^{\frac{1}{2}}} = -\frac{2}{\alpha\gamma^{\frac{1}{2}}(C(k_{ph}) + T - T_c)^{\frac{1}{2}}} , \tag{5.20}$$

with

$$C(k_{ph}) = \frac{\kappa_*/\gamma}{\left(1 + \frac{\alpha}{2}\kappa_*^{\frac{1}{2}} \ln \frac{\Lambda}{k_{ph}}\right)^2} \longrightarrow 0 \quad (k_{ph} \to 0) . \tag{5.21}$$

Using the relation $\xi^{-1} = m_R = c_1 k_{SR}$ we obtain

$$\ln \frac{m_R}{k_{ph}} = A - \frac{2}{\alpha\gamma^{\frac{1}{2}}(C(k_{ph}) + T - T_c)^{\frac{1}{2}}} , \tag{5.22}$$

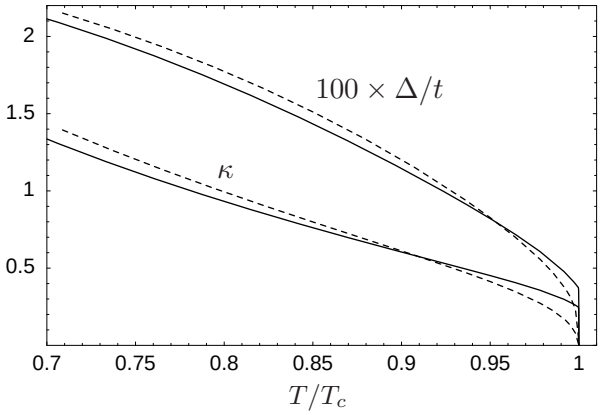

Figure 5.3: Temperature dependence of d-wave superconducting order. We plot the renormalized superfluid density κ and the fermionic gap $\Delta(0, \frac{\pi}{2})/t$. Solid/dashed lines are based on eq. (5.14)/(5.2).

where

$$A = \frac{2\kappa_*^{-\frac{1}{2}}}{\alpha} + \ln \frac{c_1 \Lambda}{k_{ph}}. \tag{5.23}$$

This yields essential scaling relation (5.15) with b and c being non-universal constants following from eq. (5.22).

The finite size correction $C(k_{ph}) \sim (1+\frac{\alpha}{2}\kappa_*^{\frac{1}{2}} \ln \frac{\Lambda}{k_{ph}})^{-2}$ vanishes logarithmically for $k_{ph} \to 0$. Close to the critical temperature the omission of the finite size correction (i.e. $C(k_{ph} = 0)$) yields to a substantial derivation from the straight line in figure 2.

For $T > T_c$ one finds that $\kappa(k)$ reaches zero at a scale $k_{SR} > k_{ph}$. Continuing the flow in the symmetric regime for $k_{SR} > k > k_{ph}$ yields $m_R = 0.50\, k_{SR}$. We show $m_R(T)$ in figure 5.2 (same t', λ_ψ^d, μ in all figs.) and find that essential scaling is smoothened due to $k_{ph} > 0$.

From figure 5.1 we can also extrapolate the pseudo-critical temperature T_{pc}. This corresponds to the temperature where $\kappa(k)$ bends over immediately after becoming non-zero at $k = k_{SSB}$ and is driven to zero again more or less at the same scale $k_{SR} \approx k_{SSB}$. In other words, T_{pc} corresponds to the highest temperature for which the initial flow in the symmetric regime hits a vanishing mass term $\bar{m}^2$ and therefore a divergent effective four fermion vertex $\sim \bar{m}^{-2}$. Often this temperature is associated with the critical temperature. We find $T_{pc}/t = 0.0372$, only slightly above the value of the critical temperature $T_c/t = 0.0368$.

It is characteristic for two dimensions that the renormalized order parameter κ jumps at T_c even though the transition shows scaling behavior. Strictly

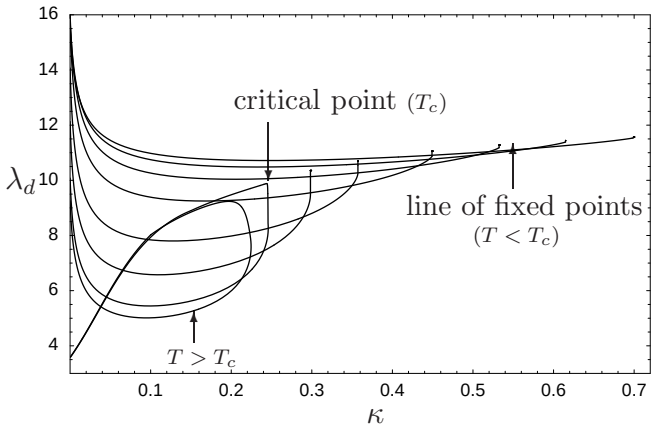

Figure 5.4: Critical line in the $\lambda_d - \kappa$ plane.

speaking, this discontinuity only occurs for $k_{ph} \to 0$ whereas it is smoothened for nonzero k_{ph}. The scaling solution at T_c corresponds to a fixed point κ_* where $\beta_\kappa(\kappa_*) = 0$ with $\beta_\kappa(\kappa < \kappa_*) > 0$. In the region $\kappa(k) < \kappa_*$ the flow drives κ to zero and the system is in the symmetric phase. In contrast, for $\kappa > \kappa_*$ the flow can never cross the fixed point. Therefore $\kappa(k_{ph})$ remains larger than κ_*, resulting in a minimal value for κ in the ordered phase. For $k_{ph} \to 0$ this results in a jump $\Delta\kappa = \kappa_*$ between the two phases. In superfluids $\kappa(k_{ph})$ determines the renormalized superfluid density. The value resulting in the vortex picture [61, 62] is $\kappa_* = \frac{1}{\pi}$. Our truncation (5.14) is already parameterized in terms of κ_*. In figure 5.3 we plot the value of the superfluid density $\kappa(k_{ph})$ as well as the gap in the electron propagator $\Delta(0, \frac{\pi}{2})$ in a fixed momentum direction. In the present truncation Δ would vanish for $k_{ph} \to 0$, whereas κ would remain nonzero. In order to settle this issue more precisely one would have to follow the flow of the Yukawa coupling that we have neglected here. For $t = 0.3$ eV and $T = T_c/2$ we obtain $\Delta(0, \frac{\pi}{2}) = 7.7$ meV.

In figure 5.4 flow trajectories for different temperatures in the $\lambda_d - \kappa$ plane are plotted. The flow starts on the scale k_{SSB} which is associated with the onset of local ordering. Per construction κ vanishes for all temperatures at k_{SSB}. However, a lowering of the scale and penetration of the broken regime reveals two qualitatively different situations. For temperatures $T < T_c$ the flow trajectories approach after some fast initial running a line of fixed points. The system is now in the scaling regime and this line ends at the critical point associated with the critical temperature T_c. For temperatures $T_{pc} > T > T_c$ fermionic fluctuations generate a finite κ. However, since $\kappa < \kappa^*$ during the flow, κ is driven to zero at a scale k_{SR} depending on the temperature. Compare with figures 5.1 and 5.3.

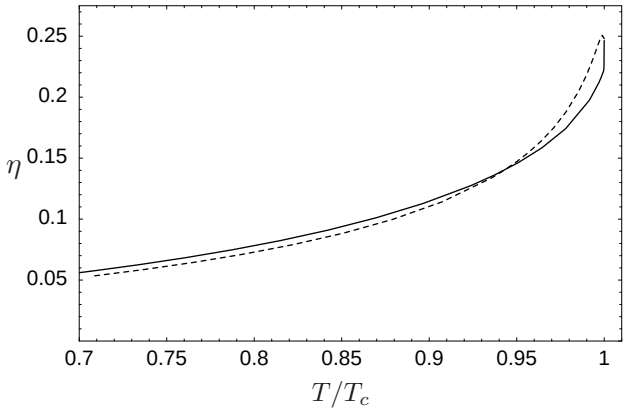

Figure 5.5: Temperature dependence of the critical exponent η. The solid line is based on eq. (5.14), the dashed line on eq. (5.2).

5.3 Anomalous Dimension

We finally turn to the anomalous dimension for $T \leq T_c$. For weakly inhomogeneous fields (low $\mathbf{q}^2$) the gradient terms in the effective theory (Landau theory) for the composite bosons d take the form

$$\Gamma = \frac{1}{T}\int_q d^*(q) A(\mathbf{q}^2, k_{ph})\, \mathbf{q}^2 d(q)\,. \tag{5.24}$$

Our truncation (5.5) has not yet taken the $\mathbf{q}^2$-dependence of A into account: the flow equations apply for $A(k) = A(\mathbf{q}^2 = 0, k)$. Nevertheless, the momentum dependence of A can be easily inferred by noting that $\mathbf{q}^2$ also acts as an infrared cutoff such that R_d^k becomes ineffective for $k^2 < \mathbf{q}^2$. A reasonable approximation uses $\partial_k A(\mathbf{q}^2, k) = \partial_k A(\mathbf{q}^2 = 0, k)\Theta(k^2 - \mathbf{q}^2)$. The solution at k_{ph} reads for $\mathbf{q}^2 > k_{ph}^2$, $q = \sqrt{\mathbf{q}^2}$,

$$A(q^2) = \bar{A}(q/\bar{q})^{-\eta}\,, \quad \eta = \int_{\ln q}^{\ln \bar{q}} d\ln k\, \eta(k)/\ln(\bar{q}/q)\,. \tag{5.25}$$

In figure 5.5 we show η for $\bar{q}/q = e^5$ and observe the characteristic dependence on T. As a result the static correlation function $\langle d(\mathbf{r}) d^*(0)\rangle_c$ decreases $\sim r^{-\eta}$ for large r. Furthermore, Coleman's no go theorem for free massless particles in two dimensions [80] is avoided since $\eta > 0$. For a superconductor one replaces in eq. (5.24) $\mathbf{q}^2$ by $-(\nabla - 2i|e|\mathbf{A})^2$ with $\mathbf{A}$ the space components of the electromagnetic potential. Inserting $d = d_0$ this results in an anomalous Landau theory for the magnetic field $B = \partial_1 A_2 - \partial_2 A_1$. Instead of the photon mass term $\sim \mathbf{A}^2$ responsible for ordinary superconductivity in three dimensions we now find a term $|\mathbf{A}|^{2-\eta}$. This may open a window for a measurement of the anomalous dimension.

Chapter 6

Summary and Outlook

High temperature superconductivity is one of the most challenging problems in condensed matter physics. A typical class of materials which show this surprisingly high transition temperature to the superconducting phase are cuprate high temperature superconductors. Of particular interest is the investigation of their comprehensive phase diagram. A common feature of these materials is an anisotropic layer structure consisting of CuO_2 layers separated by layers containing other atoms which basically define the concentration of electrons or holes in the copper-oxide layers. This concentration governs the physical properties of the material drastically. At sufficiently low temperatures it ranges from an antiferromagnetic insulator, if the number of electrons and holes are equal in the energetically accessible band, to superconductivity with d-wave pairing symmetry if holes (or electrons) are added. These extremes are separated by a region of doping where a lot of different degrees of freedom seem to play a role. However, the basic degrees of freedom and their interplay are still unclear in this pseudo-gap regime and further experimental and theoretical effort is needed. Particularly, it is speculated that an understanding of this regime may be crucial with regard to an investigation of the origin of high temperature superconductivity.

Our view is that the interlayer hopping of the charge carriers provides only a weak coupling between the copper-oxide layers. Basic features such as the d-wave Cooper-pairing mechanism reside in the two-dimensional copper-oxide planes. Furthermore, the electrons are tightly bound to the core atoms and are assumed to interact on high momentum scales only via a screened Coulomb repulsion. Other influences such as electron-phonon interactions which may also be responsible for the pairing are disregarded here. We consider the two-dimensional Hubbard model as minimal microscopic model for the electrons in the copper-oxide planes of these cuprates.

In the near future experiments with ultra-cold fermionic atoms in two-dimensional optical lattices may provide insight into the origin of high temperature superconductivity in cuprates. Under the assumption that two kinds of fermionic atoms are present differing by generalized spin-$\frac{1}{2}$ projections the

system can be described by the Hubbard model for sufficiently low temperatures where the atoms are confined to the lowest Bloch band. Furthermore, the ratio (U/t) of coupling to hopping amplitude can be tuned. In particular, a transition to antiferromagnetism or to superfluid states with e.g. d-wave pairing depending on the parameters (such as doping) can be probed in a very clean environment.

A theoretical approach to the two-dimensional Hubbard model is challenging. It has to deal with a situation where qualitatively different degrees of freedom such as antiferromagnetic spin correlation and fluctuations in the d-wave Cooper-pairing channel, which appear on different momentum scales, require and influence each other. This interplay of different degrees of freedom and different energy scales hampers approaches which treat all scales at once since they are based on the same approximation scheme on all scales. In low dimensions, perturbation theory is plagued by infrared divergencies and therefore it is often not applicable even at weak coupling. However, within a renormalization group approach the fluctuations on different scales are integrated out successively starting from the highest momentum scale which is present in the microscopic description. This fact can be used to explore different approximation schemes on different scales.

Our approach is based on a functional integral formulation and we interpolate smoothly by a one-parameter family of effective average actions between the microscopic action and the (quantum) effective action which contains the full physical information about the system. The transition from the microscopic model to the (quantum) effective action is described by an exact flow equation for the effective average action. This flow equation is equivalent to an infinite hierarchy of coupled differential flow equations for the 1-PI Greens or vertex functions. Of course, this hierarchy has to be truncated somewhere in order to make progress. In practice, various versatile approximation schemes beyond perturbation theory exist and this method is flexible enough to apply different approximations at different scales. Furthermore, infrared singularities are treated properly by successively integrating out the fluctuations scale by scale.

In most of the earlier functional renormalization group studies of the Hubbard model a purely fermionic language is used, and the scale dependence of the fermionic coupling is analyzed. However, although these studies demonstrate the power of the functional renormalization group in the context of the Hubbard model impressively, we believe that it is advantageous to make the interesting degrees of freedom more explicit in the formulation. Within our approach, we partially bosonize the fermionic coupling of the antiferromagnetic and the d-wave pairing channel, thereby the interaction between the fermions is mediated by bosonic fields. This is achieved by means of a Hubbard-

Stratonovich transformation. The penetration of a symmetry broken phase is limited in a purely fermionic language by the divergence of the fermionic coupling on a finite scale in the renormalization flow. The onset of local ordering is indicated by this scale. Particularly, this divergence is translated into a vanishing of a bosonic mass term in our language. The symmetry broken phase can be studied and is indicated by a finite expectation value of the corresponding bosonic field. Furthermore, higher fermionic operators which are needed to study phase transitions are included comparatively straightforward in terms of bosonic interactions.

Within our approach we focus on antiferromagnetism and d-wave superconductivity. On initial scale we bosonize the fermionic coupling which we set $U/t = 3$ completely into the antiferromagnetic channel. In the context of high temperature superconductivity a coupling larger than the bandwidth $U/t > 8$ would be more realistic. However, many of the important features of the Hubbard model are expected already for smaller values for U. On lower momentum scales a coupling in the d-wave channel is generated by the antiferromagnetic fluctuations. This coupling is bosonized by the method of scale dependent field transformations. Antiferromagnetic and d-wave pairing fluctuations as well as their mutual influence are studied over a wide range of chemical potential in terms of a Yukawa-like theory with two species of bosonic fields coupled to the fermions.

We calculate the pseudo-critical temperature T_{pc}, which is defined as the highest temperature at which the system enters the broken phase in the renormalization flow, for both instabilities. This temperature is often associated with the critical temperature T_c in the literature, but the true critical temperature is still below T_{pc}. More precisely, T_{pc} defines the boundary in temperature between flow trajectories where the bosonic mass stays finite ($T > T_{pc}$) and flow trajectories where the mass vanishes. For temperatures T with $T_{pc} > T > T_c$ the symmetry is spontaneously broken in the renormalization flow (below a scale k_{SSB}) but restored at the end of the flow, while for $T < T_c$ the symmetry remains spontaneously broken for $k < k_{SSB}$. See chapter 5 for a more extensive discussion.

The behavior of the system depends strongly on the chemical potential and therewith on the topology of the Fermi surface. With restriction to nearest neighbor hopping, a vanishing chemical potential corresponds to a half-filled lattice with the perfect-nesting property and the system depends only on the absolute value of the chemical potential $|\mu|$. Near $\mu = 0$ the antiferromagnetic channel dominates and becomes instable for temperatures below T_{pc} which takes the highest value at vanishing chemical potential. For increasing absolute values of the chemical potential, T_{pc} decreases, see figure 4.10. The transition into the symmetry broken regime is continuous in the renormalization flow up

to a certain value of the chemical potential $|\mu'|$. This point is indicated by the fact that for larger chemical potential the quartic coupling $\bar{\lambda}_a$ becomes negative in the renormalization flow before the mass of the boson vanishes. Hence, for $|\mu| > |\mu'|$ a transition to the symmetry broken regime is discontinuous which means that the expectation value of the bosonic fields jumps discontinuously to a finite value in the renormalization flow. However, since the spontaneous breaking of a continuous symmetry in two dimensions at non-zero temperature is forbidden by the Mermin-Wagner theorem, antiferromagnetism at non-zero temperature is a finite volume effect, see [25] for a discussion. In the sense of [25] the transition to antiferromagnetism is expected to be of first order for $|\mu| > |\mu'|$.

For larger values of the chemical potential the different topology of the Fermi surface changes the situation drastically. In particular, the d-wave pairing channel rather than the antiferromagnetic channel becomes critical, see figure 4.10. The maximum of the pseudo-critical temperature is located at $|\mu|/t \approx 0.28$ and the transition into the symmetry broken regime is everywhere continuous in the renormalization flow. In addition the nature of the antiferromagnetic fluctuations also changes with the chemical potential. At vanishing chemical potential the antiferromagnetic fluctuations are commensurate while at finite chemical potential and for sufficiently low temperatures incommensurate antiferromagnetic fluctuations prevail. However, in the range of chemical potential and temperature where antiferromagnetism becomes critical, commensurate antiferromagnetic fluctuations dominate.

In the intermediate regime of chemical potential between a dominance of either antiferromagnetic or d-wave pairing fluctuations the truncation has to be improved. For instance, this is necessary in order to decide whether a discontinuous transition into the symmetry broken regime of antiferromagnetism or a continuous transition into the symmetry broken regime of d-wave superconductivity in the renormalization flow are on hand. Such an improvement can be achieved by an inclusion of higher fermionic operators, corresponding to bosonic interactions in our language, which couples the two different bosons.

The temperature dependence of d-wave superconducting order is studied within a simplified model characterized by a coupling solely in the d-wave channel on lower momentum scales. For the phase transition from the high temperature symmetric phase to the low temperature superconducting phase we find essential scaling of the correlation length as the critical temperature is approached from above, a temperature dependent anomalous dimension and a gap in the electron propagator for temperatures below the critical temperature. These features are characteristic for a Kosterlitz-Thouless phase transition which is a natural candidate for a universality class with a global $U(1)$-symmetry in two dimensions. Importantly, this picture emerges directly from

the renormalization flow, and it is not necessary to include vortex configurations explicitly as proposed in earlier work to describe the Kosterlitz-Thouless behavior.

In summary, we have demonstrated how competing instabilities and symmetry broken phases in the Hubbard model can be addressed by the functional renormalization group with partial bosonization. However, our truncation can be further improved in various ways. A first step might be an improvement of the projection prescription onto the coupling in the d-wave channel which better accounts for the momentum dependences. The inclusion of other channels such as the s-wave, the extended s-wave pairing channel, and the charge density channel would also be desirable. Moreover, a study of possible spontaneous breaking of the point group symmetry of the square lattice by a (d-wave) Pomeranchuk instability [81, 15] would be interesting within our approach. Additional higher fermionic operators, which correspond to bosonic interactions in our formulation, can be included very efficiently. In this way a coupling between the different bosonic fields can be included. This may help to shed some light on the intermediate regime between antiferromagnetism and d-wave superconductivity in the phase diagram of the two-dimensional Hubbard model.

Appendix A

Conventions and Notation

This part of the appendix is supposed to summarize the most important conventions and notations. We use natural units with $\hbar = c = k_B = 1$. Fields are indicated by a $\hat{}$ over the symbol ($\hat{\psi}, \hat{\mathbf{a}}, \hat{d}, \dots$) while the $\hat{}$ is omitted for the corresponding expectation values ($\psi, \mathbf{a}, d, \dots$). However, there is subtlety in notation since the effective potential is a function of invariants under symmetry transformations of the expectation values, e.g. $U(\alpha, \delta)$, with $\alpha = \frac{1}{2}\mathbf{a} \cdot \mathbf{a}$, $\delta = d^* d$. The minima of the effective potential in broken phases are denoted by a node, e.g. α_0, δ_0. For composite objects like fermion bilinears we introduce a $\tilde{}$ over the symbol ($\tilde{\rho} = \hat{\psi}^\dagger \hat{\psi}, \tilde{\mathbf{a}} = \hat{\psi}^\dagger \boldsymbol{\sigma} \hat{\psi}, \dots$).

We define generalized positions and momenta by

$$X = (\tau, \mathbf{x}), \quad Q = (\omega_Q, \mathbf{q}), \quad QX = \omega_Q \tau + \mathbf{x} \cdot \mathbf{q}\,. \tag{A.1}$$

The Matsubara frequencies are defined as $\omega_Q = (2n+1)\pi T$ for fermions and $\Omega_Q = 2n\pi T$ for bosons with $n \in \mathbb{Z}$, respectively. Generalized sums and delta distributions are defined as follows

$$\begin{aligned} \sum_X = \int_0^\beta d\tau \sum_{\mathbf{x}}, \quad \sum_Q = T \sum_{n=-\infty}^{\infty} \int_{-\pi}^{\pi} \frac{d^2 q}{(2\pi)^2}\,, \\ \delta(X - X') = \delta(\tau - \tau') \delta_{\mathbf{x},\mathbf{x}'}\,, \\ \delta(Q - Q') = \beta \delta_{n,n'} (2\pi)^2 \delta(\mathbf{q} - \mathbf{q}')\,. \end{aligned} \tag{A.2}$$

We measure all components of X and Q in units of the lattice distance a, i.e. $\mathbf{x} \to a\mathbf{x}$, $\mathbf{q} \to \mathbf{q}/a$, they aquire therefore the same canonical dimension. Here we set $a = 1$. All functions are periodic in 2π in the space-like momenta.

Fourier transforms are defined for local fields as

$$\hat{\psi}(X) = \sum_Q \hat{\psi}(Q) e^{iQX}, \quad \hat{\psi}^\dagger(X) = \sum_Q \hat{\psi}^\dagger(Q) e^{-iQX}\,, \tag{A.3}$$

for the fermionic fields and similar for bosonic fields.

Appendix B

Matrices for Computation of 1-PI Vertex Functions

Both the calculation of the one-loop correction to the vertex functions and the derivation of the flow equations for the couplings are based on the matrices $\mathcal{P}_{(k)}$, $\mathcal{P}^{-1}_{(k)}$ and $\mathcal{F}$ or parts of them. We summarize these matrices and also often used abbreviations in this part of the appendix.

With the $\tilde{}$ over the symbol P we mean

$$\tilde{P}_d(P) = P_d(P) + \bar{M}_d^2 \text{ with } \bar{M}_d^2 = \begin{cases} \bar{m}_d^2 + 2\bar{\lambda}_d\delta + 3\bar{\gamma}_d\delta^2|_{\delta=0}\,, & SYM \\ \bar{\lambda}_d(2\delta - \delta_0)|_{\delta=\delta_0}\,, & SSB \end{cases}, \quad \text{(B.1)}$$

where $\delta = d^*d$. In SSB it is $\delta = \delta_0$. In the presence of the regulator it is

$$\tilde{P}_d^k(P) = P_d^k(P) + \bar{M}_d^2 = P_d(P) + R_d^k(P) + \bar{M}_d^2\,. \quad \text{(B.2)}$$

Further we use

$$N_d^{(k)}(P) = \tilde{P}_d^{(k)}(P)\tilde{P}_d^{(k)}(-P) - (\bar{\lambda}_d + 2\bar{\gamma}_d\delta)^2\delta^2\,, \quad \text{(B.3)}$$

which is the determinant of the d-boson part of the propagator matrix. For the fermion part with vanishing **a**-field ($\alpha = 0$) we define a generalized square of the inverse propagator

$$N_F^{(k)}(P) = P_F^{(k)}(P)P_F^{(k)}(-P) + \Delta^2(\mathbf{p})\,, \quad \text{(B.4)}$$

where $\Delta^2(\mathbf{p}) = 4\bar{h}_d^2(2\mathbf{p})\delta$ defines the square of the gap function.

We decompose $\Gamma^{(2)}$ into $\Gamma^{(2)} = \mathcal{P} + \mathcal{F}$. It is

$$\mathcal{P}(P_1,P_2) = \begin{pmatrix} \big(P_a(P_1)\delta_{ij}+\hat{M}^2_{a,ij}\big)\delta(P_1-P_2) & & & \\ & \begin{pmatrix} \bar{\lambda}_d\, d^*d^* & \tilde{P}_d(-P_1) \\ \tilde{P}_d(P_1) & \bar{\lambda}_d\, dd \end{pmatrix}\delta(P_1-P_2) & & \\ & & \begin{matrix} -2\bar{h}_d(2P_1)\, d^*\epsilon_{\alpha\beta}\delta(P_1-P_2) & -P_F(-P_1)\delta_{\alpha\beta}\delta(P_1-P_2) \\ P_F(P_1)\delta_{\alpha\beta}\delta(P_1-P_2) & +\bar{h}_a(0)[\mathbf{a}\cdot\boldsymbol{\sigma}^T]_{\alpha\beta}\delta(P_1-P_2-\Pi) \\ -\bar{h}_a(0)[\mathbf{a}\cdot\boldsymbol{\sigma}]_{\alpha\beta}\delta(P_1-P_2-\Pi) & 2\bar{h}_d(2P_1)\, d\epsilon_{\alpha\beta}\delta(P_1-P_2) \end{matrix} \end{pmatrix}, \tag{B.5}$$

with $\hat{M}^2_{a,ij} = [\bar{m}_a^2 + \bar{\lambda}_a(\alpha-\alpha_0)]\delta_{ij} + \bar{\lambda}_a a_i a_j\,,\ i,j=1,2,3.$

$$\mathcal{F}(P_1,P_2) \;=\; \begin{pmatrix} \begin{matrix} \bar{\lambda}_a[\mathbf{a}\cdot\delta\mathbf{a}(P_1-P_2)\delta_{ij}+\delta a_i(P_1-P_2)a_j+a_i\delta a_j(P_1-P_2)] \\ +\bar{\lambda}_a\sum_K[\frac{1}{2}\delta\mathbf{a}(K)\cdot\delta\mathbf{a}(P_1-P_2-K)\delta_{ij}+\delta a_i(K)\delta a_j(P_1-P_2-K)] \end{matrix} & 0 & 0 \\ 0 & \begin{matrix} 2\bar{\lambda}_d\, d^*\delta d^*(P_2-P_1) \\ +\bar{\lambda}_d\sum_K \delta d^*(K)\delta d^*(P_2-P_1-K) \end{matrix} & \begin{matrix} 2\bar{\lambda}_d[d^*\delta d(P_1-P_2)+d\delta d^*(P_2-P_1) \\ +\sum_K \delta d^*(K)\delta d(K+P_1-P_2)] \end{matrix} \\ 0 & \begin{matrix} 2\bar{\lambda}_d[d^*\delta d(P_1-P_2)+d\delta d^*(P_2-P_1) \\ +\sum_K \delta d^*(K)\delta d(K+P_1-P_2)] \end{matrix} & \begin{matrix} 2\bar{\lambda}_d d\,\delta d(P_1-P_2) \\ +\bar{\lambda}_d\sum_K \delta d(K)\delta d(P_1-P_2-K) \end{matrix} \\ \begin{matrix} \bar{h}_a(P_2)\psi^*_\gamma(P_2-P_1+\Pi)\boldsymbol{\sigma}_{\gamma\alpha} \\ -\bar{h}_a(P_2)\boldsymbol{\sigma}_{\alpha\gamma}\psi_\gamma(P_1-P_2-\Pi) \end{matrix} & \begin{matrix} 0 \\ 2\bar{h}_d(2P_1-P_2)\epsilon_{\alpha\gamma}\psi^*_\gamma(P_2-P_1) \end{matrix} & \begin{matrix} -2\bar{h}_d(P_2-2P_1)\epsilon_{\alpha\gamma}\psi_\gamma(P_1-P_2) \\ 0 \end{matrix} \end{pmatrix}$$

$$\begin{pmatrix} -\bar{h}_a(-P_1)\psi^*_\gamma(P_2-P_1+\Pi)\boldsymbol{\sigma}_{\gamma\beta} & \bar{h}_a(-P_1)\boldsymbol{\sigma}_{\beta\gamma}\psi_\gamma(P_1-P_2-\Pi) \\ 0 & -2\bar{h}_d(2P_2-P_1)\epsilon_{\beta\gamma}\psi^*_\gamma(P_2-P_1) \\ 2\bar{h}_d(P_1-2P_2)\epsilon_{\beta\gamma}\psi_\gamma(P_1-P_2) & 0 \\ -2\bar{h}_d(P_1+P_2)\delta d^*(P_2-P_1)\epsilon_{\alpha\beta} & \bar{h}_a(P_1-P_2-\Pi)[\delta\mathbf{a}(P_1-P_2-\Pi)\cdot\boldsymbol{\sigma}^T]_{\alpha\beta} \\ -\bar{h}_a(P_1-P_2-\Pi)[\delta\mathbf{a}(P_1-P_2-\Pi)\cdot\boldsymbol{\sigma}]_{\alpha\beta} & 2\bar{h}_d(P_1+P_2)\delta d(P_1-P_2)\epsilon_{\alpha\beta} \end{pmatrix}. \tag{B.6}$$

In the symmetric regime concerning antiferromagnetism ($\alpha = 0$), eq. (B.5) simplifies to

$$\mathcal{P}(P_1,P_2) = \begin{pmatrix} \big(P_a(P_1)+\bar{m}_a^2\big)\delta_{ij} & & \\ & \begin{pmatrix} \bar{\lambda}_d\, d^*d^* & \tilde{P}_d(-P_1) \\ \tilde{P}_d(P_1) & \bar{\lambda}_d\, dd \end{pmatrix} & \\ & & \begin{matrix} -2\bar{h}_d(2P_1)\, d^*\epsilon_{\alpha\beta} & -P_F(-P_1)\delta_{\alpha\beta} \\ P_F(P_1)\delta_{\alpha\beta} & 2\bar{h}_d(2P_1)\, d\epsilon_{\alpha\beta} \end{matrix} \end{pmatrix}\delta(P_1-P_2)\,. \tag{B.7}$$

For the expansion of $\frac{1}{2}\mathrm{STr}\left\{\tilde{\partial}_k \ln(\mathcal{P}+\mathcal{F})\right\}$ in powers of the fields, we need the inverse of $\mathcal{P}(P_1,P_2)$:

$$\mathcal{P}^{-1}(P_1,P_2) = \begin{pmatrix} \left(P_a(P_1)+\bar{m}_a^2\right)^{-1}\delta_{ij} & 0 & 0 & 0 & 0 \\ 0 & -\frac{\bar{\lambda}_d\, dd}{N_d(P_1)} & \frac{\tilde{P}_d(-P_1)}{N_d(P_1)} & 0 & 0 \\ 0 & \frac{\tilde{P}_d(P_1)}{N_d(P_1)} & -\frac{\bar{\lambda}_d\, d^*d^*}{N_d(P_1)} & 0 & 0 \\ 0 & 0 & 0 & \frac{2\bar{h}_d(2P_1)\, d}{N_F(P_1)}\epsilon_{\alpha\beta} & \frac{P_F(-P_1)}{N_F(P_1)}\delta_{\alpha\beta} \\ 0 & 0 & 0 & \frac{-P_F(P_1)}{N_F(P_1)}\delta_{\alpha\beta} & \frac{-2\bar{h}_d(2P_1)\, d^*}{N_F(P_1)}\epsilon_{\alpha\beta} \end{pmatrix} \delta(P_1-P_2)\,. \tag{B.8}$$

$\mathcal{P}_k$ ($\mathcal{P}_k^{-1}$) can be obtained simply by adding the regulator functions to the inverse propagators, see eqs. (4.37) and (4.31).

Appendix C

Explicit Flow Equations

In this chapter we provide all flow equations within our truncation and regulator scheme.

The functions $S_{1,\ldots,11}$, $F_{1,2,3}$, G, g, and h are defined in appendix D.

C.1 Effective Potential

$$k\partial_k \bar{m}_a^2 = -\frac{5}{2}\frac{\bar{\lambda}_a A_a k^2 T}{(2\pi T)^4 Z_a^2} I_i S_5(a) + \frac{\bar{h}_a^2(0)(k\partial_k T_k)T}{2T_k^3}\int_{-\pi}^{\pi}\frac{d^2p}{(2\pi)^2} G(\Xi_1,\Xi_3)\,, \tag{C.1}$$

with

$$a = \sqrt{\frac{A_a k^2 + \bar{m}_a^2}{Z_a (2\pi T)^2}}\,, \tag{C.2}$$

and $\Xi_1 = \frac{\xi_{\mathbf{p}}}{2T_k}$, $\Xi_3 = \frac{\xi_{\hat{k}\mathbf{e_x}+\mathbf{p}+\boldsymbol{\pi}}}{2T_k}$.

$$\begin{aligned} k\partial_k \bar{\lambda}_a = {} & 11\frac{\bar{\lambda}_d^2 A_a k^2 T}{(2\pi T)^6 Z_a^3} I_i S_6(a) - 7\frac{\bar{\gamma}_a A_a k^2 T}{(2\pi T)^4 Z_a^2} I_i S_5(a) \\ & - \frac{\bar{h}_a^4(0)(k\partial_k T_k)T}{2T_k^5}\int_{-\pi}^{\pi}\frac{d^2p}{(2\pi)^2}\left(\frac{\tanh\Xi_1 - \tanh\Xi_2}{(\Xi_1-\Xi_2)^3}\right. \\ & \left. + \frac{\Xi_2 + \Xi_1(\Xi_1-\Xi_2)\tanh\Xi_1}{(\Xi_1-\Xi_2)^3\cosh^2\Xi_1} - \frac{\Xi_1 - \Xi_2(\Xi_1-\Xi_2)\tanh\Xi_2}{(\Xi_1-\Xi_2)^3\cosh^2\Xi_2}\right), \end{aligned} \tag{C.3}$$

where $\Xi_2 = \frac{\xi_{\mathbf{p}+\boldsymbol{\pi}}}{2T_k}$.

$$\begin{aligned} (k\partial_k \bar{\gamma}_a)^B = {} & -9\frac{\bar{\zeta}_a A_a k^2 T}{(2\pi T)^4 Z_a^2} I_i S_5(a) + 102\frac{\bar{\lambda}_a \bar{\gamma}_a A_a k^2 T}{(2\pi T)^6 Z_a^3} I_i S_6(a) \\ & - 174\frac{\bar{\lambda}_a^3 A_a k^2 T}{(2\pi T)^8 Z_a^4} I_i S_8(a)\,. \end{aligned} \tag{C.4}$$

$$\begin{aligned}\left(k\partial_k\bar{\gamma}_a\big|_{\delta=0}\right)^F = \frac{\bar{h}_a^6(0)(k\partial_k T_k)T}{4T_k^7}\int_{-\pi}^{\pi}\frac{d^2p}{(2\pi)^2}\Bigg(&6\frac{\tanh\Xi_1-\tanh\Xi_2}{(\Xi_1-\Xi_2)^5}\\ &-\frac{\Xi_1}{(\Xi_1-\Xi_2)^3\cosh^4\Xi_1}+\frac{\Xi_2}{(\Xi_1-\Xi_2)^3\cosh^4\Xi_2}\\ &+\frac{6\Xi_2+3(\Xi_1^2-\Xi_2^2)\tanh\Xi_1+2\Xi_1(\Xi_1-\Xi_2)^2\tanh^2\Xi_1}{(\Xi_1-\Xi_2)^5\cosh^2\Xi_1}\\ &-\frac{6\Xi_1-3(\Xi_1^2-\Xi_2^2)\tanh\Xi_2+2\Xi_2(\Xi_1-\Xi_2)^2\tanh^2\Xi_2}{(\Xi_1-\Xi_2)^5\cosh^2\Xi_2}\Bigg)\,.\end{aligned} \tag{C.5}$$

$$\begin{aligned}\left(k\partial_k\bar{\zeta}_a\big|_{\delta=0}\right)^F = \frac{\bar{h}_a^8(0)(k\partial_k T_k)T}{2T_k^9}\int_{-\pi}^{\pi}\frac{d^2p}{(2\pi)^2}\Bigg(&\frac{2\Xi_1+\Xi_2+2\Xi_1(\Xi_1-\Xi_2)\tanh\Xi_1}{(\Xi_1-\Xi_2)^5\cosh^4\Xi_1}\\ &-3\frac{\Xi_1+2\Xi_2-\Xi_2(\Xi_1-\Xi_2)\tanh\Xi_2}{(\Xi_1-\Xi_2)^5\cosh^4\Xi_2}\\ &-\frac{1}{(\Xi_1-\Xi_2)^7\cosh^2\Xi_1}\Big\{15\Xi_2+(\Xi_1-\Xi_2)\tanh\Xi_1\big[6\Xi_1+9\Xi_2\\ &+2(\Xi_1-\Xi_2)(2\Xi_1+\Xi_2)\tanh\Xi_1+\Xi_1(\Xi_1-\Xi_2)^2\tanh^2\Xi_1\big]\Big\}\\ &+\frac{1}{(\Xi_1-\Xi_2)^7\cosh^2\Xi_2}\Big\{15\Xi_1+2\Xi_1^3-6\Xi_1\Xi_2^2+4\Xi_2^3\\ &-(\Xi_1-\Xi_2)\big(9\Xi_1+(6+\Xi_1^2)\Xi_2-2\Xi_1\Xi_2^2+\Xi_2^3\big)\tanh\Xi_2\Big\}\\ &-15\frac{\tanh\Xi_1-\tanh\Xi_2}{(\Xi_1-\Xi_2)^7}\Bigg)\,.\end{aligned} \tag{C.6}$$

For bosonic contributions of the d-boson we present the flow equations with both linear and quadratic frequency dependence of the inverse bosonic propagator. With linear frequency dependence the flow equation for the mass is

$$(k\partial_k\tilde{m}_d^2)^B = -\frac{2\bar{\lambda}_d A_d k^2}{(2\pi Z_d)^2 T}\,I_i S_2(\alpha_1)\,, \tag{C.7}$$

where

$$\alpha_1 = \frac{A_d k^2+\bar{m}_d^2}{2\pi T Z_d}\,. \tag{C.8}$$

With quadratic frequency dependence it is

$$(k\partial_k\tilde{m}_d^2)^B = -\frac{2\bar{\lambda}_d A_d k^2 T}{(2\pi T)^4 Z_{d2}^2}\,I_i S_5(\alpha_2)\,, \tag{C.9}$$

where

$$\alpha_2 = \sqrt{\frac{A_d k^2 + \tilde{m}_d^2}{Z_{d2}(2\pi T)^2}}\,. \tag{C.10}$$

$$(k\partial_k \bar{m}_d^2)^F = \frac{T(k\partial_k T_k)}{T_k^3} \int_{-\pi}^{\pi} \frac{d^2p}{(2\pi)^2} \bar{h}_d^2(2\mathbf{p}) F_1(\Xi_1)\,. \tag{C.11}$$

$$\begin{aligned}(k\partial_k \bar{\lambda}_d)^B = {} & \frac{\bar{\lambda}_d^2 A_d k^2}{(2\pi Z_d)^3 T^2}\, I_i\{8S_3(\alpha_1) + 2\alpha S_5(\alpha_1)\} \\ & -6\frac{\bar{\gamma}_d A_d k^2}{(2\pi Z_d)^2 T}\, I_i S_2(\alpha_1)\,,\end{aligned} \tag{C.12}$$

with linear frequency dependence of the inverse bosonic propagator, and

$$(k\partial_k \bar{\lambda}_d)^B = 10\frac{\bar{\lambda}_d^2 A_d k^2 T}{(2\pi T)^6 Z_{d2}^3}\, I_i S_6(\alpha_2) - 6\frac{\bar{\gamma}_d A_d k^2 T}{(2\pi T)^4 Z_{d2}^2}\, I_i S_5(\alpha_2)\,, \tag{C.13}$$

with quadratic frequency dependence.

$$(k\partial_k \bar{\lambda}_d)^F = -\frac{T(k\partial_k T_k)}{2T_k^5} \int_{-\pi}^{\pi} \frac{d^2p}{(2\pi)^2}\, \bar{h}_d^4(2\mathbf{p}) F_2(\Xi_1)\,. \tag{C.14}$$

$$\begin{aligned}(k\partial_k \bar{\gamma}_d)^F = {} & \frac{T(k\partial_k T_k)}{4T_k^7} \int_{\pi}^{\pi} \frac{d^2p}{(2\pi)^2} \bar{h}_d^6(2\mathbf{p}) \Bigg(\frac{3 - 4\Xi_1^2}{2\Xi_1^4 \cosh^2 \Xi_1} + \frac{3}{\Xi_1^2 \cosh^4 \Xi_1} \\ & - \frac{3\tanh \Xi_1}{2\Xi_1^5} \Bigg)\,.\end{aligned} \tag{C.15}$$

C.2 Kinetic Terms

$$
\begin{aligned}
k\partial_k \hat{A}_a = -\frac{\bar{h}_a^2 T(k\partial_k T_k)}{4T_k^3}\int_{-\pi}^{\pi}\frac{d^2p}{(2\pi)^2}\Bigg\{ & \frac{2B^2+A(\Xi_1-\Xi_3)}{(\Xi_1-\Xi_3)^2}\Bigg(\frac{\Xi_1}{(\Xi_1-\Xi_3)\cosh^2\Xi_1} \\
& -\frac{\Xi_3}{(\Xi_1-\Xi_3)\cosh^2\Xi_3}+\frac{\tanh\Xi_1-\tanh\Xi_3}{\Xi_1-\Xi_3}\Bigg) \\
& +\frac{4B^2}{(\Xi_1-\Xi_3)^2}\Bigg(\frac{\Xi_1\tanh\Xi_3-1}{\cosh^2\Xi_3}\Bigg)+\frac{2A}{\Xi_1-\Xi_3}\Bigg(\frac{\Xi_3\tanh\Xi_3-1}{\cosh^2\Xi_3}\Bigg) \\
& +\frac{2B^2\tanh\Xi_3(1-2\Xi_3\tanh\Xi_3)}{(\Xi_1-\Xi_3)\cosh^2\Xi_3}+\frac{2B^2\Xi_3}{(\Xi_1-\Xi_3)\cosh^4\Xi_3}\Bigg\} \\
+\frac{\bar{h}_a^2 T(k\partial_k \hat{k})}{4T_k^2}\int_{-\pi}^{\pi}\frac{d^2p}{(2\pi)^2}\Bigg\{ & 2B^3\Bigg(-3\Bigg(\frac{\tanh\Xi_1-\tanh\Xi_3}{(\Xi_1-\Xi_3)^4} \\
& +\frac{(\Xi_1-\Xi_3)\tanh\Xi_3-1}{(\Xi_1-\Xi_3)^3\cosh^2\Xi_3}\Bigg)+\frac{2\tanh^2\Xi_3-1/\cosh^2\Xi_3}{(\Xi_1-\Xi_3)\cosh^2\Xi_3}\Bigg) \\
& -6AB\Bigg(\frac{\tanh\Xi_1-\tanh\Xi_3}{(\Xi_1-\Xi_3)^3}+\frac{(\Xi_1-\Xi_3)\tanh\Xi_3-1}{(\Xi_1-\Xi_3)^2\cosh^2\Xi_3}\Bigg) \\
& +B\Bigg(\frac{\tanh\Xi_1-\tanh\Xi_3}{(\Xi_1-\Xi_3)^2}-\frac{1}{(\Xi_1-\Xi_3)\cosh^2\Xi_3}\Bigg)\Bigg\}, \qquad \text{(C.16)}
\end{aligned}
$$

where

$$
A=\frac{-(t-2t'\cos p_y)\cos(p_x+\hat{k})}{T_k}\,,B=\frac{-(t-2t'\cos p_y)\sin(p_x+\hat{k})}{T_k}\,. \qquad \text{(C.17)}
$$

The flow equations $k\partial_k A_a$ can be obtained from eq. (C.16) by setting $\hat{k}=0$ and $\partial_k\hat{k}=0$.

$$
\begin{aligned}
k\partial_k Z_a = -\frac{(k\partial_k T_k)\bar{h}_a^2}{8\pi^2 T T_k^3}\int_{-\pi}^{\pi}\frac{d^2p}{(2\pi)^2}\Bigg\{ & G(\Xi_1,\Xi_2)-\frac{(\Xi_1-\Xi_2)(\Xi_1F_1(\Xi_1)-\Xi_2F_1(\Xi_2))}{(\Xi_1-\Xi_2)^2+\pi^2} \\
& -\frac{2\pi^2(\Xi_1-\Xi_2)(\tanh\Xi_1-\tanh\Xi_2)}{((\Xi_1-\Xi_2)^2+\pi^2)^2}\Bigg\}. \qquad \text{(C.18)}
\end{aligned}
$$

$$
\begin{aligned}
k\partial_k A_d = \frac{\bar{h}_d^2 T(k\partial_k T_k)}{16t^2}\int_{-\pi}^{\pi}\frac{d^2p}{(2\pi)^2}\Bigg\{ & -\frac{1}{T_k^3}F_1(\Xi_1)(B\cos p_1-\sin^2 p_1) \\
& -\frac{\Xi_1}{T_k^4}F_2(\Xi_1)B(\frac{B}{2}\cos p_1-\sin^2 p_2)(2t+4t'\cos p_2) \\
& +\frac{1}{T_k^5}F_3(\Xi_1)B^2\sin^2 p_1(2t+4t'\cos p_2)^2\Bigg\}. \qquad \text{(C.19)}
\end{aligned}
$$

$$k\partial_k Z_d = -\frac{(k\partial_k T_k)}{2T_k^3}\int_{-\pi}^{\pi}\frac{d^2p}{(2\pi)^2}\bar{h}_d^2(2\mathbf{p})\frac{\tanh\Xi_1}{\cosh^2\Xi_1}\,, \tag{C.20}$$

based on eq. (4.124), or alternatively based on a discrete prescription

$$k\partial_k Z_d = -\frac{(k\partial_k T_k)}{4T_k^3}\int_{-\pi}^{\pi}\frac{d^2p}{(2\pi)^2}\bar{h}_d^2(2\mathbf{p})\Big\{\frac{2\Xi_1^2\tanh\Xi_1}{(\Xi_1^2+(\frac{\pi}{2})^2)^2}-\frac{2\tanh\Xi_1}{\Xi_1^2+(\frac{\pi}{2})^2} -\frac{\Xi_1}{\cosh^2\Xi_1(\Xi_1^2+(\frac{\pi}{2})^2)}\Big\}\,. \tag{C.21}$$

C.3 Yukawa Couplings

$$\begin{aligned}\beta^d_{\bar{h}_a} =& -\frac{T(k\partial_k T_k)\bar{h}_a^3}{4T_k^3}\int_{-\pi}^{\pi}\frac{d^2p}{(2\pi)^2}\frac{G(\Xi_1,\Xi_2)}{\tilde{P}_a^k(\mathbf{p})}\\ &-\frac{T}{4T_k^2}\frac{A_a k^2\bar{h}_a^3}{\left(A_a k^2+\bar{m}_a^2\right)^2}\int_{-\pi}^{\pi}\frac{d^2p}{(2\pi)^2}\big(2-\eta_a(1-\frac{\mathbf{p}^2t^2}{k^2})\big)\\ &\qquad\times\Theta(k^2-\mathbf{p}^2t^2)g(\Xi_1,\Xi_2)\\ &+\frac{T(k\partial_k T_k)\bar{h}_a}{T_k^3}\int_{-\pi}^{\pi}\frac{d^2p}{(2\pi)^2}\frac{\bar{h}_d^2(\mathbf{p})}{\tilde{P}_d^k(\mathbf{p})}G(\Xi_1,\Xi_2)\\ &+\frac{T}{T_k^2}\frac{A_d k^2\bar{h}_a}{\left(A_d k^2+\bar{m}_d^2\right)^2}\int_{-\pi}^{\pi}\frac{d^2p}{(2\pi)^2}\big(2-\eta_d(1-\frac{\mathbf{p}^2t^2}{k^2})\big)\Theta(k^2-\mathbf{p}^2t^2)\\ &\qquad\times\bar{h}_d^2(\mathbf{p})g(\Xi_1,\Xi_2)\,.\end{aligned} \tag{C.22}$$

$$\begin{aligned}\beta^d_{\bar{h}_d(2\mathbf{q})} &= (k\partial_k\bar{h}_d)^d f_d(2\mathbf{q})\\ &= \frac{3T(k\partial_k T_k)\bar{h}_d\bar{h}_a^2}{4T_k^3}\int_{-\pi}^{\pi}\frac{d^2p}{(2\pi)^2}\frac{f_d(2\mathbf{q}+2\mathbf{p})}{\tilde{P}_a^k(\mathbf{p})}F_1\big(\frac{\xi_{\mathbf{q}+\mathbf{p}-\pi}}{2T_k}\big)\\ &\quad+\frac{3T}{4T_k^2}\frac{A_a k^2\bar{h}_d\bar{h}_a^2}{\left(A_a k^2+\bar{m}_a^2\right)^2}\int_{-\pi}^{\pi}\frac{d^2p}{(2\pi)^2}\big(2-\eta_a(1-\frac{\mathbf{p}^2t^2}{k^2})\big)\Theta(k^2-\mathbf{p}^2t^2)\\ &\qquad\times f_d(2\mathbf{q}+2\mathbf{p})h\big(\frac{\xi_{\mathbf{q}+\mathbf{p}-\pi}}{2T_k}\big)\,.\end{aligned} \tag{C.23}$$

$$\beta^{rb}_{\bar{h}^2_a} = \bar{h}^4_a \bar{m}^2_a \frac{T(k\partial_k T_k)}{2T_k^3} \int_{-\pi}^{\pi} \frac{d^2p}{(2\pi)^2} \frac{1}{\tilde{P}^k_a(\mathbf{p})\tilde{P}^k_a(\pi-\mathbf{p})} \big\{ G(\Xi_1,\Xi_2) + F_1(\Xi_1) \big\}$$
$$+ \bar{h}^4_a \bar{m}^2_a \frac{T}{2T_k^2} \int_{-\pi}^{\pi} \frac{d^2p}{(2\pi)^2} \frac{k\partial_k R^k_a(\mathbf{p})}{\tilde{P}^k_a(\mathbf{p})^2 \tilde{P}^k_a(\pi-\mathbf{p})}$$
$$\times \big\{ 2g(\Xi_1,\Xi_2) + h(\Xi_1) + h(\Xi_2) \big\} . \tag{C.24}$$

In the following it is

$$\Xi_1 = \frac{\xi_{\mathbf{p}+(0,\pi)}}{2T_k} \quad \text{and} \quad \Xi_2 = \frac{\xi_{\mathbf{p}+(\pi,0)}}{2T_k} . \tag{C.25}$$

$$k\partial_k \lambda^d_\psi = -\frac{3}{8} \bar{h}^4_a \int_{-\pi}^{\pi} \frac{d^2p}{(2\pi)^2} k\tilde{\partial}_k \Bigg\{ \frac{1}{\tilde{P}^k_a(\mathbf{p})\tilde{P}^k_a(\mathbf{p}-\pi)} \frac{T}{2\pi^2 T_k^4} \frac{\pi^2 + 2(\Xi_1-\Xi_2)^2}{\pi^2 + (\Xi_1-\Xi_2)^2}$$
$$\times \frac{\tanh\Xi_1 - \tanh\Xi_2}{\Xi_1 - \Xi_2}$$
$$+ \frac{1}{\tilde{P}^k_a(\mathbf{p})^2} \frac{T}{2\pi^2 T_k^4 \cosh^2\Xi_2} \Bigg\} . \tag{C.26}$$

$$(k\partial_k \lambda^\psi_d)^F = \frac{3T(k\partial_k T_k)}{8\pi^2 T_k^5} \bar{h}^4_a \int_{-\pi}^{\pi} \frac{d^2p}{(2\pi)^2} \Bigg\{ \frac{1}{\tilde{P}^k_a(\mathbf{p})\tilde{P}^k_a(\mathbf{p}-\pi)}$$
$$\times \Bigg[\frac{\pi^2 + 2(\Xi_1-\Xi_2)^2}{2(\pi^2 + (\Xi_1-\Xi_2)^2)} \frac{1}{\Xi_1-\Xi_2} \left(\frac{\Xi_1}{\cosh^2\Xi_1} - \frac{\Xi_2}{\cosh^2\Xi_2} \right)$$
$$+ \frac{\pi^2(\Xi_1-\Xi_2)(\tanh\Xi_1 - \tanh\Xi_2)}{(\pi^2 + (\Xi_1-\Xi_2)^2)^2}$$
$$+ \frac{3(\pi^2 + 2(\Xi_1-\Xi_2)^2)}{2(\pi^2 + (\Xi_1-\Xi_2)^2)} \frac{\tanh\Xi_1 - \tanh\Xi_2}{\Xi_1-\Xi_2} \Bigg]$$
$$+ \frac{1}{\tilde{P}^k_a(\mathbf{p})^2} \frac{2 - \Xi_2 \tanh\Xi_2}{\cosh^2\Xi_2} \Bigg\} . \tag{C.27}$$

$$(k\partial_k \lambda^\psi_d)^B = \frac{3T\bar{h}^4_a}{8\pi^2 T_k^4} \int_{-\pi}^{\pi} \frac{d^2p}{(2\pi)^2} A_a k^2 \big(2 - \eta_a(1 - \frac{\mathbf{p}^2}{k^2})\big) \Theta(k^2 - \mathbf{p}^2)$$
$$\times \Bigg\{ \frac{1}{\tilde{P}^k_a(\mathbf{p})^2 \tilde{P}^k_a(\mathbf{p}-\pi)} \frac{\pi^2 + 2(\Xi_1-\Xi_2)^2}{\pi^2 + (\Xi_1-\Xi_2)^2} \frac{\tanh\Xi_1 - \tanh\Xi_2}{\Xi_1-\Xi_2}$$
$$+ \frac{1}{\tilde{P}^k_a(\mathbf{p})^3} \frac{1}{\cosh^2\Xi_2} \Bigg\} . \tag{C.28}$$

Appendix D

Useful Formulae

D.1 Spinor Matrices

The calculation of the flow equations involves an evaluation of products of spinor matrices. This appendix is supposed to provide some helpful relations.

The group $\mathrm{GL}(2,\mathbb{C})$ consists of all complex 2×2 matrices. A convenient basis is the identity plus the three Pauli matrices in standard representation

$$\sigma^0 = \begin{pmatrix} 1 & 0 \\ 0 & 1 \end{pmatrix}, \sigma^1 = \begin{pmatrix} 0 & 1 \\ 1 & 0 \end{pmatrix}, \sigma^2 = \begin{pmatrix} 0 & -i \\ i & 0 \end{pmatrix}, \text{and } \sigma^3 = \begin{pmatrix} 1 & 0 \\ 0 & -1 \end{pmatrix}. \quad \text{(D.1)}$$

They obey the well known (anti)-commutation relations[1]

$$\{\sigma^i, \sigma^j\} = 2\delta^{ij}\,, \quad [\sigma^i, \sigma^j] = 2i\epsilon^{ijk}\sigma^k\,, \quad \text{and} \quad \sigma^i = (\sigma^i)^\dagger = (\sigma^i)^{-1}\,, \quad \text{(D.2)}$$

where $i = 1, 2, 3$. We introduce a condensed notation $\sigma^\mu = (\sigma^0, \boldsymbol{\sigma})$, $\bar{\sigma}^\mu = (\sigma^0, -\boldsymbol{\sigma})$, $\epsilon = i\sigma^2$ and the metric $g_{\mu\nu} = \mathrm{diag}(1, -1, -1, -1)$. It holds

$$(\sigma^\mu)_{\alpha\beta}(\sigma_\mu)_{\gamma\delta} = 2\epsilon_{\alpha\gamma}\epsilon_{\beta\delta}\,, \quad \text{and} \quad \epsilon\sigma^\mu = (\bar{\sigma}^\mu)^T\epsilon\,, \quad \text{(D.3)}$$

from which we obtain

$$\begin{aligned} \sigma^i_{\alpha\beta}\sigma^i_{\gamma\delta} &= \delta_{\alpha\beta}\delta_{\gamma\delta} - 2\epsilon_{\alpha\gamma}\epsilon_{\beta\delta} \\ \sigma^i\sigma^j &= \delta^{ij} + i\epsilon^{ijk}\sigma^k \\ \sigma^i\sigma^j\sigma^i &= -\sigma^j \\ \epsilon(\sigma^i)^T\epsilon &= \sigma^i \\ \sigma^i\epsilon(\sigma^i)^T &= -3\epsilon\,. \end{aligned} \quad \text{(D.4)}$$

and

$$\begin{aligned} (\sigma^i\sigma^j)_{\alpha\delta}(\sigma^j\sigma^i)_{\gamma\beta} &= 5T_{\alpha\gamma;\delta\beta} - 3S_{\alpha\gamma;\delta\beta} \\ (\sigma^i\sigma^j)_{\alpha\delta}(\sigma^i\sigma^j)_{\gamma\beta} &= T_{\alpha\gamma;\delta\beta} + 9S_{\alpha\gamma;\delta\beta}\,, \end{aligned} \quad \text{(D.5)}$$

[1] Summation over repeated indices.

where S and T are the projectors on spin singlet and spin triplets in a two spin-$\frac{1}{2}$ particle state, respectively. They are

$$\begin{aligned} S_{\alpha\gamma;\beta\delta} &= \frac{1}{2}(\delta_{\alpha\beta}\delta_{\gamma\delta} - \delta_{\gamma\beta}\delta_{\alpha\delta}) \\ T_{\alpha\gamma;\beta\delta} &= \frac{1}{2}(\delta_{\alpha\beta}\delta_{\gamma\delta} + \delta_{\gamma\beta}\delta_{\alpha\delta})\,. \end{aligned} \tag{D.6}$$

In addition it is

$$\mathrm{tr}(\sigma^{i_1}\sigma^{i_2}\cdots\sigma^{i_{2n}})a_{i_1}a_{i_2}\cdots a_{i_{2n}} = 2^{n+1}(\frac{1}{2}\mathbf{a}\cdot\mathbf{a})^n\,. \tag{D.7}$$

D.2 Integrals

Due to our regularization scheme for the bosons, the following integral with case differentiation appears:

$$I_i = \int_{-\pi}^{\pi} \frac{d^2p}{(2\pi)^2}(2 - \eta_d(1 - \frac{\mathbf{p}^2}{k^2}))\Theta(k^2 - \mathbf{p}^2)\,, \tag{D.8}$$

with $i = 1, 2$ depending on the scale. Note, that the scale is in units of the hopping parameter t.

- i=1 corresponds to $0 \leq k \leq k\pi$:

$$\begin{aligned} I_1 &= \frac{2\pi}{(2\pi)^2}\int_0^k dx x(2 - \eta_d(1 - \frac{x^2}{k^2})) \\ &= \frac{k^2}{8\pi}(4 - \eta_d)\,. \end{aligned} \tag{D.9}$$

- i=2 corresponds to $\pi \leq k \leq \sqrt{2}\pi$:

$$\begin{aligned} I_2 &= 4\frac{2(\phi - \frac{\pi}{4})}{2\pi}I_1 \\ &+ 8\frac{1}{(2\pi)^2}\int_0^{\pi} dp_x \int_0^{p_x\cot\phi} dp_y(2 - \eta_d(1 - \frac{\mathbf{p}^2}{k^2})) \\ &= \frac{(\phi - \frac{\pi}{4})k^2}{2\pi^2}(4 - \eta_d) \\ &+ (\cot\phi)\big(2 - \eta_d\big(1 - \frac{\pi^2(1 + \frac{1}{3}\cot^2\phi)}{2k^2}\big)\big)\,, \end{aligned} \tag{D.10}$$

with

$$\sin\phi = \frac{\pi}{k}\,, \quad \text{where} \quad \frac{\pi}{4} \leq \phi \leq \frac{\pi}{2}\,.$$

D.3 Matsubara Sums

Here we introduce shortcuts for all Matsubara sums.

$$S_1(x) = \sum_{n\in Z} \frac{1}{x^2+(2n+1)^2} = \frac{\pi}{2}\frac{\tanh(\frac{\pi x}{2})}{x}\,, \tag{D.11}$$

$$S_2(x) = \sum_{n\in Z} \frac{1}{(in+x)^2} = \sum_{n\in Z} \frac{x^2-n^2-2inx}{(n^2+x^2)^2} = \frac{\pi^2}{\sinh^2(\pi x)}\,, \tag{D.12}$$

$$S_3(x) = \sum_{n\in Z} \frac{1}{(in+x)^3} = -\frac{1}{2}\frac{\partial}{\partial x}S_2 = \frac{\pi^3\coth(\pi x)}{\sinh^2(\pi x)}\,, \tag{D.13}$$

$$S_4(x) = \sum_{n\in Z} \frac{1}{n^2+x^2} = \frac{\pi\coth(\pi x)}{x}\,, \tag{D.14}$$

$$S_5(x) = \sum_{n\in Z} \frac{1}{(n^2+x^2)^2} = -\frac{1}{2x}\frac{\partial}{\partial x}S_4 = \frac{\pi\coth(\pi x)}{2x^3} + \frac{\pi^2}{2x^2\sinh^2(\pi x)}\,, \tag{D.15}$$

$$\begin{aligned} S_6(x) &= \sum_{n\in Z} \frac{1}{(n^2+x^2)^3} = -\frac{1}{4x}\frac{\partial}{\partial x}S_5 \\ &= \frac{3\pi\coth(\pi x)}{8x^5} + \frac{\pi^2 x(3+2\pi x\coth(\pi x))}{8x^5\sinh^2(\pi x)}\,, \end{aligned} \tag{D.16}$$

$$\begin{aligned} S_7(x) &= \sum_{n\in Z} \frac{1}{(x^2+(2n+1)^2)^2} = -\frac{1}{2x}\frac{\partial}{\partial x}S_1 \\ &= \frac{\pi\tanh(\frac{\pi x}{2})}{4x^3} - \frac{\pi^2}{8x^2\cosh^2(\frac{\pi x}{2})}\,, \end{aligned} \tag{D.17}$$

$$\begin{aligned} S_8(x) &= \sum_{n\in Z} \frac{1}{(n^2+x^2)^4} = -\frac{1}{6x}\frac{\partial}{\partial x}S_6 \\ &= \frac{5\pi\coth\pi x}{16x^7} + \frac{5\pi^2+4\pi^3 x\coth(\pi x)+\frac{4}{3}\pi^4x^2\coth^2(\pi x)}{16x^6\sinh^2(\pi x)} \\ &+ \frac{\pi^4}{24x^4\sinh^4(\pi x)}\,, \end{aligned} \tag{D.18}$$

$$
\begin{aligned}
S_9(x) &= \sum_{n\in Z} \frac{1}{(n^2+x^2)^5} = -\frac{1}{8x}\frac{\partial}{\partial x} S_8 \qquad \text{(D.19)}\\
&= \frac{35\pi \coth \pi x}{128 x^9} + \frac{\pi^4(5+4\pi x \coth(\pi x))}{96 x^6 \sinh^4(\pi x)}\\
&+ \frac{\pi^2(105+90\pi x\coth(\pi x)+40\pi^2 x^2\coth^2(\pi x)+8\pi^3 x^3 \coth^3(\pi x))}{384 x^8 \sinh^2(\pi x)}\,,
\end{aligned}
$$

$$
S_{10}(x) = \sum_{n\in Z} \frac{1}{(in+x)^4} = -\frac{1}{3}\frac{\partial}{\partial x} S_3 = \frac{\pi^4(2+\cosh(2\pi x))}{3\sinh^4(\pi x)}\,, \qquad \text{(D.20)}
$$

$$
\begin{aligned}
S_{11}(x) &= \sum_{n\in Z} \frac{1}{(in+x)^3(-in+x)}\\
&= \frac{\pi\coth(\pi x)}{4x^3} + \frac{\pi^2(1+2\pi x\coth(\pi x))}{4x^2\sinh^2(\pi x)}\,. \qquad \text{(D.21)}
\end{aligned}
$$

D.4 Abbreviations

The here defined functions often appear in fermionic one-loop calculations.

$$
\begin{aligned}
F_1(x) &= \frac{\tanh x}{x} + \frac{1}{\cosh^2 x}\,,\\
F_2(x) &= \frac{\tanh x}{x^3} + \frac{2x\tanh x - 1}{x^2\cosh^2 x}\,,\\
F_3(x) &= \frac{\tanh x}{4x^3} + \frac{\tanh^2 x}{\cosh^2 x} - \frac{\tanh x}{x\cosh^2 x} - \frac{1}{2\cosh^4 x} - \frac{1}{4x^2\cosh^2 x}\,,\\
h(x) &= \frac{\tanh x}{x}\,,\\
g(x,y) &= \frac{\tanh x - \tanh y}{x-y}\,,\\
G(x,y) &= \frac{xF_1(x) - yF_1(y)}{x-y}\,. \qquad \text{(D.22)}
\end{aligned}
$$

In the fermionic part of the flow equation for the effective potential (4.106) the function

$$
\gamma_\epsilon(\alpha,\delta) = \frac{1}{2T_k}\sqrt{\left[\mu_{\text{eff},1} - \epsilon'_{\mathbf{q}} + \epsilon\sqrt{\epsilon^2_{\mathbf{q}} + 2\bar{h}^2_a\alpha}\right]^2 + 4\bar{h}^2_d(2\mathbf{q})\delta}\,, \qquad \text{(D.23)}
$$

is used, where

$$
\xi_{\mathbf{q}} = -\mu + \epsilon_{\mathbf{q}} + \epsilon'_{\mathbf{q}}\,, \qquad \text{(D.24)}
$$

with

$$\epsilon_{\mathbf{q}} = -2t(\cos q_x + \cos q_y) \quad \text{and} \quad \epsilon'_{\mathbf{q}} = -4t' \cos q_x \cos q_y \,. \tag{D.25}$$

Bibliography

[1] J. Hubbard. *Proc. R. Soc. London, Ser. A*, 276:238, 1963.

[2] J. Kanamori. *Prog. Theor. Phys.*, 30:275, 1963.

[3] M. C. Gutzwiller. *Phys. Rev. Lett.*, 10:159, 1963.

[4] P. W. Anderson. *Science*, 235:1196, 1987.

[5] D. J. Scalapino. *Physics Reports*, 250:329, 1995.

[6] C. C. Tsuei and J. R. Kirtley. *Rev. Mod. Phys.*, 72:969, 2000.

[7] W. Hofstetter, J. L. Cirac, P. Zoller, E. Demler, and M. D. Lukin. *Phys. Rev. Lett.*, 89:220407, 2002.

[8] A. Georges. arXiv:cond-mat/0702122.

[9] F. J. Wegner and A. Houghton. *Phys. Rev. A*, 8:401, 1973.

[10] C. Wetterich. *Phys. Lett. B*, 301:90, 1993.

[11] K. G. Wilson and J. Kogut. *Phys. Rep. C*, 12:75, 1974.

[12] J. Polchinski. *Nucl. Phys. B*, 231:269, 1984.

[13] D. Zanchi and H. J. Schulz. *Z.Phys.*, B103:339, 1997.

[14] D. Zanchi and H. J. Schulz. *Europhys. Lett.*, 44:235, 1998.

[15] C. J. Halboth and W. Metzner. *Phys. Rev. Lett.*, 85:5162, 2000.

[16] C. J. Halboth and W. Metzner. *Phys. Rev. B*, 61:7364, 2000.

[17] I. Grote, E. Koerding, and F. Wegner. *J. Low Temp. Phys.*, 126:1385, 2002 [arXiv:cond-mat/0106604].

[18] M. Salmhofer and C. Honerkamp. *Prog. Theor. Phys.*, 105:1, 2001.

[19] C. Honerkamp, M. Salmhofer, N. Furukawa, and T. M. Rice. *Phys. Rev. B*, 63:035109, 2001 [arXiv:cond-mat/9912358].

[20] C. Honerkamp, M. Salmhofer, and T. M. Rice. *Eur. Phys. J. B*, 27:127, 2002 [arXiv:cond-mat/0204063].

[21] W. Metzner, J. Reiss, and D. Rohe. *Phys. stat. sol. (b)*, 243:46, 2006 [arXiv:cond-mat/0509412].

[22] J. Reiss, D. Rohe, and W. Metzner. arXiv:cond-mat/0611164.

[23] J. Hubbard. *Phys. Rev. Lett.*, 3:77, 1959.

[24] R. L. Stratonovich. *Soviet. Phys. Doklady*, 2:416, 1958.

[25] T. Baier, E. Bick, and C. Wetterich. *Phys. Rev. B*, 70:125111, 2004.

[26] H. C. Krahl and C. Wetterich. *Phys. Lett. A*, doi: 10.1016/j.physleta.2007.03.028, 2007 [arXiv:cond-mat/0608667].

[27] J. G. Bednorz and K. A. Müller. *Z.Phys.*, B64:189, 1986.

[28] P. A. Lee, N. Nagaosa, and X.-G. Weng. *Rev. Mod. Phys.*, 78:17, 2006.

[29] B. Batlogg and C. M. Varma. *Phys. World*, 2, 2000.

[30] J. Bardeen, L. N. Cooper, and J. R. Schrieffer. *Phys. Rev.*, 106:162, 1957.

[31] J. Bardeen, L. N. Cooper, and J. R. Schrieffer. *Phys. Rev.*, 108:1175, 1957.

[32] C. C. Tsuey et al. *Phys. Rev. Lett.*, 73:593, 1994.

[33] J. R. Kirtley et al. *Nature*, 373:255, 1995.

[34] H. Tasaki. *Prog. Theor. Phys.*, 99:1445, 1998 [arXiv:cond-mat/9512169], [arXiv:cond-mat/9712219].

[35] E. H. Lieb and F. Y. Wu. *Phys. Rev. Lett.*, 20:1445, 1968.

[36] J. W. Negele and H. Orland. *Quantum Many-Particle Systems*, Addison Wesley, Redwood City, 1988.

[37] F. Wegner. *Graßmann-Variable*, lecture notes, Heidelberg, 1998 [http://www.tphys.uni-heidelberg.de/wegner/].

[38] E. Demler, W. Hanke, and Shou-Cheng Zhang. *Rev. Mod. Phys.*, 76, 2004.

[39] M. Salmhofer, C. Honerkamp, W. Metzner, and O. Lauscher. *Prog. Theor. Phys.*, 112:943–970, 2004.

[40] T. Baier. *PhD thesis*, Heidelberg, 2002.

[41] E. Bick. *PhD thesis*, Heidelberg, 2002.

[42] J. Heinonen. *Diploma thesis*, Heidelberg, 2005.

[43] J. Müller. *Diploma thesis*, Heidelberg, 2007.

[44] T. Baier, E. Bick, and C. Wetterich. *Phys. Rev. B*, 62:15471, 2000.

[45] M. E. Peskin and D. V. Schröder. *An Introduction to Quantum Field Theory*, Addison Wesley, 1995.

[46] J. Zinn-Justin. *Quantum Field Theory and Critical Phenomena*, 3rd ed., Oxford university press, 1996.

[47] S. Weinberg. *The Quantum Theory of Fields*, Cambridge University Press, 1996.

[48] J. Berges, N. Tetradis, and C. Wetterich. *Phys. Rep.*, 363:223, 2002.

[49] J.M. Pawlowski. *Annals Phys.*, doi: 10.1016/j.aop.2007.01.007, 2007 [arXiv:hep-th/0512261].

[50] M. Salmhofer. *Renormalization: An Introduction*, Springer, Heidelberg, 1999.

[51] J. Feldman and E. Trubowitz. *Helv. Phys. Acta*, 63:157, 1990, ibid. 64:213, 1991.

[52] R. Shankar. *Physica A*, 177:530, 1991.

[53] R. Shankar. *Rev. Mod. Phys.*, 66:129, 1994.

[54] W. Metzner. *Prog. Theor. Phys.*, 160:58, 2005.

[55] H. Gies and C. Wetterich. *Phys. Rev. D*, 65:065001, 2002.

[56] H. Gies. arXiv:hep-ph/0611146.

[57] D. F. Litim. *Phys. Rev. D*, 64:105007, 2001.

[58] H. J. Schulz. *Phys. Rev. Lett.*, 64:1445, 1990.

[59] W. Kohn and J. M. Luttinger. *Phys. Rev. Lett.*, 15:524, 1965.

[60] W. H. Press, V. T. Vetterling, S. A. Teukolsky, and B. P. Flannery. *Numerical recipes in C*, Cambridge Univesity Press, 1992.

[61] J. M. Kosterlitz and D. J. Thouless. *J. Phys. C.*, 6:1181, 1973.

[62] D. R. Nelson. *Phase transitions and critical phenomena*, Vol. 7, Academic Press, J. L. Lebowitz, 1983.

[63] N. Goldenfeld. *Lectures on Phase transitions and the Renormalization Group*, Addison-Wesley, 1992.

[64] N. D. Mermin and H. Wagner. *Phys. Rev. Lett.*, 17:1133, 1966.

[65] C. Wetterich. *Z.Phys.*, C57:451, 1993.

[66] A. Rufenacht et al. *Phys. Rev. Lett.*, 96:227002, 2006.

[67] J. Corson et al. *Nature*, 398:221, 1999.

[68] Y. Wang et al. *Phys. Rev. B*, 73:024510, 2006.

[69] L. Lie et al. *Europhys. Lett.*, 72:451, 2005.

[70] K. Miyake et al. *Phys. Rev. B*, 34:6554, 1986.

[71] D. J. Scalapino et al. *Phys. Rev. B*, 34:8190, 1986.

[72] N. E. Bickers et al. *Int. J. Mod. Phys. B*, 1:687, 1987.

[73] S. Sachdev. *Quantum Phase Transitions*, Cambridge University Press, 1999.

[74] P. Coleman and A. J. Schofield. *Nature*, page 433, 2005.

[75] J. A. Hertz. *Phys. Rev. B*, 14:1165, 1976.

[76] A. J. Millis. *Phys. Rev. B*, 48:7183, 1993.

[77] M. Vojta, Y. Zhang, and S. Sachdev. *Phys. Rev. Lett.*, 85:4940, 2000.

[78] M. Grater and C. Wetterich. *Phys. Rev. Lett.*, 75:378–381, 1995.

[79] G. v. Gersdorff and C. Wetterich. *Phys. Rev. B*, 64:054513, 2000.

[80] S. Coleman. *Comm. Math. Phys.*, 31:259, 1973.

[81] I. J. Pomeranchuk. *Soviet. Phys. JEPT*, 8:361, 1958.

Danksagung

Mein besonderer Dank gilt Herrn Prof. Dr. Christof Wetterich für die inspirierende und motivierende Betreuung dieser Arbeit.

Herrn PD Dr. Jan Martin Pawlowski danke ich herzlich für die Übernahme des Zweitgutachtens.

Für zahlreiche Diskussionen, von denen ich auch im Hinblick auf die vorliegende Arbeit sehr profitiert habe, danke ich besonders Dr. Sebastian Diehl, Philipp Strack, Jens Müller, Michael Scherer, Stefan Flörchinger, PD Dr. Jan Martin Pawlowski, PD Dr. Holger Gies, PD Dr. Thomas Gasenzer, Dr. Jörg Jäckel und Johannes Heinonen. Georg Robbers, Klaus Klingmüller und Steffen Stern danke ich für die geduldige Hilfe bei Computerproblemen.

Meinen Freunden und Bekannten innerhalb und außerhalb des Institutes danke ich für die Begleitung und Anteilnahme.

Meiner Familie bin ich für die Liebe und Unterstützung auf dem Weg durch das Studium zu großem Dank verpflichtet.

Dem Land Baden-Württemberg danke ich für die finanzielle Förderung durch ein Promotionsstipendium im Rahmen der Landesgraduiertenförderung.